Université de Montréal

# Development and application of a Human Cortical Brain atlas on MRI considering phylogeny

## Développement et emploi d'un atlas du cortex cérébral humain réalisé sur IRM et tenant compte de la phylogénie

Par Maryna Zhernovaia

Programme de sciences biomédicales
Faculté de médecine,
En extension à l'Université du Québec à Trois-Rivières

Mémoire présenté
en vue de l'obtention du grade de Maître ès sciences (M.Sc.)
en Sciences biomédicales

Octobre 2021

Université du Québec à Trois-Rivières
Département d'anatomie

Ce mémoire intitulé

# Development and application of a Human Cortical Brain atlas on MRI considering phylogeny

## Développement et emploi d'un atlas du cortex cérébral humain réalisé sur IRM et tenant compte de la phylogénie

Présenté par

**Maryna Zhernovaia**

A été évalué par un jury composé des personnes suivantes

**Benjamin Boller**
Président-rapporteur

**Josefina Maranzano**
Directrice de recherche

**Simona Brambati**
Membre du jury

# Résumé

Le cortex cérébral est une structure en couches complexe qui remplit différents types de fonctions. Au cours de l'histoire des neurosciences, plusieurs atlas corticaux ont été développés pour classifier différentes régions du cortex en tant que zones aux caractéristiques structurelles ou fonctionnelles communes, afin d'étudier et de quantifier les changements aux états sain et pathologique. Cependant, il n'existe pas d'atlas suivant une approche phylogénétique, c'est-à-dire, basée sur les critères d'évolution communs.

Ce mémoire présente les étapes de création d'un nouvel atlas dans un modèle d'imagerie par résonance magnétique (IRM) en espace standard (pseudo-Talairach) : le PAN-Atlas, basé sur l'origine phylogénétique commune de chaque zone corticale, et son application sur des scans d'IRM de dix individus pour évaluer sa performance.

D'abord, nous avons regroupé les différentes régions corticales en cinq régions d'intérêt (RdI) d'origine phylogénétique connue (archicortex, paléocortex, périarchicortex, proïsocortex, isocortex ou néocortex) sur la base de protocoles de segmentation validés histologiquement par d'autres groupes de chercheurs. Puis, nous avons segmenté ces régions manuellement sur le modèle d'IRM cérébrale moyen MNI-ICBM 2009c, en formant des masques.

Par la suite, on a utilisé un pipeline multi-étapes de traitement des images pour réaliser le recalage des masques de notre atlas aux scans pondérés T1 de dix participants sains, en obtenant ainsi des masques automatiques pour chaque RdI. Les masques automatiques ont été évalués après une correction manuelle par le biais de l'indice Dice-kappa, qui quantifie la colocalisation des voxels de chaque masque automatique vs. le masque corrigé manuellement. L'indice a montré une très bonne à excellente performance de notre atlas. Cela a permis l'évaluation et comparaison des volumes corticales de chaque région et la quantification des valeurs de transfert de magnétisation (ITM), qui sont sensibles à la quantité de myéline présente dans le tissu.

Ce travail montre que la division régionale du cortex en IRM avec une approche phylogénétique est réalisable à l'aide de notre PAN-Atlas en espace standard et que les masques peuvent être utilisés pour différents types de quantifications, comme les volumes corticaux, ou l'estimation des valeurs de ITM. Notre atlas pourrait éventuellement servir à évaluer les différences entre personnes saines et celles atteintes par des maladies neurodégénératives ou d'autres maladies neurologiques.



**Mots-clés** : cortex cérébral, phylogénie, atlas, IRM, volumétrie, indice de transfert magnétisation

# Abstract

The cerebral cortex is a complex layered structure that performs different types of functions. Throughout the history of neuroscience, several cortical atlases have been developed to classify/divide different regions of the cortex into areas with common structural or functional characteristics, to then study and quantify changes in healthy and pathological states. However, to date, there is no atlas following a phylogenetic approach, i.e. based on the common evolution criteria.

This thesis presents the steps of creation of a new atlas corresponding to a standard MRI template: the PAN-Atlas, based on the common phylogenetic origin of each cortical zone, and its application on MRI scans of ten healthy participants to assess its performance.

First, we grouped the different cortical regions into five regions of interest (ROI) of known phylogenetic origin (archicortex, paleocortex, periarchicortex, proisocortex, isocortex or neocortex) based on MRI protocols previously validated through histology by other groups of researchers. Then, we manually segmented these ROIs on the MNI-ICBM 2009c average brain MRI template, creating corresponding masks.

We then used a multi-step image processing pipeline to register the atlas' masks to T1 weighted images of ten healthy participants, generating automatic masks for each scan. The accuracy of these automatic atlas' masks was assessed after manual correction using Dice-kappa similarity index, to quantify the colocalization of the automatic vs. the manually corrected masks. The Dice-kappa values showed a very good to excellent performance of the automatic atlas' masks. This allowed the evaluation and comparison of cortical volumes of each ROI, as well as the quantification of magnetization transfer ratio (MTR) values, which are sensitive to myelin content.

This work shows that the division of the cortex on MRI following a phylogenetic approach is feasible using our PAN Atlas, and that the masks of the atlas can be used to perform different types of quantifications, such as the ones presented here (cortical volume and MTR per ROI). Our atlas could similarly be used to assess differences between the cortex of healthy individuals and people affected by neurodegenerative diseases and other neurological disorders.



**Keywords**: cerebral cortex, phylogeny, atlas, MRI, volumetry, magnetization transfer index

# Table of Contents

# List of Tables

# List of Figures

# List of Acronyms

AC: Anterior commissure

aCf: Anterior calcarine fissure

AD: Alzheimer's disease

ADNI: Alzheimer's Disease Neuroimaging Initiative

AG: Amygdala

AHLV: Anterior horn of lateral ventriculus

ANTS: Advanced Normalization Tools

BCC: Body corpus collosum

BOLD MRI: Blood-Oxygenation-Level-Dependent magnetic resonance imaging

CA: Cornu ammonis

CalF: Calcarine fissure

CalS: Callosal sulcus

Cas: Calcarine sulcus

cf: Crus of the fornix

CinG: Cingulate gyrus

CinS: Cingulate sulcus

CNS: Central nervous system

CS: Collateral sulcus

CSc: Collateral sulcus caudal segment

CSF: Cerebrospinal fluid

CT: Computed tomography

CTLDs: C-type of lectin-like domain proteins

DBM: Deformation based morphometry

dMRI: Diffusion-weighted (tensor) magnetic resonance images

DK: Desikan–Killiany atlas

DKT: Desikan–Killiany-Tourville atlas

EC: Entorhinal cortex

Es : Entorhinal sulcus

Fg: Fusiform gyrus

FLASH: Fast low angle shot

fMRI: Functional magnetic resonance imaging

GABA: γ-aminobutyric acid

GCC: Genu corpus collosum

GLI: Gray level index images

GM: Gray matter

GRE: Gradient echo

HB: Hippocampal body

HCP: Human connectome project

Hf: Hippocampal fissure

HH: Hippocampal head

IHLV: Inferior horn of lateral ventriculus

HT: Hippocampal tail

ICBM: International Consortium for Brain Mapping

igCAMs : Immunoglobulins cell adhesion molecules

IL-1β: Interleukin 1β

Ins: Interneurons

Itg: Inferior temporal gyrus

ITM: Index of transfer magnetisation

Its: Inferior temporal sulcus

Lg: Lingual gyrus

Li: Limen insulae

LV: Lateral ventricle

MarS: Marginal sulcus

MNI: Montreal Neurological Institute

MPRAGE: Magnetisation-prepared rapid gradient-echo

MRI: Magnetic resonance imaging

MTL: Medial temporal lobe

MTR: magnetization transfer ratio

ND: Neurodegenerative disorders

NIH: National Institute of Health

OASIS: Open Access Series of Imaging Studies

Ols: Olfactory sulcus

P: Pulvinar

PAN: PaleoArchiNeo

PC: Posterior commissure

PD: Parkinson's disease

PDw: Proton density weighted

PHg: Parahippocampal gyrus

PHLV: Posterior horn of lateral ventriculus

PirC: Piriform cortex

PNs: Projection neurons

PRC: Perirhinal cortex

PU: Parcellation units

Pu: Putamen

RCC: Rostrum corpus collosum

rfMRI: Resting-state functional magnetic resonance imaging

ROIs: Regions of interest

Schg: Gyrus of Schwalbe

SE: Spin echo

SpCC: Splenium corpus collosum

SPGR: Spoiled gradient

SPM: Statistical Parametric Mapping

Ssa: Sulcus semiannularis

STs: Superior temporal sulcus

TBM: Tensor based morphometry

TD: Talairach Daemon atlas

tfMRI: Task functional magnetic resonance imaging

Th: Thalamus

THVL: Temporal horn of ventriculus lateralis

TNF-$\alpha$: Tumor necrosis factor $\alpha$

TP: Temporal pole

TPs: Temporopolar sulcus

T1w: T1-weighted

T2w: T1-weighted

VBM: Voxel based morphometry

WM: White matter

## Acknowledgements

First, I want to thank the director of the program, Hugues Leblond, for his collegiality and ability to find the best way forward.

I would like to express my deep gratitude to my research director Josefina Maranzano, who was able to see in me the potential to carry out this work. I really appreciate the patience and the wisdom with which professor Maranzano taught, supported, guided me and with which she gave me the opportunity to develop professionally throughout the project. I would also like to thank my mentor, professor Anna Nayouf, for the incredible amount of help she provided me during the preparatory phase of this work.

I would also like to thank the researchers of the McConnel Brain Imaging Center of the Montreal Neurological Institute, especially Drs. Mahsa Dadar and Yashar Zeighami for the interest they showed and for the MRI data they provided.

I would also like to thank my parents, my husband, my family, and my colleagues for their faith in me, for their understanding and support.

# INTRODUCTION: Background and Rational

## The human cerebral cortex: why and how we study it

The human cerebral cortex is a complex convoluted, layered structure that constitutes the outer surface of both hemispheres. To this day, cortical functions, under normal or pathological conditions, are incompletely understood and remain the center of interest of neuroscientists, neurologists and phycologists (Strominger, Demarest, & Laemle, 2012).

In essence, cerebral cortical functions are: to receive and process sensory inputs, to form stable interneuron interactions that allow memory formation and a variety of cognitive processes, and to coordinate the activities of the organism to produce the appropriate behavioral and motor responses to the sensory stimuli (Watson, Kirkcaldie, & Paxinos, 2010). The wide variety of functions performed with the direct participation of the cortex can be explained by its complex structural organization and functional interconnections between different cortical regions and subcortical structures (Strominger et al., 2012); (K. D. Harris & Shepherd, 2015); (Eickhoff, Thirion, Varoquaux, & Bzdok, 2015).

The attempts to increase and streamline our knowledge of the cerebral cortex have led to the creation of classification systems and conceptual models that divide the cortex into multiple areas or parcels, which may be presented together as a brain atlas. Historically, the first descriptions of cortical areas were related to the search of regions of the brain responsible for a specific cognitive function. The studies of Broca and Wernicke, which proposed the dependence of a language deficit on damage to a specific and isolated brain portion, materialized the concept of topographic specialization, and structure-function specificity (Eickhoff, Constable, & Yeo, 2018).

The next important stage that cemented the notion of functional specificity of a given cortical area was the use of microscopy, which revealed the heterogenous microstructure of the cortex. Histologically, considering the structural characteristics of cortical cell bodies, such as shape and size (known as cytoarchitecture), and their horizontal distribution, Brodmann separated the mammalian cortex into 47 cortical areas (Brodmann & Gary, 2006) creating the standard reference.

Compared to Brodmann, a much more detailed cytoarchitectonic description of cortical layers (agranular, frontal, parietal, polar, and granular) was obtained by Von Economo and Koskinas by sectioning the whole brain perpendicularly into its fronto-occipital axis (von Economo &

Koskinas, 1925);(von Economo, Koskinas, & Triarhou, 2008). They divided the human cerebral cortex into 54 fundamental cytoarchitectonic areas with 76 variants and 107 modification areas (Triarhou, 2007).

Similar conclusions were drawn by Cécile and Oskar Vogt about the clear classification of boundaries between cortical parcels who identified 185 cortical areas separated according to the density and distribution of myelinated neuronal axons, also known as myeloarchitecture (R. Nieuwenhuys, 2013); (Eickhoff et al., 2018).

More detailed consideration of the classical cytoarchitectural areas led to the division of the cerebral neocortex into smaller units, which contain different types of cells connected vertically, perpendicular to the pial surface (Mountcastle, 1997); (K. Amunts & Zilles, 2015). These units, called microcolumns, are grouped by short range horizontal connections to form columns or modules. This columnar disposition would be determined by two factors: the ontogenetic development of a group of progenitor cells, which would determine the micro columnar organization, and the intermittent distribution of the afferents reaching the cortex, essential for the modular arrangement (Mountcastle, 1997).

Despite the various morphological classification systems dividing the cortex into distinct areas, one characteristic remains as the basis of any and all histological classifications proposed to date: there are two basic types of cortices: the *isocortex* and the *allocortex* (J. r. K. Mai & Paxinos, 2012).

The *isocortex* corresponds to the *homogenetic cortex*, as per Brodman developmental classification, representing the cerebral cortex that remains a six-layered structure laid in early stages of embryogenesis. The only exceptions here are the frontal agranular cortex without a clear layer IV; and the primary visual cortex where layer IV is enlarged and can be subdivided into sublayers IVa, IVb, and IVc (J. r. K. Mai & Paxinos, 2012).

On the other hand, the *heterogenetic cortex* of Brodman, which corresponds to the *allocortex*, does not form six layers during the developmental stage. This fact explains the heterogeneity of the allocortex as it differs in the number of layers in different areas (J. r. K. Mai & Paxinos, 2012); (K. Amunts & Zilles, 2015).

Another distinction between *isocortex (homogenetic)* and *allocortex (heterogenetic)* is that the latter does not receive thalamic inputs, while the former (*isocortex*) does (Strominger et al., 2012).

Finally, the period of cortical maturation through mammalian evolution (phylogeny) can be used to classify the cortical areas using evolutionary criteria. This phylogenetic approach could reveal the features of different cortical areas grouped together based on a common evolutionary development. Hence, we can divide the earlier formed *allocortex* in two areas: the phylogenetically oldest *paleocortex* and the ancient *archicortex* (J. r. K. Mai & Paxinos, 2012); (K. Amunts & Zilles, 2015).

The *paleocortex*, which shares common characteristics with the three-layered general cortex of reptiles (Klingler, 2017), consists of the olfactory bulb, retrobulbar (anterior olfactory nucleus), the olfactory tubercle (substantiae perforatae anterioris), prepiriform cortex (gyrus olfactorius lateralis), periamygdalar area (gyrus semilunaris), cortical part of the amygdala, the diagonal band and septum pellucidum (Kharlamova, Godovalova, Junemann, & Saveliev, 2018); (J. r. K. Mai & Paxinos, 2012).

The *archicortex* is represented by the hippocampus (Ammon's horn, dentate gyrus, and subiculum), the presubiculum, parasubiculum, entorhinal cortex, retrosplenial cortex, and a cortical band in the cingulate gyrus (J. r. K. Mai & Paxinos, 2012); (K. Amunts & Zilles, 2015).

The *isocortex* represents the evolutionarily much younger human *neocortex*, which forms most of the cerebral cortex. It comprises the primary, secondary, and tertiary sensory areas, the multimodal association areas, and the primary and non-primary motor areas.

The border between *isocortex* and *allocortex* is a smooth transition in cyto- and in myeloarchitecture. This spatial disposition allows the classification of these transitional areas in *periarchicortex*, adjacent to the *archicortex*, and *proisocortex*, between the *periarchicortex* and *neocortex* (J. r. K. Mai & Paxinos, 2012), see Figure 1 in Chapter 2.

Being present in the medial temporal lobe, the *peri-archicortex* is lining the surface of the collateral sulcus (almost throughout its entire length) and next to the parahippocampal gyrus, forming the perirhinal and parahippocampal cortices (Ulmer & Jansen, 2013).

Finally, the *proisocortex* is represented by the cortex of the anterior, middle, and posterior cingulate gyrus that surround the corpus callosum like a belt (J. r. K. Mai & Paxinos, 2012).

All of the above explains why the human cortex with its inherent complexity, cannot be studied as a whole unit and must be divided into smaller portions (called areas, or regions, or parcels) which

follow a rational either in structure and/or function, so that each region may have a recognisable identity.

The general aim of this work (this thesis) is to exploit the previous knowledge of cortical areas of common phylogenetic origin, to apply it to magnetic resonance imaging (MRI), constructing a **new atlas corresponding to a standard MRI template: the PAN-Atlas (P=paleo, P=periarchi, P=proiso, A=archicortex, N=neocortex)**. To date (to our knowledge), such an approach on MRI has not been attempted by others. We have also made the PAN-Atlas publicly available at https://gin.g-node.org/Maryna.Zhernovaia/MRI/. It is our hope that in the future, neuroscientists studying normal aging, neurodegeneration, and cortical asymmetry (between left and right hemispheres) would benefit from investigating the changes and differences in cortical areas defined in this way: considering phylogeny on MRI.

Before diving into the construction of the PAN-atlas on MRI itself (chapter 2 of this thesis), a review of the literature (chapter 1) will present the basic concepts regarding: the histological structure of the human cortex, its organization (e.g. layers and columns) and symmetry/asymmetry, some basic notions on neurodegeneration, the various MRI sequences that are used to study the cortex (including the ones used in this project), the basis of MRI registration (necessary to use the atlas at a single subject level), and the main and most frequently used brain atlases available to researchers to date. Finally (in chapter 3), the first results of the atlas applied to ten individual healthy subjects will be presented, followed by a general discussion and a conclusion.

# CHAPTER 1: Literature Review

## 1. Structure of the human cerebral cortex

The human cerebral cortex corresponds to the superficial area of the brain hemisphere where the neuronal cells with their bodies and processes are surrounded by supporting cells and the vascular network (capillaries) (Purves et al., 2018). During mammalian evolution, the human cortex has experienced the largest increase in volume compared to other species, which in turn has allowed for the evolution of its functions (Van Essen, Donahue, & Glasser, 2018). To fulfill the highest-level of cognitive functions, the cortex has acquired a high level of diversity in terms of cell types, connectivity patterns, and plasticity (K. D. Harris & Shepherd, 2015).

### 1.1. Cell types and their interactions

In absolute numbers, the human brain contains on average 86 billion neurons and 84 billion non-neuronal cells (Azevedo et al., 2009). These cells differ in their morphology, presence, number of projections, and their functional characteristics.

#### 1.1.1. Common characteristics of all neurons

The main functional unit of the cortex is the neuron or nerve cell. It promotes communication between distinct regions of the nervous system by transferring an electrical signal for longer or shorter distances (Purves et al., 2018).

A typical neuron has similarities to other cells in morphology and cytoplasmatic content, in terms of the organelles (Figure. 00) (Brady, Siegel, Albers, & Price, 2011).

**Figure 00**: Schematic representation of the neuronal morphology.

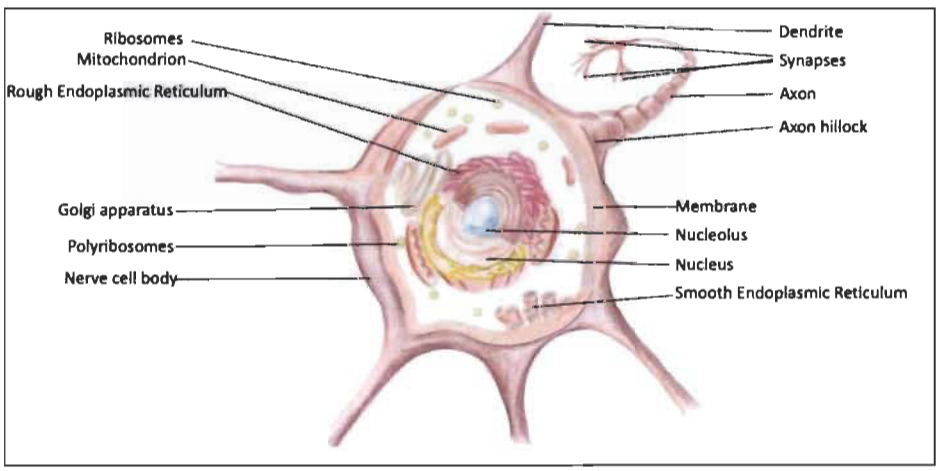

However, neurons have specificities of their own, such as: a more distinct distribution of the organelles and the presence of specialized fibrillar or tubular proteins that promote the stability of the cell and its processes, and a directional transport of molecules (Purves et al., 2018).

Most neurons have multiple extensions of their cytoplasm: the dendrites and the axons.

A dendrite is a branching outgrowth of a nerve cell and forms the sensitive pole of that cell. The dendrites perceive excitatory or inhibitory signals from other neurons or receptor cells. The number of dendrites in different cells can vary from one to many (Boivin & Nedivi, 2018); (Fernandez-Gonzalez et al., 2017).

The other type of branch of the neuron, which promotes the action potential initiation and its propagation to other cells, is the axon (Ramaswamy & Markram, 2015) which can be subdivided into the axon hillock, the initial segment, the axon proper, and the axon termination (Brady et al., 2011). Through their axons, the neurons connect different cortical areas and subcortical brain structures like the striatum, thalamus, subthalamic nucleus, inferior and superior colliculus, as well as other nuclei in the midbrain and brainstem, and to the spinal cord (Gerfen, Economo, & Chandrashekar, 2018); (Farhy-Tselnicker & Allen, 2018); (Ramaswamy & Markram, 2015).

The interaction between neurons occurs through a specific type of contact named synapsis. There are two types of synapses, the electric synapse, where the membranes of the two neurons involved are very close together and connected by gap junctions where ion channels are lined up in each membrane, allowing the direct passage of ions from one neuron (pre-synaptic) to the other neuron (post-synaptic) (Purves et al., 2018). The other type of synapse is the chemical synapse, without a physical connection, but through a contiguity disposition of the neurons involved, distinguishing between the pre- and postsynaptic neuronal membrane a space called the synaptic cleft (Purves et al., 2018). Depending on what neuronal components form the synapses, they are classified as axodendritic, axosomatic, axoaxonic, dendrodendritic, somatosomatic, and somatodendritic synapses (Brady et al., 2011). In a chemical synapse, the release of a low-molecular-weight substance, the neurotransmitter, from the presynaptic neuron to the synaptic cleft is the result of an electrical signal (action potential) activating voltage-sensitive calcium channels. This leads to an increase in the local intracellular calcium concentration and the fusion of the pre-synaptic vesicles (containing the neurotransmitter) with the cellular membrane (Batool et al., 2019); (Bae & Kim, 2017). For each neurotransmitter, whether is it excitatory or inhibitory, there are specific receptors on the postsynaptic side that activate downstream signaling (Brady et al., 2011).

Presently, neurotransmitters and their receptors can be used to classify neurons and synapses, allowing the analysis of cortical regions with greater detail than that provided by the cell morphology (Palomero-Gallagher & Zilles, 2019).

### 1.1.2. Types of neurons

To execute all types of brain functions, different neuronal subtypes are formed during corticogenesis (Oishi & Nakajima, 2018). The classification and categorization of hundreds of cortical neurons is based on morphological, ontological, electrophysiological criteria, on destination of their projections, their function, or their gene expression profile (J. Harris, Tomassy, & Arlotta, 2015); (Johnson & Walsh, 2017); (Lodato & Arlotta, 2015).

Morphologically, a basic classification of neurons divides them in two types according to the cellular body shape: 1) pyramidal (70% of all cells of the cortex) and 2) non-pyramidal cells, which include stellate cells, Martinotti, and horizontal cells (Rudolf Nieuwenhuys, 1994); (Cragg, 1976).

The pyramidal neuron bodies have conical form and a wide range of sizes, divided into small, medium, large or giant Betz cells (Strominger et al., 2012). They have a widely developed apical dendrite that extends toward the cortical surface and several basilar dendrites. Their axons reach cortical areas of the same or opposite hemisphere or terminate in subcortical regions (Rudolf Nieuwenhuys, 1994). Pyramidal neurons can be found in all the layers of the cortex, except for the most superficial layer (layer I) (Strominger et al., 2012).

Stellate cells are interneurons with bodies of different shapes (double bouquet cells, tuft cells, chandelier cells, and basket cells) and are characterized by a weak development of dendrites and a powerful development of axons, which do not go beyond the thickness of the cortex and encompass groups of pyramidal cells with their branches. Stellate cells are capable of coordinating (simultaneously inhibiting or exciting) spatially close groups of pyramidal neurons. Martinotti cells are multipolar neurons which, are encountered predominantly in the deepest cortical layers. Their long ascending axon splits up into a number of long horizontal branches, forming a local plexus. The horizontal cell (of Cajal) is a small neuron of layer I, with an axon oriented parallel to the cortical surface. They play an important role during development, but are absent or rare in adults (Brady et al., 2011); (Rudolf Nieuwenhuys, 1994).

Another type of cortical neuronal classification is based on their function and connectivity properties. Based on this criterion, there are two main groups of neurons: projection (or excitatory)

neurons (PNs) and local cortical interneurons (INs) (Molyneaux, Arlotta, Menezes, & Macklis, 2007).

Most neurons (70 to 80%) are projection neurons with typical pyramidal morphology. They use the amino-acid glutamate or aspartate as neurotransmitter and the synaptic contacts of their axonal terminals are excitatory. In this group, the cortico-cortical neurons can project their axons to the same hemisphere (forming the subgroup of associative projection neurons) or to the opposite hemisphere through the corpus callosum or the anterior commissure (composing the subgroup of commissural projection neurons). The corticofugal projection neurons conduct their axons to the targets out of the cortex, connecting the cortex and the nuclei of thalamus: corticothalamic PNs; the pons: cortico-pontine PNs; the superior colliculus: corticotectal PNs; and the spinal cord: corticospinal motor neurons (Lodato & Arlotta, 2015).

Local cortical INs are part of neocortical circuits. The subgroup of the spiny stellate interneurons receives inputs from the thalamus and are excitatory glutamatergic neurons. Conversely, aspiny cortical interneurons, use GABA (γ-aminobutyric acid) as a neurotransmitter which is the main inhibitory modulator of projection neurons (Lodato & Arlotta, 2015).

### 1.1.3. Characteristics of non-neuronal brain cells

The non-neuronal brain cells are the glial cells: the macroglia, formed of astrocytes and oligodendrocytes, and the microglia.

The largest group is represented by the astrocytes. They can be subdivided into protoplasmic astrocytes that are located in the gray matter in relation to capillaries, and fibrous astrocytes located in the white matter (Brady et al., 2011). They promote a structural support to the central nervous system (CNS) components. They also provide a metabolic interface with neurons, sending them partially metabolized glucose from the capillaries and regulating the local pH and ionic levels. Having a high proliferation ability, as a reaction to damage, astrocytes can form, in both gray and white matter, a fibrous form (state of gliosis). Also, astrocytes participate in neuronal synapse formation and synapse isolation to protect neurotransmitters released to the extracellular space (Marinelli, Basilico, Marrone, & Ragozzino, 2019); (Farhy-Tselnicker & Allen, 2018); (Brady et al., 2011).

Oligodendrocytes have variable morphology and fulfill various functions. Based on their location, the oligodendrocytes can be subdivided into perineuronal satellite oligodendrocytes that are in close proximity to neuron bodies in the gray matter (playing a role in the maintenance of the

neuron) and myelinating oligodendrocytes found in the white matter (Brady et al., 2011). The myelinating oligodendrocytes with their extended plasma membrane contribute to the myelination of segments of several axons at the same time in the CNS (Walsh, Landman, & Hughes, 2017). Along the axonal cytoplasm, there is an alternation of segments of compact myelin with a section of the unwrapped axonal plasma membrane: the nodes of Ranvier (Purger, Gibson, & Monje, 2016). Being a lipoprotein by chemical structure, myelin optimizes the action potential transmission along the axon by saltatory conduction. Oligodendrocytes also play a role in the metabolic support of axons as they can generate lactate as a source for further ATP formation (Kuhn, Gritti, Crooks, & Dombrowski, 2019). Finally, oligodendrocytes can regulate axonal volumes by reduction of axonal microfilaments phosphorylation (Brady et al., 2011).

Different types of injury factors may produce regions of demyelination in the CNS, which may persist for variable periods of time, as a result of slow and poor proliferative abilities of oligodendrocytes (Brady et al., 2011) and slower metabolic turnover of myelin compared with the other neuronal membranes (Morell & Norton, 1980).

Microglia cells are part of the immune system and promote immune surveillance of the CNS (Strominger et al., 2012). They are the only cell type in the CNS that has a distinct embryological linage, mesodermal instead of ectodermal (Brady et al., 2011). Considering their functional state, they can be subdivided into resting microglia, reactive or nonphagocytic microglia, and phagocytic macroglia with macrophage activity. These cells form a complex network with neurons and astrocytes. In response to injury, they are activated with production of pro- and anti-inflammatory cytokines. Also, they can activate neurotoxic processes mediated by stimulation of interleukin 1β (IL-1β) receptors or tumor necrosis factor α (TNF-α) receptors (Malva, 2007).

## 1.2. Cortical organization: cortical architecture

### 1.2.1. The cytoarchitectonic approach

This type of classification is based on the size, shape, and arrangement of the neuronal cell bodies in each different layer of the cortex. The number of layers varies from region to region, depending on the phylogenetic origin of the cortex (J. r. K. Mai & Paxinos, 2012) (Ch. 23).

The mammalian paleocortex has a simple trilaminar structure comprising: (I) a first marginal cell-sparse plexiform layer composed of dendrites of neurons from deeper layers; (II) a well-defined

second granular layer of pyramidal cell somata; (III) a polymorphous (slightly larger pyramidal cells and other neurons) cell layer (J. r. K. Mai & Paxinos, 2012) (Ch. 34).

Studying post-mortem paleocortical areas in human fetuses by immunohistochemistry, Kharlamova and colleagues (Kharlamova et al., 2018) determined that in comparison with other cortical regions, the prepiriform area develops first. Additionally, they found that the cytoarchitecture of the frontal and temporal areas of paleocortex were similar.

Amygdaloid nuclei can be subdivided by their developmental origin into deep cortex-like nuclei, a superficial "cortical" region, and a centromedial group of nuclei (J. r. K. Mai & Paxinos, 2012) (Ch. 22). The superficial cortex-like amygdaloid region, considered part of the paleocortex, has a layered organization with a cortex-like cytoarchitecture: (I) the most superficial molecular layer; (II) the outer cell-dense layer; (III) the deep inner cellular layer with a looser cellular arrangement (J. r. K. Mai & Paxinos, 2012) (Ch. 22).

The archicortex is more complex in structure with a number of layers that varies. For example, in the hippocampus, which can be subdivided into three distinct fields (CA3, CA2, and CA1), the distribution of the pyramidal cells is so homogeneous that it can be considered as essentially one cellular layer: the pyramidal cell layer (J. r. K. Mai & Paxinos, 2012)(Ch. 24); (R. Nieuwenhuys, Voogd, & Huijzen, 2008). However, based on the thickness of pyramidal cell compartmentalisation, a multilaminar structure can be observed (J. r. K. Mai & Paxinos, 2012)(Ch. 24). The plexiform layer with axons of that pyramidal cell is called the alveus. Opposite to it, we find the layer of apical dendrites of the pyramidal cells (R. Nieuwenhuys et al., 2008).

In contrast to the CA fields, the dentate gyrus, also part of the hippocampus, has a tri-laminate cortex. (I) the upper molecular layer populated by the unipolar dendritic tree of neurons from the underlying level to form synapses with afferents from the entorhinal cortex; (II) the principal cell layer (granule cell layer) with the granule neuron cells, the dendrites of which enter the molecular layer and the axons enter the Ammon's horn; and (III) the polymorphic layer with numerous intrinsic neurons (the hilus of the dentate gyrus) (J. r. K. Mai & Paxinos, 2012) (Ch. 24); (R. Nieuwenhuys et al., 2008).

Another portion of the archicortex, the entorhinal cortex, is a multilaminar structure. Despite the fact that the entorhinal cortex has a six-layered organization, it is quite distinct from the neocortical organisation: (I) an acellular or plexiform layer; (II) a cellular layer presented by modified pyramidal and stellate cells; (III) a homogeneous medium-sized pyramidal cell layer; (IV) the

lamina dissecans (an acellular region of dense fibers); (V) a layer of primarily large pyramidal cells with three sublaminae; and (VI) a broad and diffuse layer presenting a sharp border with white matter caudally, and less sharp rostrally (J. r. K. Mai & Paxinos, 2012) (Ch. 24).

The cortex between the hippocampus and the entorhinal cortex is the subiculum, also part of the archicortex, and the origin of subcortical projections to the septal complex, nucleus accumbens, anterior thalamus, and to the entorhinal cortex. The laminar organization of the subiculum is given by: (I) the superficial molecular layer containing the apical dendrites of the subicular pyramidal cells, and (II) the pyramidal cell layer that can be subdivided into (IIa) the external sublaminae (next to the molecular layer) and (IIb) internal sublaminae (J. r. K. Mai & Paxinos, 2012) (Ch. 24).

In the neocortex, six layers can be identified (see Figure 2) (J. r. K. Mai & Paxinos, 2012) (Ch. 23):

(I) the molecular layer, which is the most superficial, characterized by a very small number of cells, mainly represented by neuroglia cells and small associative horizontal Cajal cells. Their axons run parallel to the surface of the brain forming a tangential plexus of nerve fibers. However, the bulk of the fibers of this plexus is represented by dendritic branches of the underlying layers (Ross & Pawlina, 2011); (Eroschenko & Di Fiore, 2017).

(II) the outer granular layer, formed by numerous small pyramidal and stellate (excitatory) neurons, which give the granular appearance to the layer. The apical dendrites of pyramidal cells go towards layer I and their axons project from the base of the cell (Eroschenko & Di Fiore, 2017).

(III) the external pyramidal layer (Strominger et al., 2012), which is the widest layer of the cerebral cortex, contains pyramidal neurons and Martinotti cells. The density of non-pyramidal cells is lower in this layer than the adjacent layers, making it possible to distinguish from the neighboring layers (Ross & Pawlina, 2011); (Eroschenko & Di Fiore, 2017) The pyramidal layer mainly performs associative functions. (Rudolf Nieuwenhuys, 1994).

(IV) the inner granular layer, which is very developed in some areas of the cortex: granular regions (e.g. visual and auditory cortex), weakly developed in other areas: dysgranular regions (e.g. Broca's speech region), and absent in some regions: agranular regions (e.g. primary motor area) (J. r. K. Mai & Paxinos, 2012)(Ch.23). This layer is predominantly formed by small stellate (excitatory) neurons and different neuroglia cells that form complex connections with the pyramidal cells (Ross & Pawlina, 2011); (Eroschenko & Di Fiore, 2017).

(V) the internal pyramidal layer (Strominger et al., 2012), which is formed by large pyramidal cells. The area of the primary motor cortex (precentral gyrus) contains giant pyramidal cells, which were first described by V.A. Betz (J. r. K. Mai & Paxinos, 2012; Ross & Pawlina, 2011) (Ch.27, Ch23). The apical dendrites of these cells reach the 1st layer. The axons of the pyramidal cells project to subcortical structures like the striatum, thalamus, subthalamic nucleus, inferior and superior colliculus, the nuclei in the midbrain and brainstem, and to the spinal cord. The longest axons of the Betz cells reach the caudal segments of the spinal cord in the pyramidal tract (Gerfen et al., 2018). In addition to these vertical (projection) pathways, in this layer, as in the previous one, there are also horizontal nerve fibers (J. r. K. Mai & Paxinos, 2012) (Ch.23).

(VI) the multiform layer contains polymorphic cells whose concentration decreases closer the white matter. The axons of these cells go into the white matter as part of the efferent pathways, and the dendrites reach the molecular layer (Ross & Pawlina, 2011); (Eroschenko & Di Fiore, 2017).

**Figure 01**: Schematic representation of the cytoarchitecture of the human isocortex. I molecular; II outer granular layer; III external pyramidal layer; IV inner granular layer; V internal pyramidal; VI multiform. (Modified from Amunts, Zhilles, 2015)

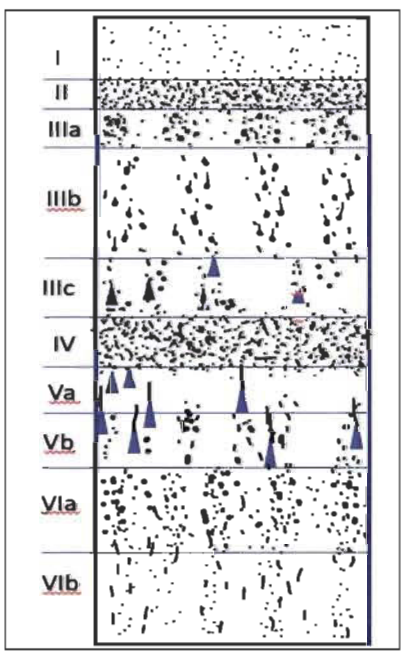

### 1.2.2. The myeloarchitectonic approach

This classification is based on local differences in the thickness and density of myelin fibers. There are various ways to approach the myelo-architecture of the cortex.

The most commonly used myeloarchitectural classification of the cortex is determined by the length and strength of the radial bundles (R. Nieuwenhuys, 2013). In correspondence with the cytoarchitectonic layers (but using Arabic numbers instead of roman numbers), the myeloarchitectonic layers are:

(1) the zonal layer, with four sublayers, the narrow sublayer $1^{o}$, with very few fibres, and the external, intermediate and deep sublayers 1a, 1b and 1c. The sublayer 1a contains more fibres than 1b and 1c,

(2) the dysfibrous layer with very few fibres,

(3) the suprastriate layer with three sublayers: 3a1 rich in fibres, and 3a2 and 3b with the end-segments of the radial bundles,

(4) the external stria (outer stripe of Baillarger) layer with tightly packed, tangential fibres.

(5.a) the intrastriate layer, which is poor in tangential fibres,

(5.b) the internal stria (inner stripe of Baillarger) with tightly packed tangentially oriented fibres,

(6) this layer is subdivided into the 6a1 and 6a2 laminae, and the 6b1 and 6b2, which forms a transitional zone with the subcortical white matter (R. Nieuwenhuys, 2013).

According to Vogt, another way of considering the classification of the cortical myeloarchitecture is based exclusively on the lamination of the tangential fibers. This classification categorises four myeloarchitectonic types: bistriate, unistriate, unitostriate and astriate. The separation of these myeloarchitectonic types depends on whether myelin-rich bands (bands of Baillarger) are identified or not (R. Nieuwenhuys, 2013); (Dinse et al., 2015). In the case of the astriate type, the myelination is maximal (heaviest) and it is impossible to separate any individual band. In the bistriate type, correspondingly, the areas of maximal myelination produce two visible bands. The unitostriate type represents a complex of multiple layers that are visible as a single one, and finally the unistriate type has only one band (R. Nieuwenhuys, 2013) (Figure 02).

Finally, a last way to approach the myeloarchitectural classification of the cortex is according to the disposition of the bundles of radial fibres. Following this approach, three types of areas can be distinguished: euradiate (where the radii do not extend beyond the level of the suprastriate layer); supraradiate (where the bundles traverse almost the entire width of the cortex and reach the zonal

layer); and infraradiate (where the radii are very short and terminate already in the fifth layer at the level of the inner stripe of Baillarger) (R. Nieuwenhuys, 2013).

**Figure 02**. Representation of four different types of myeloarchitecture according to Vogt: a: astriate; b: bistriate; c: unitostriate; d: unistriate. The red boxes represent the bands of Baillarger (inspired by a figure of Nieuwenhuys R. 2013)

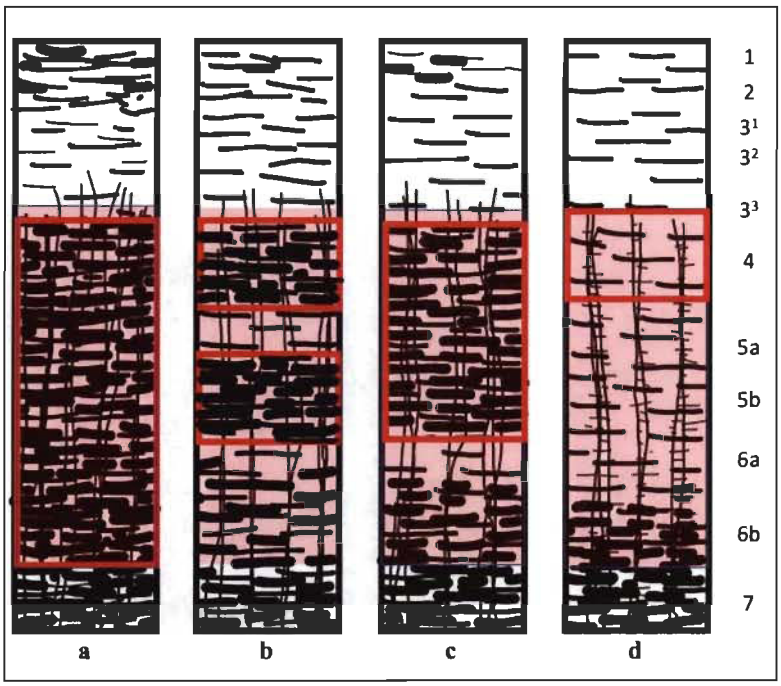


## 1.3. Asymmetries in the cerebral cortex

Our two brain hemispheres are different at a functional level, as shown by language dominance and handedness (lateralized specialization), as well as at the cytoarchitectural and neurochemical levels (Toga & Thompson, 2003).

The development of the asymmetries in cortical areas along with the corresponding cellular changes start during the period of early cortical development, during the proliferation of the progenitor cells (Toga & Thompson, 2003). The stage of pathway selection, characterized by the complex interaction of genetic factors and the influences of endogenous extracellular signals, leads to the specificity of the immature neuron subtype (Strominger et al., 2012) and their layer specific position (Oishi & Nakajima, 2018). This is followed by the stage of target selection, characterized by the chemotrophic guidance of axons on their pathway of elongation and expansion (Strominger et al., 2012). But changes leading to structural specifications and asymmetries continue to occur

even after birth (Li et al., 2014). The activity-dependent and experience-dependent specialisation of neurons promote extensive circuitry and connectivity formation between the nervous cells (Strominger et al., 2012). For example, on post-mortem brains of different ages, Amunts and colleagues detected cytoarchitectonic differences that were age-dependent in the cortical areas of language dominance (Katrin Amunts, Schleicher, Ditterich, & Zilles, 2003).

Macroscopically, the regional hemispheric asymmetries that can be observed in right-handers, manifest by the larger posterior protrusion of the left occipital pole compared with the right one, and the right frontal lobe anterior protrusion compared to the left one (J. r. K. Mai & Paxinos, 2012) (Ch.23); (Toga & Thompson, 2003).

While the total right hemispheric cortex volume is considered larger than that of the left one (J. r. K. Mai & Paxinos, 2012) (Ch. 23), the inter- hemispheric cortical volume difference per lobe might show larger volumes on the left (Carne, Vogrin, Litewka, & Cook, 2006). For example, the left temporal lobe cortex is larger than its right counterpart (Carne et al., 2006); (Katrin Amunts et al., 2003). This could be explained by the location of the cortex around the superior temporal sulcus, which is one of the longest sulci of our brain, being even longer and shallower in the left hemisphere (Specht & Wigglesworth, 2018).

The entorhinal cortex presents a clear functional asymmetry with left dominance, which can be explained by its involvement in verbal processing (Simic et al., 2005). The location of the neurons and their interconnections on that area can explain the formation of a structural asymmetry, as shown by the *verrucae entorhinalis*. It was determined that the surface of these entorhinal islands (*verrucae entorhinalis)* is significantly higher in the left hemisphere compared to the right one (Simic et al., 2005).

Regarding the hippocampus, the asymmetries found varied depending on the type of study. A histological study found larger left hippocampi, but without reaching statistical significance (J. r. K. Mai & Paxinos, 2012) (Ch. 23). Another study, considering handedness, reported a larger size of the right hippocampi (Szabo, Xiong, Lancaster, Rainey, & Fox, 2001).

Measured on MRI-based studies, the left frontal cortex has been reported to be significantly larger than the right one (Carne et al., 2006). Specifically, the volume of the medial frontal cortex, is higher in the hemisphere where a paracingulate sulcus is present, which is accompanied by the corresponding decrease of the adjacent anterior cingulate cortex volume (Fornito et al., 2008).

Asymmetries also affect the visual association cortex projected on the parieto-occipital fissure. The asymmetry in the surface area depends on the depth of the junction between the occipito-parietal fissure and the calcarine sulcus: in the right hemisphere, this junction has been detected as significantly deeper (Lyttelton et al., 2009).

Finally, a relevant observation is that cortical differences across hemispheres may be significant when comparing the cortex volumetrically (voxel-base analysis), but studies based on surface analysis may reveal no significant differences across hemispheres (J. r. K. Mai & Paxinos, 2012). Hence, when comparing results obtained by different groups, it is vital to consider the method used to detect the asymmetries.

The studies mentioned above present examples of the wide variety of hemispheric cortical asymmetries, affecting different cortical areas. This points to the relevance of considering (and measuring) hemispheric asymmetries when performing MRI measurements, either in health or in pathological states. Our atlas is an MRI tool that could be used to probe these differences (details in Chapter 3).

## 1.4. Cortex and neurodegeneration

Neuronal damage is a pathological feature of neurodegenerative disorders (NDs) such as Alzheimer's and Parkinson's disease, amyotrophic lateral sclerosis, Huntington's disease, spinocerebellar ataxia, and multiple sclerosis (de Flores, La Joie, & Chételat, 2015) (Heim, Krismer, De Marzi, & Seppi, 2017); (Rüb et al., 2016); (Liu et al., 2019).

The etiological factors of neuronal disease can be very different. Among them, the most commonly considered are infections, genetic mutations, neuroinflammation, oxidative stress (Simpson & Oliver, 2020); (Stephenson, Nutma, van der Valk, & Amor, 2018) and specific protein aggregations (Llorens et al., 2017).

All NDs are characterized by a progressive loss in the number of neurons. This loss of neurons at the cortical level leads to a loss of function, which results in the development of cognitive impairment, dementia, affected motor and sensory control, and ultimately death (Erkkinen, Kim, & Geschwind, 2018).

NDs can be classified according to the first clinical symptoms (cognitive disorders, dementia, Parkinsonism) (Jahn, 2013); (Kalia & Lang, 2015);(McKhann et al., 2011), or according to the specific anatomical location of the neurodegeneration (frontotemporal degeneration,

extrapyramidal disorders, or spinocerebellar degeneration) (Dickerson & Wolk, 2012); (Brickman et al., 2018), or based on the main molecular defect (α-synuclein protein in Parkinson's disease, Lewy body dementia, and multiple system atrophy -synucleinopathies-) (Dugger et al., 2014); (Leverenz et al., 2007).

Ultimately, during the evolution of a given ND, there will be characteristic changes affecting certain regions of the cerebral cortex and/or subcortical structures (de Flores et al., 2015), (Bartel et al., 2019), (Kutová, Mrzílková, Riedlová, & Zach, 2018). For example, in the early stages of Alzheimer's Disease (AD), the entorhinal cortex, perforant path projections and hippocampi are preferentially affected (Adams et al., 2017). The hippocampus and the entorhinal cortex are both part of the archicortex, a portion of the cortex with a common phylogenetic origin. Recent studies in another ND (Huntington disease) have shown that all four cerebral lobes undergo thinning of their cortical mantle and a layer-specific neuronal loss in various areas of the cerebral allocortex and neocortex (Rüb et al., 2016).

Cortical analyses based on a phylogenetic classification are not part of the standard imaging approaches currently used in NDs' assessments (McKhann et al., 2011), (Partridge, Deelen, & Slagboom, 2018). However, we speculate that the study of the cortex considering phylogeny (via the use of our atlas) would contribute to the evaluation of neurodegeneration in different ND.

## 2. MRI cortical studies in human brain research

The histological myelo- and cyto-architectural classification of the cortex is an invasive approach, only feasible *ex vivo,* which is considered as the gold standard for brain parcellation (Ding et al., 2016). The use of these methods *in vivo* is limited to biopsy material, or surgical resection of the lobes. Different medical imaging modalities (e.g. computed tomography, positron emission tomography, MRI) have emerged to visualize the brain *in vivo*. MRI is the method that provides the highest anatomical detail and strongest grey-to-white matter contrast (Symms, Jäger, Schmierer, & Yousry, 2004), therefore, it has become a promising technique to study the cerebral cortex, dividing it into meaningful parcels or regions of interest (ROIs) (Trampel, Bazin, Pine, & Weiskopf, 2019); (Paus, 2018). In this section, we present the MRI modalities and image processing tools that were used in our atlas project.

### 2.1. Structural MRI

Structural MRI can be considered as an imaging modality that provides static anatomical information, qualitatively and quantitatively describing the shape, size, and integrity of gray and white matter structures of the brain (Symms et al., 2004). The MRI signal varies between tissue types, since the gray matter contains more cell bodies (neurons and glial cells) than the white matter, which is mostly made up of long-range nerve fibers (myelinated axons), as well as supporting glial cells. Morphometric techniques can help us measure the volume or shape of the gray matter structures, such as the hippocampus (Na et al., 2020), and the volume, thickness or cortical layers in different cortical areas of the cerebral neocortex (Trampel et al., 2019).

**The T1-weighted sequence**

T1-weighted (T1w) is the most widely used pulse sequence for brain volumetry and for structural imaging in the research setting (Trampel et al., 2019). The sequence captures high tissue contrast and provides high spatial resolution with full brain coverage. T1 (longitudinal) relaxation time is the time constant that determines the speed at which excited protons return to equilibrium. It is a measure of the time that it takes for protons to rotate to realign themselves with the external magnetic field. The contrast created in the image is determined, in particular, by the difference in the T1 relaxation times between fat and water.

T1w is the ideal contrast for visualizing the anatomy (the cortex, subcortical white matter, basal ganglia, etc.) and for identifying and obtaining the volume of regions of interest in the cortex (Heim et al., 2017).

MRI scanners generate different types of T1w images, depending on the type of pulse sequence selected. The different sequences differ on how the excitation of protons is achieved: using only radio-frequency pulses, we can obtain spin-echo T1w images and combining a radio frequency pulse with a gradient reversal, we can generate gradient-echo T1w images (Carpenter & Williams, 1999). Additionally, the use of preparation pulses prior to the excitation pulses, for example a magnetization pulse, may influence the gray-to-white matter contrast. This is the case for T1w magnetisation-prepared rapid gradient-echo (MPRAGE) sequence. Many cortical atlases and studies that quantify the voxels of specific ROIs use T1w, specifically MPRAGE, as it provides better contrast than other T1w sequences (Brant-Zawadzki, Gillan, & Nitz, 1992).

In this project, we used T1w images for the atlas construction and volumetric assessment of the cortical areas (details in chapters 2 and 3)

## 2.2. Myelin imaging and magnetization transfer imaging

Magnetization transfer imaging method is a technique sensitive to the exchange of magnetization between the pool of free protons and the pool of protons bound to macromolecules (Symms et al., 2004). The amount of this exchange can be quantified by calculating the index of magnetisation transfer or magnetization transfer ratio (MTR). In the brain tissue, bound protons are primarily associated to macromolecules like myelin lipids and proteins. Therefore, the concentration and integrity of myelin is reflected by MTR values. In other words, MTR is a semi-quantitative measure of the amount of magnetization transfer that occurs between the bound-to-myelin and mobile water molecules in a given region (Griauzde & Srinivasan, 2018). The values of MTR decrease when pathological changes occur in different disorders (e.g. demyelination). MTR has been used as a sensitive method to mark pathological changes in neurological conditions, such as schizophrenia, dementia, brain injury, multiple sclerosis and tumors (Symms et al., 2004).

In this project, we used MTR images to assess and compare the content of myelin in various areas of the cortex marked by our atlas (details in chapter 3).

## 2.3. Image registration

To study the anatomy of the normal and pathological brain, the changes that it experiences over time, and to compare the brain of multiple subjects, MRI brain scans must be aligned to a common coordinate system where the aligned anatomical structures can be visualized for comparison (Spalletta, Piras, & Gili, 2018). This "alignment process" is called image registration and its key role is to form a correspondence between a subject image and a target image that will make possible to compare regions of interest and surface shapes. The correspondence is established between two brain scans by the process of deformation or warping. In this deformation field, the geometrical differences in the images (in two homologous points of the image) are captured by a mathematical transformation. The application of the mathematical transformation to one image (image to be registered) is what allows the registration to the other image (target image) (Spalletta et al., 2018).

There are two main types of registration applied to T1w images:

1) **surface-based registration**: its goal is the registration of the cerebral cortex. It uses a triangular mesh representation of cortical surfaces produced by specific software: BrainSuite

(http://brainsuite.org), FreeSurfer (https://surfer.nmr.mgh.harvard.edu/), Brain-Visa (http://brainvisa.info/) (Spalletta et al., 2018).

2) **volume-based registration**: it registers the full brain volumes (cortical and subcortical structures). It is an extensively used technique mostly based on the voxel intensity information of T1w images, which may apply different transformations (rigid or affine) at a global level (linear registration) or a local level (non-linear registration using Advanced Normalization Tools -ANTS-) (Maintz & Viergever, 1998).

In our project, we used a volume-based registration (ANTS) method to assess the utility of our atlas (in standard/stereotactic T1w MNI ICBM space: target image) applied to the scans of ten healthy participants (T1w scans registered to the target standard T1w) (details in Chapter 3).

## 2.4. Stereotactic space

A stereotactic coordinate system (space) is a common reference space (sometimes also called the standard space) that allows the identification of a specific point in that space by using an external, three-dimensional frame of reference based on a coordinate system with three axes: y (anterior-to-posterior), x (right-to-left) and z (superior-to-inferior). In the field of neurosurgery, a standardized coordinate frame was used early on to guide blind stereotaxic neurosurgical procedures (e.g., thalamotomy, pallidotomy). Nowadays, this coordinate system is widely used by the neuroscientific community interested in the comparison and interpretation of their brain imaging results to retain relevant 3D information (Evans, Janke, Collins, & Baillet, 2012).

The first attempt to use a common coordinate orientation to facilitate surgical exploration was made by Jean Talairach, and it was later updated as a brain-based proportional stereotaxic atlas created by Talairach and Tournoux based on a series of sagittal and coronal sections of the two hemispheres of a single post-mortem 60-year-old brain specimen. From the sagittal and coronal anatomical images, the transverse representations in the atlas were created (Petrides, 2012); (Evans et al., 2012). The coordinate system was constructed from a point of origin located on the midline at the superior and anterior aspect of the anterior commissure (AC) and 3 axes running from it: 1) the y-axis, represented by a line joining the point of origin with the inferior aspect of the posterior commissure (PC) (AC-PC line), with the positive values in the anterior direction; 2) the x-axis, extending medio-laterally from the y-axis, with positive values to the right; and 3) the z-axis, perpendicular to the y-axis, with positive values in the superior direction (Petrides, 2012).

Unfortunately, this first Talairach and Tournoux coordinate space did not consider left-right hemispheric asymmetries and did not represent the anatomical variabilities of a large population, as it was created based on a single brain specimen (Evans et al., 2012). Also, this method divided the whole brain into 12 volumes and uses 7 scaling factors (3 anterior-to-posterior, 2 left-to-right and 2 superior-to-inferior) to minimize anatomical variability within the coordinate system. This approach works well for deep structures targeted by surgery, but variability at the cortical level is still present (Petrides, 2012).

The unfolding of MRI processing technology has improved the transformation of a subject's neuroimaging data to stereotactic space. At the Montreal Neurological Institute (MNI), a series of average stereotactic MRI templates were created, to facilitate the registration of individual MRI scans to the template. One of the first templates was the Average250-T1-Model, which was constructed as a voxel-by-voxel intensity average of 250 subjects. It represents the average brain shape of a large population with low anatomical variability for the deep brain structures (they remain clearly visible) and higher residual variability for the cortical structures, not accounted for by the linear transformation used in this model (i.e. the cortex appeared blurred) (Petrides, 2012). This approach used a manual alignment method.

The template that followed the Average250-T1 was the Average305-T1-Model, which took advantage of new software developed to optimize the transformation parameters in an automatic fashion, by maximizing the cross-correlation of intensities. This template was generated based on the original 250 scans, with the addition of 55 extra scans, resulting in the Average305-T1-Model, which had the advantage of being created using a fully automatic, robust registration procedure, avoiding intra and inter-rater variability (Petrides, 2012).

Another template, the Colin27-T1-Model was created from a single subject with the aim of improving the structural definition of the cortex, as well as deep brain structures (Petrides, 2012). As it was done based on a single brain, the anatomical variations were not considered. After non-linear registration to the average 305Model, it has been adapted as a stereotactic template (Evans et al., 2012).

Most recently, the International Consortium for Brain Mapping (ICBM) proposed the construction of an average brain template using images with higher resolution (i.e. 1 $mm^3$ isotropic voxels) and multiple MRI contrasts (T2-weighted -T2w- and Proton Density -PDw- in addition to T1w). This effort led to the construction of the Montreal Neurological Institute (MNI) 152 Model (Mazziotta

et al., 2001). The high-resolution brain images of 152 young adults with 1.5 Tesla T1w, T2w, and PDw pulse sequences increased the contrast of the template and allowed for the creation of image intensity and tissue type maps (gray matter, wight matter, and cerebral spinal fluid) (Evans et al., 2012). Over the years, this model has benefitted from improvements in non-linear registration techniques (now done using multiple hierarchical iterations) that increase the detail of the cortical surfaces, despite being an area of high anatomical variability (Petrides, 2012). The MNI-ICBM2009c is the most recent version of the MNI-ICBM152 brain average. It represents the average anatomy of the population and is left-right symmetric, allowing the interpretation of possible individual variabilities and providing better alignment of cerebral structures using non-linear registration (A. Manera, Dadar, Fonov, & Collins, 2019).

In our project, we used the T1w MNI-ICBM2009c brain average template to create our atlas.

## 2.5. MRI study designs for assessing the cortex

When considering MRI studies of the cerebral cortex, different approaches have been used:

1- *Ex vivo* MRI studies to develop optimal MRI acquisition protocols: these studies explore the increase in image resolution (highest possible resolution equivalent to smallest voxel size) as well as signal-to-noise ratio and assess relaxation times in various cortical areas. This approach uses human post-mortem samples for investigation, allowing long scanning sessions without motion, reaching very high resolution, which is central to decreasing partial volume effects and providing maximum accurate delineation of brain anatomical structures (Sengupta et al., 2018). The neuroscientific community is interested in using ultra-high field MRI scanners to achieve microscopic resolution, forging the path of MRI-based histology *ex vivo* and, eventually, *in vivo* (Sengupta et al., 2018). These attempts are currently possible *ex vivo*, using research scanners (e.g. 9.4T scanners with tailored manufactured coils) not yet available for *in vivo* imaging nor clinical settings (Sengupta et al., 2018). Furthermore, reaching the necessary microscopic resolution to unveil the microscopic cortical layered structure *in vivo* (without partial volume effects) is currently not possible (Lifshits et al., 2018). *Ex vivo* studies have reached 60-micron resolution, while *in vivo* resolution has reached around 280-microns (S. Eickhoff et al., 2005).

2- *Ex vivo* MRI and histology studies on the same specimens: This type of approach is used as a validation technique to parcellate the cerebral cortex on the *ex vivo* MRI following cytoarchitectonic boundaries (e.g. Brodmann areas) that can only be captured by histology (Ding

et al., 2016); (Frankó, Insausti, Artacho-Pérula, Insausti, & Chavoix, 2014). It allows us to establish the correspondence between the microstructural/histological boundaries and the macroscopic anatomical landmarks visible on the MRI. This technique can be applied for specific areas of the brain, for example medial temporal lobe cortices (Frankó et al., 2014), or for the whole cerebral cortex, which is a much more complex and time-consuming enterprise, hence performed in a very reduced number of specimens, or even only a single brain specimen (Ding et al., 2016).

3- *In vivo* MRI scans based on previous *ex vivo* MRI-histological validated data: This approach is based on the previous one. It relies on the validation of the *ex vivo* MRI images against histological findings of the same area, correlated with the macroscopic MRI anatomical landmarks (S. Eickhoff et al., 2005); (Fatterpekar et al., 2002). Then, these landmarks can be described on the three anatomical planes (coronal, axial and sagittal) and used to construct the guidelines/steps of MRI segmentation protocols to be applied on newly collected *in vivo* MRI data (Pruessner et al., 2002), (Frankó et al., 2014).

Some researchers have used data from multiple *ex vivo* subjects to construct probabilistic maps on an average whole brain template that could be subsequently registered to *in vivo* MRI scans (Augustinack, van der Kouwe, & Fischl, 2013). However, the use of this approach for *in vivo* MRI segmentation is still somewhat limited by the low number of *ex vivo* samples, which do not account for all the possible individual anatomical variabilities.

4- *In vivo* MRI followed by *ex vivo* MRI-histology post-autopsy: This approach employs MRI data obtained during the life of a person, followed by *ex vivo* images of the same subject after autopsy. One example of this approach has been used on hippocampi imaging, where the authors concluded that this comparison helped to identify certain macro- and microstructural features *in vivo* (Wisse et al., 2017). Although this approach can provide detailed information regarding tissue properties, it is confounded by the time lapse between the last *in vivo* image and first post-mortem *ex vivo* image and subsequent histology, since several biological and pathological changes may arise during the elapsed time.

5- *In vivo* MRI scans with (ultra)high resolution: these scans can be used to divide the cortex into specific regions according to anatomical or functional classifications based exclusively on *in vivo* structural or functional MRI scans (Destrieux, Fischl, Dale, & Halgren, 2010); (Yeo et al., 2011). These divisions can be used to build cortical atlases on MRI, which allow the analysis of patient scans, following a specific approach. For example, a cortical atlas with a pure macro-anatomical

approach makes it possible to investigate whether the cortical volumes of the upper, middle, and lower frontal gyrus are more affected than the volumes of the parietal gyri in frontotemporal dementia (Manera, Dadar et al. 2019); (A. L. Manera, Dadar, Collins, & Ducharme, 2019).

In our project, we used approaches 3 and 5, constructing some of the parcels of our atlas using MRI protocols previously validated with histology, and combining them with an anatomical division of the neocortex (details in chapter 2).

## 3. Brain atlases

As stated in the introduction, brain atlases aim to divide the organ into a number of regions that have common and meaningful structural and/or functional characteristics and constitute a fundamental tool to quantify changes in healthy and pathological states.

In the previous section, we presented the different study designs that employ MRI to study the human cortex. Some of those studies have led to the creation of *ex vivo* and *in vivo* atlases, using histological or MRI criteria or both, and extrapolating histology (*ex vivo*) to *in vivo* MRI images. To simplify the review of the numerous available human cortical atlases, we have grouped them as belonging to one of three main categories: 1) those that are exclusively based on histology, 2) those based on MR images, and finally 3) those that combine MRI and histology information (Table 00 at the end of this section summarises the main characteristics, references, and web-links of each atlas).

### 3.1. Histological atlases

Histological atlases provide cellular level resolution of the cerebral substructures through microscopic examination of the brain tissue. The brain parcellation is carried out according to precise cellular structural differences of brain regions based on histochemical markers or staining (e.g. Nissl staining) (Hess, Hinz, Keliris, & Boehm-Sturm, 2018).

Starting in the early 20$^{th}$ century, when *in vivo* brain imaging methods did not exist, histology was the most accurate tool used to explore differences in the human cortex. To this day, histology is considered as the gold standard tool to study and classify/parcellate the brain cortex (Hess et al., 2018); (K. Amunts & Zilles, 2015). The most used cytoarchitecture-based human brain atlas has been Brodmann's cortical map (Brodmann & Gary, 2006). However, other (less popular)

histological atlases exist (Triarhou, 2007), and one of them has received recent attention and translation to MRI: the Von-Economo Koskina's atlas.

***Brodmann's atlas***

In this atlas, the original cortical parcellation was done exclusively based on the microscopic characteristics of the cell bodies that span the thickness of the cortex, from the pial surface to the white matter junction. Brodmann based his classification on the distribution, density, shape, and size of the Nissl-stained cell bodies, delineating in total 43 areas, each of which was given a number, the sequence of which did not consider cytoarchitectural similarities (Triarhou, 2007); (Zilles & Amunts, 2010).

Brodmann's approach was based on the idea (not proven at the time) that each cortical area with cellular structural similarities fulfilled a specific function within a larger network (Amunts Zilles 2015). This concept of structure-function interdependence has passed the test of time, since despite the numerous advances and multiplication of cortical classification systems, Brodmann's areas have reached the fMRI era and are still extensively used (K. Amunts & Zilles, 2015); (Ding et al., 2016).

Additionally, Brodmann incorporated phylogenetic concepts into his work, not only by performing a developmental division of the cortex into homogenetic (equivalent to what we call today isocortex) and heterogenetic (equivalent to the allocortex), but also by parcellation of the cortex of other primates and mammals. He assigned the same number to each cortical parcel of the different species, based on shared anatomical location and cytoarchitectonic characteristics. If the characteristics of a given parcel were missing in one species, then that number was not used, which is the reason behind certain numerical gaps in his numeral naming system. For example, he found three areas (14 to 16) in the insular cortex of the Cercopithecus, and four (13 to 16) in the insular cortex on the Lemuridae, but he could not find homologous areas in the human cortex. As a result, Broadmann's human atlas has parcels that go from 1 to 52, but the areas with numbers 12 to 16 and 48 to 51 are not present (Zilles & Amunts, 2010); (Guillery, 2000); (Brodmann & Gary, 2006).

Although Brodmann's atlas has been extensively used, it is not without neuroanatomical limitations, the main one being that it does not distinguish areas on the gyral surface (crown of the gyrus) from cortical areas in the sulcal depths (Triarhou, 2007), which makes Brodmann system particularly noninformative in regions with high gyral and sulcal folding (Zilles & Amunts, 2010); (K. Amunts & Zilles, 2015); (Van Essen, Glasser, Dierker, Harwell, & Coalson, 2012).

***Von-Economo-Koskinas' atlas***

This parcellation was more than just a more detailed version of Brodmann's Atlas (von Economo & Koskinas, 1925). Although also based on cytoarchitecture using Nissl staining, it introduced a fundamental methodological change: blocks of tissue were cut perpendicular to the surface of the gyri along the whole cortex. This way of cutting the cortex prevented the oblique cuts of most of the gyri that inevitably occur when the entire hemisphere is cut. This technique allowed for more accurate quantification of the cortical thickness and better appreciation of the layered pattern.

This atlas had a system of letters and numbers to identify each area, giving the cortex of the lobes a Roman capital, followed by the designation of the gyri using a calligraphic capital, and a Latin or Greek subscript to indicate the microscopic features (Triarhou, 2007). These areas were then classified into 54 fundamental cytoarchitectonic areas with 76 variants and 107 modifications (35 frontal, 13 limbic superior and 14 inferior or hippocampal, 6 insular, 18 parietal, 7 occipital, and 14 temporal). This atlas also considered the developmental differences of the homogenetic and heterogenetic cortices already adopted by Brodmann, but added another consideration to the isocortex, describing it as homotypic, when all six layers were easy to identify, or heterotypic when they were more difficult to depict. From this developmental perspective, the atlas comprises 22 allogenetic or allocortical areas and the isogenetic or isocortex includes 63 'homotypic' and 22 'heterotypic' cortical areas (Triarhou, 2007). Finally, Von-Economo and Koskinas estimated the volume of the cerebral cortex at 555 $cm^3$ and its surface area at 200 000 $mm^2$ (Triarhou, 2007).

Given the more accurate evaluation of the cortical thickness and the more detailed description of a higher number of cortical areas, this atlas has been recently translated into an MRI version (Scholtens, de Reus, de Lange, Schmidt, & van den Heuvel, 2018), since the neuroscientific community finds it useful for the assessment of functional MRI studies and cortical thickness studies (Scholtens, de Reus, & van den Heuvel, 2015).

***Vogt-Vogt atlas***

In close collaboration with Brodmann, who was focused on the cytoarchitectonic map of the cerebral cortex, the myeloarchitectonic mapping of the human neocortex was performed by Cécile Vogt and Oskar Vogt (known as the Vogt-Vogt school) also in an attempt to explain the structural and functional relations in the brain (R. Nieuwenhuys, 2013).

Using the Nissl stain for neuronal cell bodies and the Weigert stain and its variants for myelinated nerve fibres, Oskar and Cécile Vogt conducted their analysis on serial sections of human and animal brains (R. Nieuwenhuys, 2013).

Vogt developed a general concept of the myeloarchitectonic organization of the neocortex where the myelinated fibers were considered as morphological as well as functional units. Considering the cytoarchitectonic layered cortical structure, the myelinated fibres' location was described in corresponding myeloarchitectonic layers. Anticipating the confusion between these two layered classifications, the Roman numerals were used for the cytoarchitectonic layers, while the myeloarchitectonic layer designations used Arabic numbers. The boundaries between the myeloarchitectonic areas were defined by differences in the number and density of the tangential and radial myelinated fibres. The authors delineated 185 distinct cortical areas: 70 frontal, 6 insular, 30 parietal, 19 occipital, and 60 temporal areas. One of the achievements of Vogt's school was the very detailed description and differentiation of myeloarchitectonic variations by types (description presented in the 1.2.2. section) (R. Nieuwenhuys, 2013).

To date, the Vogt-Vogt myeloarchitectonic cortical parcellation has not been translated to standard MRI templates (R. Nieuwenhuys, 2013). However, MRI signal at the cortical level is mainly determined by myelin: up to 84% of the signal variation is related to heterogeneous myelin distribution, and only 9 to 16% of the MRI signal is driven by the density and number of cellular bodies (K. Amunts & Zilles, 2015). As a consequence, new MRI myelin density maps are emerging and can be used as a stand-alone map or in combination with cytoarchitectonic and macro-anatomical atlases (K. Amunts & Zilles, 2015).

## 3.2. Neuroimaging atlases

### 3.2.1. Volumetric atlases

#### *Talairach Daemon (TD) atlas*

This atlas allowed the inferential translation of the two-dimensional Brodmann atlas to the three-dimensional Talairach atlas (Lancaster et al., 1997).The atlas operates as a forward-transformed method, using the x-y-z coordinate system to indicate the locations within the brain to retrieve the corresponding label. The Talairach atlas uses a hierarchical approach to segment the different regions: level 1 includes the cerebrum, cerebellum, brainstem, and its component structures of level 2, the lobes, followed by level 3, the gyri, level 4, the tissue type, and level 5, the

cytoarchitecture, which represents the Broadman parcellation in the Talairach coordinate system (Lancaster et al., 1997). For example, the Talairach coordinates −40, −25, −54 correspond to the left cerebrum, parietal lobe, post-central gyrus, gray matter, Brodmann area 3 (Maldjian, Laurienti, Kraft, & Burdette, 2003).

The labeling of the various regions that composed the atlas was done within a 3D image at a resolution of 1 $mm^3$ with x-y-z dimensions of 170 × 200 × 210 $mm^3$, using Alice™ and Dipstation™ image processing software from the Hayden Image Processing Group (Boulder, CO). The segmentation and labels of 160 regions are available as a web-based application. More recently, the TD data has been included in the Pickatlas (Maldjian et al., 2003) to probe fMRI data using the atlas labels as ROIs for the functional analysis, and it has been incorporated as an extension to Statistical Parametric Mapping (SPM, University College London, Queen Square Institute of Neurology) tool (Evans et al., 2012).

***MNI atlases***

Various atlases have been developed at the MNI (Evans et al., 2012). Starting in 1996, regional probability maps were generated from the MNI152 database. The approach used was the manual segmentation of 142 regions in a single subject, and subsequent non-linear registration of the multiple subjects' MRI scans to this single subject, so that the labels of the 142 regions could be mapped to each individual scan. Finally, the multiple subjects' masks were linearly mapped to the MNI 152 template, generating regional probability maps for each area (Evans et al., 2012).

The most recent MNI atlas, **the Cerebrum Atlas (CerebrA)** (A. L. Manera, Dadar, Fonov, & Collins, 2020), is a probabilistic atlas created by non-linear registration of the "Mindboggle-101" average template to the symmetric version of the MNI-ICBM 2009c average template. This non-linear transformation allowed at the same time to resample the labels of "Mindboggle-101" to MNI-ICBM 2009c template. Manual correction of the right hemisphere's labels was performed to address inaccuracies in labels' registration. For example, several labels of the regions whose boundaries are determined by a different tissue type (e.g. lateral ventricles, fourth ventricle) had inaccuracies that were corrected by using an intensity threshold for tissue differentiation.

Subsequently, the visually assessed and corrected labels were carried over to the left hemisphere. In total, 51 cortical and subcortical labels from each hemisphere were delineated. All labels were

corrected using the interactive software package 'Display', part of the MINC Tool Kit (https://github.com/BIC-MNI) developed at the McConnell Brain Imaging Center of the MNI.

***The Harvard-Oxford atlas*** (Caviness, Meyer, Makris, & Kennedy, 1996)

This work presented a neocortical parcellation on MRI based on a topography-based system instead of a structural or functional approach. According to this system, boundaries of different regions were identified by specific anatomical landmarks or specified single points (42 in total) along the anterior-to-posterior axis and the longitudinal course of the fissures. These points, either as conjunctions of two fissures or diverse anatomical structures, determined the anterior and posterior boundaries of a given region and the longitudinal course of the fissure specified their medial and lateral boundaries.

The study was performed on 1.5T sagittal images of T2-weighted sequences and coronal 3D Tl-w spoiled gradient echo images of 15 normal adults. For each brain MRI scan, the coordinate system was defined according to Talairach & Tournoux. For all the coronal images, gray-white matter segmentation was performed. This subdivision was based on natural gray matter boundaries determined by differences of signal intensities on the T1-w images. Drawing parcellation lines at points specified by the course of boundary determining fissures, the neocortex was subdivided into 48 parcellation units (PU) per hemisphere. This parcellation was based only on the visible anatomical gyral landmarks within lobes. To guide the process of parcellation, four instructional tables were constructed: 1) the table of coordinate points where the position of anatomical landmarks specified the anterior and posterior boundaries of the PUs; 2) the table of anterior posterior PU limits indicating the coronal image planes that formed the anterior and posterior boundaries for each PU; 3) the table of fissures that indicated the lateral and medial boundaries of the PU; and 4) the PUs' tables that listed all PUs present on each coronal image plane in the order they aligned from the medial to the lateral, to the inferior surface of the hemisphere. As each PU was color coded and represented by voxels, the volumetric analysis was performed calculating the corresponding number of voxels.

This atlas only focused on the cortical parcellation of the neocortex and did not consider other cortices (e.g. paleocortex, archicortex), nor all other gray matter structures. The process of segmentation was exclusively topographic as it was based on the configuration of specific neocortical fissures of individual subjects and did not consider either interindividual variabilities, or cytoarchitectonic boundaries.

*Disease-specific atlases*

One of the disadvantages of atlases based on MRI scans of healthy adults is that they do not adapt well to the analysis of specific pathologies that affect the brain structure of specific areas (Evans et al., 2012). As a result, some groups have worked on creation of atlases that are applicable to specific diseases.

One of these atlases is the **Brain MRI atlas of a Parkinson's disease cohort** (Xiao et al., 2017) which is a population-averaged atlas derived from the 3T MRI scans of 25 Parkinson disease (PD) patients. The authors used a multimodal protocol that collected a T1w MPRAGE sequence along with a multi-echo FLASH MRI protocol. The brain masks were generated after the MPRAGE images were registered to the FLASH images. Each subject's data was nonlinearly registered to the common MNI ICBM152 stereotactic space. The derived averaged atlas contains tissue segmentations (including the cortex) and subcortical structures in one image with different resolutions: $1\times1\times1$ $mm^3$ and $0.5\times0.5\times0.5$ $mm^3$, which cover the entire brain, and a $0.3\times0.3\times0.3$ $mm^3$ template comprising only the subcortical nuclei. The final version of the Atlas also contains a histology-based digitized atlas of 123 subcortical anatomical structures from nonlinearly registered histological data of the Gilles-Mallar atlas (Chakravarty, Bertrand, Hodge, Sadikot, & Collins, 2006).

The advantage of this atlas is that it represents a disease-specific anatomy applicable to PD patients. At the same time, the use of multiple MRI contrasts provides better visualisation and anatomical detail of cortical and subcortical structures.

### 3.2.2. Surface-based atlases

The use of surface based cortical atlases, constructed on the inflated-spherical surface of the brain, has been considered as a tool that significantly simplifies the analysis of a highly folded structure, such as the cortex. Also, this surface approach would better present the interindividual differences of the cortex, compared to the volume approaches. This has led to generation of multiple protocols, which have been incorporated into brain software processing tools/packages developed by different centers: the FreeSurfer software suite created by the Laboratory of Computational Neuroimaging of Harvard University: https://surfer.nmr.mgh.harvard.edu; FSL created by the Analysis Group of Functional MRI Brain (FMRIB) of the University of Oxford:

https://fsl.fmrib.ox.ac.uk/fsl/fslwiki; and the SPM toolbox developed at the Institute of Neurology of University College London: https://www.fil.ion.ucl.ac.uk/spm/.

***Desikan–Killiany (DK) atlas***

The main goal of the authors was to create a probabilistic atlas with an automated anatomical cortex labeling system that could be applied to a large variety of subjects. The atlas was constructed on 40 T1w MPRAGE scans of healthy participants including young, middle-aged, and elderly adults, as well as patients with Alzheimer's disease. The atlas includes 34 regions of interest in each hemisphere, defined on MRI images using the guidance of previously published anatomical brain descriptions (Duvernoy, 1999), (Ono, Kubik, & Abernathey, 1990) and consultation with two experts: Drs Douglas Rosene and Thomas Kemper. The regions were separated using a curvature based (gyral-based) approach: each region was manually segmented starting at the deepest point of a sulcus and ending at the deepest point of the adjacent sulcus, incorporating the corresponding gyrus in between (Desikan et al., 2006).

Once the 40 scans were manually labeled, they were co-registered (using Freesurfer tools) to the spherical surface representation of the brain. They were then probabilistically assigned a neuroanatomical region to every point on the cortical surface. This procedure produces a spherical surface-based coordinate system adapted to the folding pattern of each individual subject. As a result, this approach increases the precision across subjects.

The strength of this work was that the labels defined on the inflated surface improved the delineation accuracy of the manual cortical ROIs, as it allowed for simultaneous visualization in both the sulci and the gyri.

The approach used in the generation of this atlas expanded its practical value beyond the normal healthy population, since it included cases with a large range of atrophy in a group of subjects with neurodegenerative pathology.

***Destrieux atlas***

This atlas shares some characteristics with the previously described atlas: it also provides a fully automated parcellation of the human cortex on T1w MRI scans, using a standard gyral and sulcal division, following rules of standard anatomical nomenclature, based on Duvernoy's anatomical brain description (Duvernoy, 1999), (Destrieux et al., 2010). It translates the parcellation of the gyri and sulci to the inflated surface of the cortex.

The main differences of this atlas reside in the population chosen for its construction (in this case all healthy young adults) and in the geometrical threshold taken to define a surface as sulcal vs. gyral.

On T1w MPRAGE scans of 24 healthy participants the entire cortex was divided into sulcal and gyral cortices based on the values of average convexity and mean curvature obtained with FreeSurfer software. An empirical threshold (expressed as a percentage of the mean convexity) checked by visualization of the crown of the gyrus on the convexity of the brain was employed. There were some areas where the mean curvature threshold was not used as a factor to label the cortex: namely, the insular lobe and opercula due to their deep localisation in the lateral sulcus. Also, for the cingulate gyrus, additional sub-parcellation was based on cytoarchitectonic criteria described by Vogt (Vogt, Vogt, & Laureys, 2006). The cortical surface was divided in frontal, temporal, parietal, occipital, insular and limbic lobes, and 74 labels per hemisphere were delineated.

***Yeo 2011 functional atlas***

This work studies the organization and properties of large-scale networks in the human brain (Yeo et al., 2011).

This atlas is based on hierarchical clustering analysis of resting-state fMRI of 1000 healthy young adults and presents the analysis of the whole brain and the more detailed analysis of the primary visual area, the middle temporal area complex, the lateral intraparietal area, and the frontal eye fields together with the functional connectivity of the parietal and prefrontal association cortices. Supplementary fMRI data (N=20) helped to get information regarding passive tasks at the time of resting-state fMRI and during visual stimulation. Also, cytoarchitectonic areas were defined using probabilistic histological maps in FreeSurfer surface space.

The atlas provides a parcellation of the cerebral cortex into 7 networks and 17 sub-networks of functionally coupled regions. The 7-network analysis showed clear discrimination of the motor and sensory cortex (validated by histological maps resampled to the fMRI data) from the association cortex. The association networks were consistent with previously described networks (i.e. the dorsal and ventral attention, the frontoparietal control, and the default mode network). The 17 sub-networks that emerged from the hierarchical analysis showed some expected networks (e.g. parahippocampal-retrosplenial-lateral parietal network) and some unexpected: subnetworks within

the visual and motor cortices that did not respect areal boundaries, but align with topographic organization. All MRI scans were processed in FreeSurfer surface space where each subject's cortical surface was inflated into a sphere.

The advantage of this work was the inclusion of a large number of subjects that represent a wide range of variability of the overall population. Compared with 3D volumetric registration, the spherical representation of the cortex in this work generated more accurate anatomical details and has improved cytoarchitectonic and functional correspondences.

***Mindboggle-101 atlas***

The principal goal of this study was to create a new automatic-initiated cortex labeling protocol based on robust anatomical landmarks, which would be easy to correct by a rater, generating a large, publicly available dataset of 101 corrected cortical masks (Klein & Tourville, 2012).

T1w brain MRI scans of 101 healthy participants were considered as a part of a multi-modal acquisition (T2-weighted, diffusion-weighted scans). The scans that comprise the Mindboggle-101 data set come from different sources: 20 test-retest participants from the OASIS data, the 21 test-retest participants from the Multi-Modal Reproducibility Resource data, two additional subjects scanned using the same protocol in 3T and 7T scanners, 20 participants from the Nathan Kline Institute Test-Retest data, 12 subjects of the Human Language Network, the Colin Holmes 27 template, two identical twins, and one brain imaging colleague (A. Manera et al., 2019).

Cortical surfaces were constructed using FreeSurfer's standard image processing pipeline with subsequent application of the DK cortical parcellation protocol. To reduce the number of errors during automatic labeling and to make the region definitions more consistent and better suited to FreeSurfer's classifier algorithm, the DK protocol was modified: the frontal and temporal poles and the banks of the superior temporal sulcus were eliminated. Boundaries of the major regions were determined (as in other atlases that follow sulci and gyral divisions) considering the cortical surface curvature features: the sulcal fundi (deepest point of sulci) and gyral crowns (superficial convexity of the gyrus).

As a result, two variants of cortical labeling protocols were created: DKT31 (consisting of 31 cortical regions per hemisphere) and DKT25 (consisting of 25 regions per hemisphere, where subregions of a larger gyral formation were considered as a unit).

This new surface-based cortical labeling protocol considered the large variety of cortical topographies. Here, the cortical regions were defined more consistently, and the region boundaries were well suited to FreeSurfer's classifier algorithm. The advantage of this atlas is in the initial automatization of the labeling process, minimising the number of errors at the time of labeling.

***The Human Connectome Project: Multi Modal Parcellation***

The cortex parcellation scheme proposed in this study aimed to identify the boundaries across different properties of the cerebral cortex: cytoarchitecture, functions, connectivity, and topography (Glasser et al., 2016). This parcellation protocol used MRI data from the Human Connectome Project (HCP) (Van Essen et al., 2013) an initiative of Washington University, University of Minnesota, and Oxford University (WU-Minn HCP) to generate the map of human brain connectivity and function in a large population of 1200 healthy adults. The main goal of the HCP was to allow comparisons between brain circuits, behavior, and genetics. The neuroimaging data of the project consists of structural MRI (T1w and T2w scans), resting-state fMRI, task fMRI, diffusion MRI and MEG/EEG (resting-state and task-evoked) imaging modalities. Processing of the brain scans included: volumetric registration to MNI152 space using FSL's linear FLIRT tool for good alignment of subcortical structures and FreeSurfer for cortical surface alignment. To analyze genetic and environmental influences, the project was conducted using adult mono- and dizygotic twins and their non-twin siblings as subjects (Glasser et al., 2016).

The Multi-Modal Parcellation version 1.0 (MMP 1.0) used surface-based registrations of multimodal (T1w and T2w structural, diffusion-weighted MRI, task-based, and resting state-based fMRI) images of 449 healthy young adults from the Human Connectome Project. The semi-automated neuroanatomical approach in this work was the basis for a fully automated algorithmic approach: a machine-learning classifier (Glasser et al., 2016).

The atlas includes 180 cortical areas (97 new areas and 83 previously reported areas) the limits of which are marked by sharp changes in cortical architecture, function, connectivity, and/or topography that were identified on inflated and flattened cortical surfaces in both left and right hemispheres. The machine-learning classifier detected the presence of 96.6% of the cortical areas in new subjects, correctly replicating the group parcellation.

The advantage of this study was that it offered the opportunity to find results in the same cortical area using several different neuroimaging modalities, with improved neuroanatomical precision.

## 3.3. Histological and MRI atlases

***Medial temporal cortices atlas by Insausti et al.***

This protocol was designed to conduct a volumetric analysis of temporal lobe cortical structures on MRI scans, with histologic validation that justify the selection of the boundaries on MRI (Insausti et al., 1998).

The MRI scans (tilted coronal 1.5T 3D MPRAGE) of 52 healthy participants were used to perform an entorhinal, perirhinal, and associated temporopolar cortices segmentation. The participants were separated in two groups according to age (a younger and an older group). For the histology analysis, 44 autopsy brains, cut in 50 μm thick coronal sections, were stained with thionine. To match and align the structures on MRI scans with the corresponding histological boundaries, the brain coronal sections, as well as the MR images were oriented perpendicular to the line drawn between the anterior and posterior commissures. The anatomical landmarks of cortices were drawn manually on coronal MR images and were correlated with the cytoarchitectonic borders considering the cytoarchitectural subdivision by Brodmann. For each of the cortical regions, the detailed description of the major anatomic landmarks on MRI was presented in a series of steps (Insausti et al., 1998).

This transposition of cytoarchitectonic boundaries onto the MRI makes it possible to delineate the anatomical structures in future in vivo studies without direct histological analysis of the same specimen. Another prominent finding of the volumetric analysis during this study showed that the age-related cortex reduction can be found in all temporal lobe cortical areas.

***Medial temporal lobe parcellation by Pruessner et al.***

This work focused on a pure MRI segmentation protocol to volumetrically measure the hippocampus, amygdala (Pruessner et al., 2000) and temporopolar, perirhinal, entorhinal, and parahippocampal cortex (Pruessner et al., 2002) within the medial temporal lobe.

The scans of 40 young healthy normal subjects from the International Consortium of Brain Mapping initiative were used. In this protocol, the T1, T2, and PD-weighted MRI scans were acquired with 1 mm slice thickness. All images underwent linear stereotaxic transformation to the MNI space. The volumetric analysis was done using the software package 'Display' (from the Brain Imaging Centre of the MNI) that allows simultaneous viewing of the various sequences (T1w, T2w, and PDw) and precise editing in the coronal, sagittal and axial planes. Manual

segmentation of the ROIs on MRI was performed according to macroscopic borders and anatomical landmarks identified from histological data described by the protocol of Insausti et al. (Insausti et al., 1998). For the parahippocampal cortex, the anatomical delineation was adapted from work of Van Hoesen (Pruessner et al., 2002). The labeling description in this protocol was performed in the coronal view, where the anterior, posterior, medial and lateral borders were indicated. The fronto-temporal junction and collateral sulcus were identified prior to the individual cortices' segmentations.

If anatomical landmarks were only partly identified on MRI and/or the delineation was difficult, a more arbitrary approach, although also based on anatomical landmarks, was employed. For example, a structure such as the tail of the hippocampus was discriminated from the adjacent crux of the fornix by a horizontal line tangential to the superior border of the quadrigeminal cistern. Also, to exclude partial volume in each segmented ROI, one or two rows of voxels were excluded from the perimeter of the structure.

The advantage of this protocol resides in the use of a three-dimensional and multi-contrast (multi-sequence) MRI dataset, allowing simultaneous visualisation of the three planes to segment the brain structures of interest more precisely. As the boundaries and neuroanatomical landmarks were adapted from a combined MRI-histological study, this protocol can serve as reference for other works using temporal lobe structures delineation on MRI. The possibility to cross-validate the coronal description of the boundaries with the sagittal and horizontal planes in standard space is an advantage in cases where it is impossible to determine the borders exclusively in the coronal plane. The 1 $mm^3$ isotropic voxels of the images allowed an accurate examination and precise manual segmentation of the ROIs. At the same time, this work presented volumes of the described structures that can be used in further comparative analysis.

***The JuBrain Cytoarchitectonic atlas: probabilistic cytoarchitectonic atlas***

Being a part of the Human Brain Project/Neuroinformatics research, this study had as a goal to develop an SPM software package to correlate the micro-structural data (under the form of three-dimensional probabilistic cytoarchitectonic maps) with structural (T1w MNI anatomical template) and functional MRI scans of the human cerebral cortex (S. B. Eickhoff et al., 2005).

The process of generating probabilistic cytoarchitectonic maps consisted of the following steps: 1) T1w MRI scans of 10 human post-mortem brains were acquired prior to the histological

processing; 2) whole brain sectioning and staining; 3) cytoarchitectonic definition of the borders of each area; 4) 3D reconstruction of the histological volume; 5) transfer of each area to the corresponding sections of the 3D volume; 6) registration of the reconstructed brains to the T1w MNI single subject template; 7) superimposition of the homologous areas in template space; and 8) probabilistic map formation for each area (S. B. Eickhoff et al., 2005).

The definition of the cytoarchitectonic borders (step 3) were based on previously published probabilistic individual post-mortem cytoarchitectonic maps of motor, somatosensory, visual, auditory, and language related brain regions (S. B. Eickhoff et al., 2005), (Caspers, Eickhoff, Zilles, & Amunts, 2013). The procedure was based on digitalization of coronal, sagittal and horizontal sections, 20 μm thick, stained for cell bodies, which were subsequently transformed into gray level index images (GLI) where the pixels reflect the volume fraction of cell bodies. The differences in cytoarchitecture were described by differences in GLI values between adjacent cortical regions, assessed through a mathematical similarity function: the Mahalanobis distance function. Once each individual brain had its own cytoarchitectural map, they were non-linearly registered to the MNI space, which determined overlap of adjacent areas given by interindividual differences. Hence, to produce a combined single map, with no overlaps between adjacent areas, the assignment of each voxel to a particular cortical area was determined by the frequency (the highest probability) with which a cytoarchitectonic area was observed at the voxel specific position in the template (Caspers et al., 2013).

This cytoarchitectonic probabilistic atlas has three main advantages: first, it recognises and captures the interindividual variabilities at the cytoarchitectonic level; second, it is not manually performed by an observer, being then independent of observer bias, since the limits are mathematically calculated using GLI values and a similarity function; and third, it is fully operational in the SPM toolbox, which also allows the integrated analysis of structural and functional MRI data, generating anatomical labeling of functional activated clusters (S. B. Eickhoff et al., 2005), (Caspers et al., 2013). The main disadvantage of this atlas is that it does not cover the full extent of the cortex, just the specific areas mentioned before (motor, somatosensory, visual, auditory and language areas) (S. B. Eickhoff et al., 2005).

Additionally, these probabilistic maps are also available in the software packages FSL and AFNI and can also be found in the JuBrain Web tool: https://www.fz-juelich.de/JuBrain/EN/_node.html (Caspers et al., 2013).

***BigBrain: an ultrahigh-resolution 3D human brain model***

The main goal of this work was to create a new three-dimensional reference human brain model close to cellular resolution that would provide the basis for addressing histological stereotaxic and topological positions in the full brain (K. Amunts et al., 2013).

7400 coronal sections of 20-μm thickness were produced from a single 65-year-old subject brain, with subsequent Nissl staining and digitalisation. The 3D reconstruction of the whole brain was done using the series of histological block images aligned together. All sections were registered to the MRI and nonlinearly registered together section-to-section. This procedure allowed the reconstruction of the whole brain as a contiguous volume, adding the 3D reconstructed axial and sagittal planes to the original coronal plane images. The boundaries between brain areas were defined by differences in the laminar pattern comparing the coronal and the horizontal virtual planes at the identical location (K. Amunts et al., 2013).

The advantage of the 3D analysis proposed by the BigBrain model, over 2D histological sections and light-microscope images (Caspers et al., 2013), is that this protocol enables the recognition of borders either between primary cortical areas, or between higher associative cortical areas throughout the whole cortical ribbon, as opposed to specific cytoarchitectonic areas, such as the ones presented by the probabilistic atlas of Eickhoff et al. At the same time, this brain model gives information regarding histological cortical thickness and density of body cells per column that can be registered and correlated to in vivo MRI scans resampled to MNI space.

***Atlas of the human brain by Mai J.K., Majtanik M. and Paxinos G.***

This Atlas describes the macroscopic and microscopic organisation of the human brain in detail, paying particular attention to morphological and topographical aspects (J. K. Mai, Majtanik, & Paxinos, 2015).

The fourth edition of this atlas combined two previous works. The first one: "Three Atlases of the Brain in the Head", which presented three ex vivo brains in situ (inside the head) in 1-cm thick sections. The sections were displayed either as photographs or color-coded drawings on three planes (either sagittal, axial, or coronal). These three specimens were scanned (in a low field MRI scanner) prior to being sectioned to be correlated with MRI scans of a living volunteer. The in vivo T1w and T2w MRI scans of the healthy young volunteer were presented at each atlas level and used to show the careful matching of the corresponding anatomical slices. Also, at each level, a

computed tomography (CT) scan of the ex vivo specimen sections were included, to portray the main arterial vessels and the segments of extracranial arteries.

This atlas approach, using the brain inside the skull prevented possible deformations of the brain tissue and allowed the use of extracerebral landmarks, such as bones, nerves, and vessels. The ex vivo images of the brain contributed to a better orientation in the 3D space and helped to recognize the topography of structures.

The second work included in the fourth edition of the atlas is "Myelo- and Cytoarchitectonic Atlas of the Human Brain in Stereotaxic (MNI) Space". This part of the atlas comprises the presentation of 100-μm thickness slices cut from the 1-cm slices. It includes 50 slices stained for cytoarchitecture (Nissl stain) and 99 stained for myeloarchitecture (fiber-stained sections). The high-resolution photographs which were taken during the sectioning process helped to reconstruct the 3D model of the brains.

The cell-stained plates underwent a cortical delineation by gyri and sulci and the regions were color-coded based on Brodman's, Von Economo, and Koskinas cortical areas. All photographs of the cell- and fiber-stained sections underwent 3D reconstruction and transformation to be registered to the MNI-space, creating a bridge between microscopic and macroscopic delineations. Moreover, this atlas includes fMRI and tractography. The novelty of the fourth edition was that the Nissl plates were presented as series of histological sections and that the cortical cytoarchitectonic ribbon was unfolded and presented linearly. This linear representation of the cortex enables a more accurate delineation of cortical areas and overcomes the major limitation of the classical Brodmann mapping, which did not address the cytoarchitectonic boundaries in the deep sulci surfaces. Nevertheless, the atlas has as a disadvantage that it does not address interindividual variabilities, in the way probabilistic atlases do.

***The Allen Institute Brain Atlas***

This atlas could be considered as a modern histology atlas (Ding et al., 2016) where the authors created an interactive online digital human brain atlas linking high resolution histology, chemoarchitecture, and neuroimaging performed in a very high field MRI scanner.

The atlas was performed on a single young subject brain (34-year-old female). Before histological analysis, high-resolution structural images of both hemispheres were acquired in a 7T MRI scanner, along with 3T diffusion images.

For histochemical analysis, the cerebral hemispheres along with the connected brainstem and cerebellum were divided into eight 2-cm-thick slabs, which were subsequently sectioned coronally into 50-μm-thick sections. From a total of 2716 brain sections, 679 (200-mm sampling interval) were stained for Nissl; 338 (400-mm sampling interval) for immunohistochemistry of non-phosphorylated neurofilament proteins, which stain pyramidal cells, and 339 (400-mm sampling interval) were immunostained for the calcium-binding protein parvalbumin, which stain non-pyramidal cells. All histologically stained sections were digitalised and processed in one single hemispheric image with cellular resolution using a custom-designed large-format microscopy system. From all Nissl-stained sections, 106 were selected to perform anatomical delineation of 862 cortical and subcortical structures including 117 white matter tracts (Ding et al., 2016).

To correlate the cytoarchitectural cortical parcellation based on histology with the gyral and sulcal parcellation based on neuroimaging, the Nissl-based anatomical landmarks (modified Brodmann's areas) were transposed and matched into the corresponding planes of the MRI.

The atlas is comprehensively annotated using a unified hierarchical structural ontology with color codes, acronyms, and full names. The structures on each Nissl-digital image were delineated as polygons which were interactively linked to the hierarchical ontology system and their colors codes, showing the relation between the structures and their affiliation to the similar color group.

The innovation of this atlas is that it proposed the whole brain description with multimodal high-resolution MRI and a histological exploration that used multiple stains in the same tissue, discriminating pyramidal and non-pyramidal cells. This made it possible to identify the boundaries between areas, to localise and delineate white matter tracts and to identify some novel brain subregions, not included in the original Brodmann's classification. Also, the introduction of hierarchical structural ontology helped to browse and search delineated structure polygons interactively. The correlation of histological delineation with the matching MRI scan allows the identification of the cytoarchitectonic structure on MRI data.

**Table 00:** Examples of Human Brain atlases using different modalities

| Human Brain Atlases | Modalities | Characteristics | Selected references | Links |
|---|---|---|---|---|
| **HISTOLOGICAL ATLASES** | | | | |
| **Brodmann's cortical map (1909)** | Cytoarchitecture | Single-brain (hemisphere) study<br>Nissl staining.<br>47 cortical areas.<br>Definition of borders based on visual inspection | Book:<br>Brodmann K., and Gary L. J., 2006 | https://www.google.ca/books/edition/Brodmann_s/-9p6cgAACAAJ?hl=en |
| **von Economo and Koskinas (1925)** | Cytoarchitecture | Several healthy brain samples.<br>Nissl staining.<br>107 annotated areas.<br>More detailed cytoarchitectonic parcellation | Book:<br>von Economo and Koskinas, 1925.<br>Article:<br>Triarhou, 2007 | https://www.google.ca/books/edition/Die_Cytoarchitektonik_Der_Hirnrinde_Der/mbcuywEACAAJ?hl=en<br>https://pubmed.ncbi.nlm.nih.gov/17534132/ |
| **Vogt and Vogt** | Myeloarchitecture | 185 cortical areas based on differences in the pattern of myelinated axons | Article:<br>Nieuwenhuys, 2013 | https://pubmed.ncbi.nlm.nih.gov/23076375/ |
| **VOXEL-BASED NEUROIMAGING ATLASES** | | | | |
| **Talairach Daemon** | MRI (T1w) | 38 coronal plates.<br>Cortical parcellation following Brodmann's areas.<br>65 annotated structures | Article:<br>Lancaster et al., 1997 | http://www.talairach.org/<br>https://pubmed.ncbi.nlm.nih.gov/20408222/ |
| **The Cerebrum Atlas (CerebrA)** | MRI (T1w) | Manual correction of the Mindboggle-101 atlas registered to the symmetric version of MNI-ICBM 2009c<br>51 cortical and subcortical labels for each hemisphere. | Article:<br>Manera et al., 2020. | https://github.com/templateflow/tpl-MNI152NLin2009cSym<br>http://nist.mni.mcgill.ca/?p=904 |

| | | | | |
|---|---|---|---|---|
| | | | | https://pubmed.ncbi.nlm.nih.gov/32669554/ |
| **Harvard-Oxford Atlas** | MRI (T1w; T2w) | 48 parcellation units per hemisphere.<br>Topography- based parcellation system | Article:<br>Caviness et al., 1996 | https://pubmed.ncbi.nlm.nih.gov/23961985/ |
| **DISEASE-SPECIFIC ATLASES** | | | | |
| **Brain MRI atlas of Parkinson's disease** | MRI (T1w, T2w, phase, and an R2 map) | Probabilistic maps for WM, GM, CSF.<br>123 anatomical structures.<br>Segmented labels for eight subcortical and midbrain nuclei. | Article:<br>Xiao Y. et al., 2017 | http://nist.mni.mcgill.ca/?p=1209<br>https://pubmed.ncbi.nlm.nih.gov/28491942/ |
| **SURFACE-BASED NEUROIMAGING ATLASES** | | | | |
| **Desikan–Killiany (DK)** | MRI (T1w) | Manual segmentation using a curvature based (gyral-based) approach.<br>34 gyral-based regions of interest. | Article:<br>Desikan et al., 2006 | https://surfer.nmr.mgh.harvard.edu/fswiki/CorticalParcellation<br>https://pubmed.ncbi.nlm.nih.gov/16530430/ |
| **Destrieux** | MRI (T1w) | 74 labels per hemisphere.<br>Parcellation based on sulcal depth yielding precise automated definition of cortical gyri and sulci. | Article:<br>Destrieux et al., 2010 | https://surfer.nmr.mgh.harvard.edu/fswiki/CorticalParcellation<br>https://pubmed.ncbi.nlm.nih.gov/20547229/ |
| **Yeo 2011 functional atlas** | MRI (resting-state fMRI and T1w) | 7 networks<br>17 sub-networks | Article:<br>Yeo et al., 2011 | https://surfer.nmr.mgh.harvard.edu/fswiki/CorticalParcellation_Yeo2011<br>https://pubmed.ncbi.nlm.nih.gov/21653723/ |
| **Mindboggle-101 atlas** | MRI (T1w) | Manual labeling following the DK protocol. | Article: | https://mindboggle.info/data.html |

| | | | | |
|---|---|---|---|---|
| | | DKT31 (31 cortical regions per hemisphere).<br>DKT25 (25 regions per hemisphere) | Klein A, Tourville J., 2012 | https://mindboggle.readthedocs.io/en/latest/labels.html<br>https://pubmed.ncbi.nlm.nih.gov/23227001/ |
| **Human Connectome Project (HCP)** | MRI (T1w, T2w, DWI, fMRI) MEG, EEG. | 180 cortical areas.<br>In vivo multimodal atlas. | Article:<br>Van Essen DC, Smith et al., 2013 | https://www.humanconnectome.org/<br>https://pubmed.ncbi.nlm.nih.gov/23684880/ |
| **HISTOLOGICAL-MRI ATLASES** | | | | |
| **Insausti et al.** | Cytoarchitecture<br>MRI (T1w) | Medial temporal lobe cortices: entorhinal, perirhinal and temporopolar. | Article:<br>Insausti et al., 1998 | https://pubmed.ncbi.nlm.nih.gov/9576651/ |
| **Pruessner et al.** | MRI (T1w, T2w, PDw) | Hippocampus, amygdala, temporopolar, perirhinal, entorhinal and parahippocampal cortices. | Articles:<br>Pruessner et al., 2000;<br>Pruessner et al., 2002 | https://pubmed.ncbi.nlm.nih.gov/10769253/<br>https://pubmed.ncbi.nlm.nih.gov/12427684/ |
| **BigBrain** | Cytoarchitecture<br>MRI (T1w) | 3D reconstruction of 7400 histological coronal sections of a single brain. | Article:<br>Amunts K, Lepage et al., 2013 | https://bigbrain.loris.ca/main.php |
| **JuBrain** | Cytoarchitecture<br>MRI (T1w, fMRI) | Probabilistic maps of motor, somatosensory, visual, auditory and language related cortices | Articles:<br>Eickhoff et al., 2005<br>Caspers et al., 2013 | https://jubrain.fz-juelich.de/apps/cytoviewer2/cytoviewer-maintenance.php#%23mitte<br>https://pubmed.ncbi.nlm.nih.gov/15850749/<br>https://pubmed.ncbi.nlm.nih.gov/23571419/ |

| | | | | |
|---|---|---|---|---|
| **Atlas of the human brain by Mai J.K., Majtanik M. and Paxinos G.** | Cytoarchitecture<br>Myeloarchitecture<br>MRI (T1w, T2w)<br>CT | Brodmann areas<br>Von Economo and Koskinas<br>Gyral anatomical parcellation. | Book:<br>Mai et al., 2016 | https://books.google.ca/books?id=4S01CgAAQBAJ&lpg=PP1&ots=iT8OO8wgWE&lr&pg=PP1#v=onepage&q&f=false |
| **The Allen institute Brain Atlas** | Cytoarchitecture and immunohistochemistry<br>MRI (T1w, DWI) | Cortical areas modified from Brodmann and von Economo.<br>Gyral anatomical parcellation. | Article:<br>Ding et al, 2016 | http://human.brain-map.org/<br>https://pubmed.ncbi.nlm.nih.gov/27418273/ |

# CHAPTER 2: The PaleoArchiNeo (PAN) Human Brain Atlas

The work presented in this chapter has been submitted as: Zhernovaia M, Dadar M, Mahmoud S, Zeighami Y, Maranzano, J. *The PaleoArchiNeo (PAN) Human Brain Atlas: a dataset on a standard neuroanatomical MRI template following a phylogenetic approach*, to the journal Data in Brief (accepted for publication pending minor revisions regarding data accessibility).
This article is formatted as a data article which means that it describes a dataset without providing conclusions or interpretive insights. Our data article presents the description of the atlas (which represents the dataset of interest) and how it was generated. Preliminary results regarding the application of the atlas are presented in Chapter 3.


**Abstract**

Cortical atlases constitute a consistent division of the human cortex into areas that have common structural as well as meaningful and distinctive functional characteristics. They constitute a fundamental tool to study and quantify changes in healthy and pathological states. Historically, the most widely used atlases follow the cytoarchitecture described by Brodmann and/or the myeloarchitectonic characteristics described by Vogt-Vogt. These histological approaches have since been combined to the standard anatomical nomenclature of gyri and sulci, referring to the corresponding cytoarchitectonic area(s) present in a gyrus, when applicable or necessary (e.g. area 4 of Brodmann in the pre-central gyrus). More recently, common functional features depicted by resting state functional MRI have guided the division of the cortex in functional regions of interest. However, to date, there are no human MRI atlases that divide the cortex considering the common evolutionary changes experienced by the mammalian cortex.

Hence, the present dataset describes a voxel-based atlas that divides the human cortex into five regions of interest (ROIs) following a phylogenetic approach: 1- archicortex, 2- paleocortex, 3- peri-archicortex, 4- proisocortex, 5- neocortex, and thirty neocortical sub-ROIs that follow the gyral *Terminologia Anatomica*. The masks of the ROIs and sub-ROIs were segmented on the T1-weighted MNI ICBM 152 2009c symmetric average brain MRI model, following the MRI anatomical landmarks that have been previously described, correlated, and validated with histology by other groups.

We present the PaleoArchiNeo (PAN) Human Brain Atlas.

**Key words**

Atlas; Human Brain; Cerebral Cortex; MRI; Phylogenetic; Paleocortex; Archicortex; Neocortex

**Specifications Table**

| | |
|---|---|
| **Subject** | Neuroanatomy |
| **Specific subject area** | Cortical human brain atlas |
| **Type of data** | Cortical masks of the regions of interest that constitute the PAN-Human Brain Atlas, manually segmented on the T1-weighted MNI ICBM 152 2009c symmetric average brain MRI model |
| **How data were acquired** | 1.5T Magnetic resonance imaging |
| **Data format** | MINC2 and NIFTI |
| **Parameters for data collection** | Non-applicable |
| **Description of data collection** | Non-applicable |
| **Data source location** | McGill University, Montreal, Quebec, Canada.<br>Université du Québec à Trois-Rivières, Trois-Rivières, Quebec, Canada. |
| **Data accessibility** | The dataset is made available in two repositories:<br>1) MNI ICBM 152 2009c symmetric average brain MRI model http://nist.mni.mcgill.ca/?p=904<br>2) The final masks of each ROI of the PAN-Human Brain Atlas https://gin.g-node.org/Maryna.Zhernovaia/MRI/ |
| **Related research article** | Non-applicable |

**Value of the Data**

- To date, there has been no MRI human brain atlas following a phylogenetic approach. Some groups have developed detailed segmentations of the hippocampus and amygdale. Others have described the segmentation of the piriform cortex. However, the different parcels were never grouped together considering their common evolutionary origin. Our atlas has combined all previous MRI cortical knowledge and translated it in a common single atlas that considers phylogeny as the classification factor.
- This atlas will serve all the neuroscientific research community who works using MRI to quantify changes in the human brain, either in healthy populations or in pathological states. The atlas masks are voxel-based and constructed in an average-open-source T1-weighted MRI template, which allows the registration of single individual MRI scans and translation of the masks to fit each individual scan.
- This atlas will enhance the study of changes in areas of cortex with common characteristics regarding their evolutionary development. Neuroscientists and neurologists interested in neurodegenerative diseases could explore whether pathological changes detectable by MRI (e.g. cortical volume, magnetization transfer values, etc.) preferentially affect areas of cortex with a given evolutionary chronology.

**Data Description**

The dataset that constitutes this atlas is a collection of voxel-based cortical regions of interests (ROIs) segmented in the International Consortium for Brain Mapping of the Montreal Neurological Institute (MNI-ICBM) 2009c average template [1].

The cortical ROIs were segmented following a phylogenetic approach that divides the cerebral cortex into five main regions of interest (ROIs): 1-archicortex, 2-paleocortex, 3-peri-archicortex 4-pro-isocortex, 5-neocortex [2]. Additionally, we divided the neocortex into thirty sub-regions of interest (sub-ROIs) following an anatomical gyri division, which include various sensory modalities, as well as motor and association cortices: 5.1.temporopolar, 5.2.post-central, 5.3.pre-central, 5.4.pericalcarine, 5.5.superior temporal, 5.6.middle temporal, 5.7.precuneus, 5.8.insular, 5.9.inferior parietal, 5.10.caudal anterior cingulate, 5.11.posterior cingulate, 5.12.lingual,

5.13.caudal middle frontal, 5.14.cuneus, 5.15.fusiform, 5.16.inferior temporal, 5.17.isthmus cingulate, 5.18.lateral occipital, 5.19.lateral orbitofrontal, 5.20.medial orbitofrontal, 5.21.paracentral, 5.22.pars opercularis, 5.23.pars orbitalis, 5.24.pars triangularis, 5.25.rostral anterior cingulate, 5.26.rostral middle frontal ,5.27. superior frontal, 5.28. superior parietal, 5.29. supramarginal, and 5.30. transverse temporal cortex [1].

During mammalian evolution, the archi- and paleocortex, also grouped under the name of allocortex (allocortex=cortex with a number of layers different than six), precede the development of the larger neocortex. The archicortex is represented by the hippocampus, formed by the Cornus Ammonis areas, dentate gyrus and subiculum, presubiculum, parasubiculum, entorhinal cortex, retrosplenial cortex, and a cortical band in the cingulate gyrus [2]. The paleocortex, which shares common characteristics with the three-layered general cortex of reptiles [3], is composed of the prepiriform and piriform regions, as well as part of the amygdala, the olfactory cortex, the olfactory bulb, retrobulbar (anterior olfactory nucleus), olfactory tubercle and septal region [2].

The much younger human neocortex, also called isocortex, is characterised by the six cellular layers depicted by classical Nissl stains. It comprises the sensory areas (primary somatosensory, auditory and visual areas, secondary and tertiary sensory areas), multimodal association areas, and motor areas: primary and non-primary [2].

Finally, the areas of cortices between archi- paleo- and neocortex show a gradual transformation of cytoarchitecture, which allow the classification of these transitional areas as periarchicortex, adjacent to the archicortex, and proisocortex, between the periarchicortex and neocortex [4], see Figure 1.

**Figure 1:** Schematic representation of the subdivisions of the human cerebral cortex into paleocortex (in green), archicortex (in red), periarchicortex (in blue), proisocortex (in purple) and neocortex (in yellow). Modified from Zilles and Amunts, 2012.

*Note: we created a modified sagittal representation of the MRI template by fusing various parasagittal slices that allowed the delineation of the five ROIs in the same figure.*

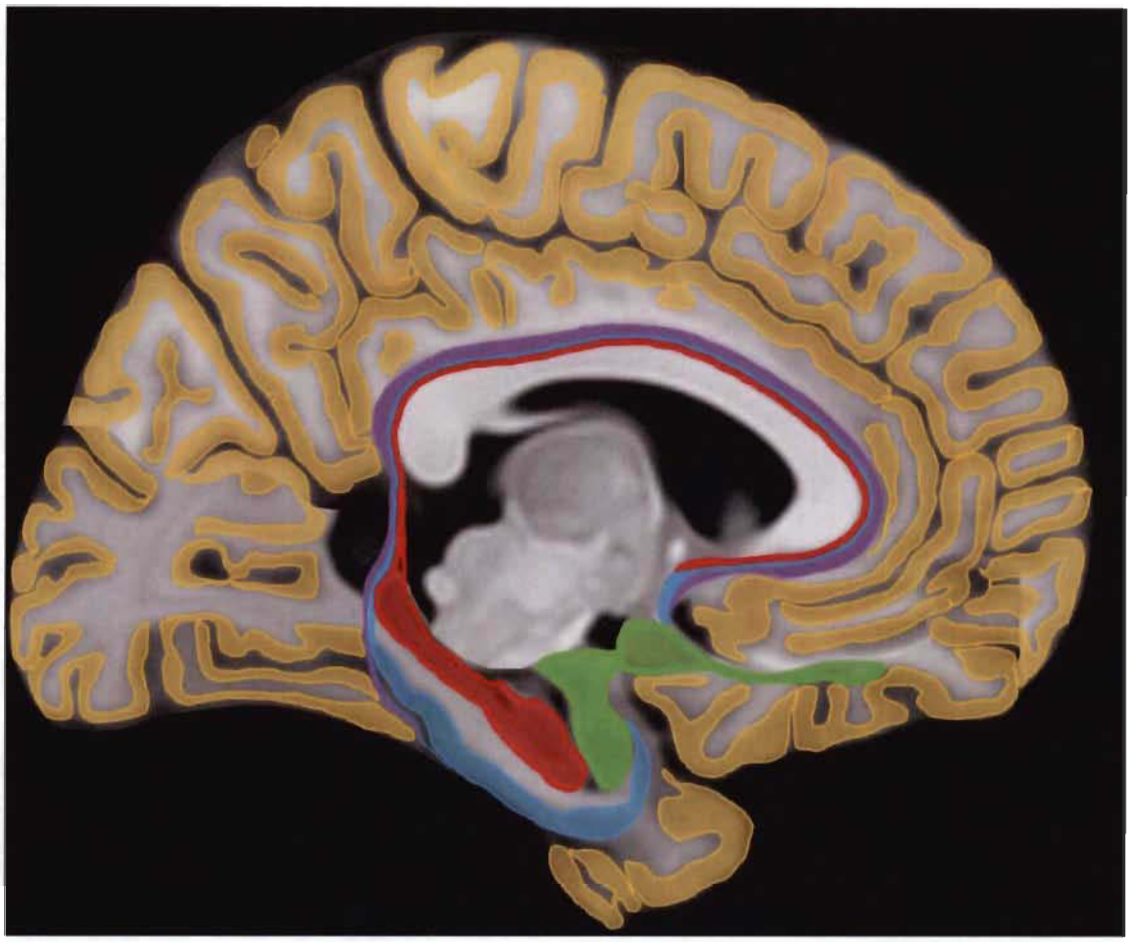

**Experimental Design, Materials and Methods**

The atlas was done following previously described MRI protocols [5, 6, 7, 8, 9, 10, 11, 12, 13, 14] that provide a detailed description of the MRI anatomical landmarks, correlated with histological studies, necessary to segment the parcels included within each or our ROIs.

We performed these segmentations manually on the MNI-ICBM 2009c average template, which is the most recent version of the MNI-ICBM152 brain average [1] and provides a higher level of anatomical details. The MNI-ICBM152 non-linear model has two main advantages: 1) it was created from a large number of subjects; hence it represents the average anatomy of the population and is unbiased, unlike single-subject models [13], and 2) the left-right symmetric version enables interpretation of asymmetries that might be found in an analysis.

The sub-ROIs of the neocortical parcels (other than the temporopolar region, which was done fully manually) were based on the manual correction of the CerebrA atlas [1], by removing voxels of

partial volume with the subarachnoid space cerebrospinal fluid (CSF) and juxtacortical white matter. We chose CerebrA because it was also created on the MNI-ICBM152 2009c average template, providing the perfect complement to our manually created labels.

Both, fully manual segmentations and correction of the CerebrA masks were done using the interactive software package 'Display', part of the MINC Tool Kit (https://github.com/BIC-MNI) developed at the McConnell Brain Imaging Center of the Montreal Neurological Institute. This program allows simultaneous viewing and segmentation in the coronal, sagittal and axial planes. Each window allows zooming in and out and a painting tool allows marking voxels with a given color (label/mask number). All the labels created for the atlas consist of cortical gray matter only. Note that this atlas, even if it follows a phylogenetic approach, was created to be used in images of the human brain exclusively and not in other species, since all MRI cortical regions are based on human anatomical landmarks correlated with human cytoarchitectonic characteristics of the specific cortices.

**Anatomical MRI landmarks of each segmented ROI**

***ROI 1. Archicortex manual segmentation:*** we included the hippocampus, presubiculum, subiculum, parasubiculum, and entorhinal cortices. We did not attempt the segmentation of the pre- and supra-commissural (indusium griseum) hippocampal portions, because the resolution of the MRI brain template precluded its conclusive segmentation.

The hippocampus is traditionally divided into a posterior portion called the hippocampal tail (HT), a more anterior part called the hippocampal body (HB) and the most anterior, the hippocampal head (HH) [5].

The hippocampus included the dentate gyrus, the cornu ammonis (CA) regions, the part of the fasciolar gyrus that is adjacent to the CA regions. The white matter portions traditionally included in the MRI segmentation of the hippocampus [5] were excluded, because our atlas aims to exclusively include cortical gray matter. Hence, the fimbria, located at the superomedial level of the HB and the alveus, which separates the HH from the amygdala at the supero-rostral level, were not included in our atlas.

The uncal recess of the inferior horn of the lateral ventricle (LV) and alveus served as landmarks for definition of the supero-anterior border of hippocampus [7]. The most posterior part of the HT

was selected in the coronal plane, where an ovoid mass of gray matter (GM) is first visible inferio-medial to the trigone of the LV [5, 13]. The lateral border of HB was identified by the inferior horn of the LV or the caudally adjacent WM: see Figure 2.

**Figure 2:** MRI anatomical landmarks of the hippocampal limits.

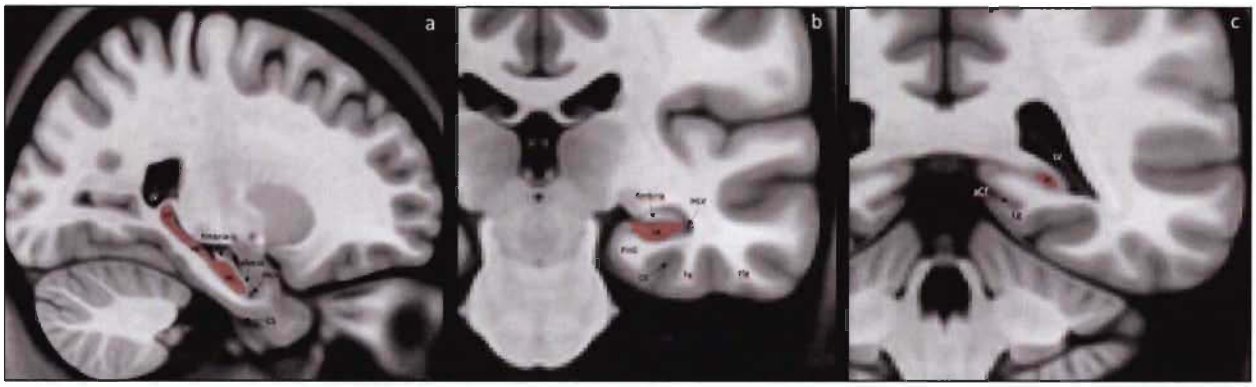


(a) Sagittal section with visualization of anterior, posterior, superior and inferior borders of the hippocampus; delineation of the fimbria that is excluded from the segmentation. (b) Coronal sections of the medial temporal lobe (MTL) with posterior end of the hippocampal body and (c) posterior end of the hippocampal tail.
IHLV= inferior horn of lateral ventriculus; LV= lateral ventriculus; CS= collateral sulcus; PHG= parahippocampal gyrus; Fg= fusiform gyrus; Itg= inferior temporal gyrus; aCf= anterior calcarine fissure; Lg= lingual gyrus; HB= hippocampal body; HT= hippocampal tail.

The entorhinal cortex (EC) was segmented by selecting the coronal view and moving from anterior to posterior, from the posterior limit of the temporopolar cortex (described in section ROI.5.1.) towards the point of transition between the HH and HB (intralimbicus gyrus) [14]. The collateral sulcus (CS) was localised prior to the segmentation and served as a guide for the subsequent localisation of the first and last slices to be labelled [15]. If the CS was spreading rostral to the limen insulae (Li), then the anterior border of the EC was taken 2 mm posterior to the first appearance of the Li (grey matter); if the CS was shorter than the Li, then the anterior border was the rostral end of the CS [11, 12]. The posterior limit was determined 1 mm posterior to the last slice containing the apex of the intralimbic gyrus [7,14]. The superio-medial limit of the EC was given by the sulcus semiannularis (ssa), and the lateral limit was always the midpoint of the medial bank of the CS: see Figure 3.

**Figure 3:** MRI anatomical landmarks of the entorhinal cortex limits.

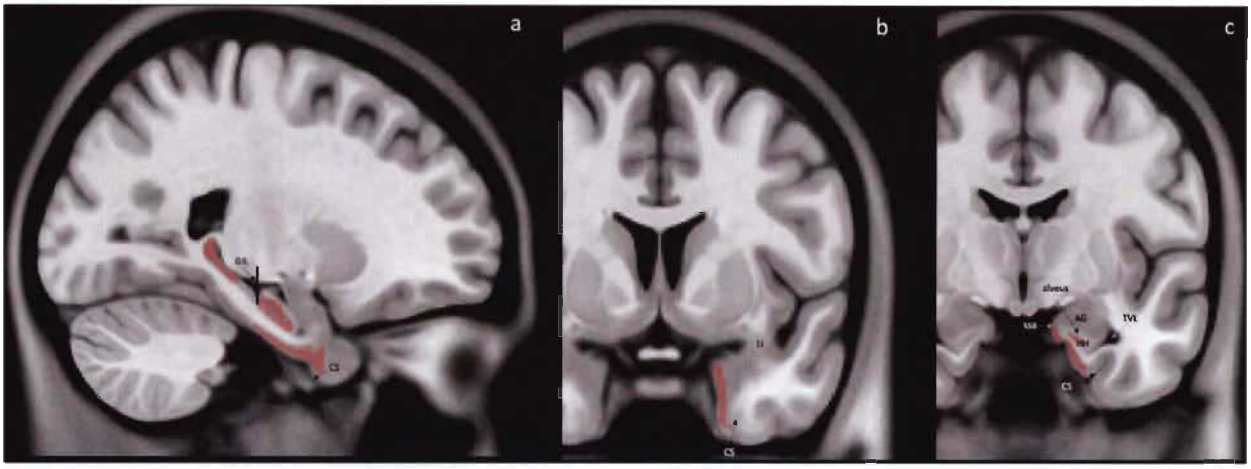


(a) Sagittal section with visualization of anterior and posterior borders of EC. (b) Coronal view of the MTL at the level of the limen insulae and (c) at the level of uncal notch is visible. The perpendicular line indicates the apex of the gyrus intralimbicus.

Li= limen insulae GIL= gyrus intralimbicus; CS= collateral sulcus; AG= amygdala; ssa= sulcus semiannularis; TVL= temporal horn of lateral ventricle.

***ROI 2. Paleocortex manual segmentation:***

The resolution of our MRI precluded the identification of the olfactory bulb and the distinction of the periamygdaloid cortex from the amygdaloid nuclei. Having a close relationship, both anatomically and functionally, the PirC and periamygdaloid cortex together with all the gray matter of the amygdala (AG) were considered in our atlas as a complex [6].

The most rostral portion was marked at the level of the Li (white matter-Li in the coronal view) [5, 7].

Superomedially, the fundus of the sulcus semiannularis separates PirC from EC and superolateraly, the fundus of the entorhinal sulcus (es) separates the paleocortex from the substantia innominata. From the level of the Li posteriorly to the rostral end of the AG, the mediolateral extent of the piriform paleocortex occupies progressively more of the surface, (between 30% and 80% of that distance) [6], see Figure 4.

**Figure 4:** MRI anatomical landmarks of the paleocortex limits.

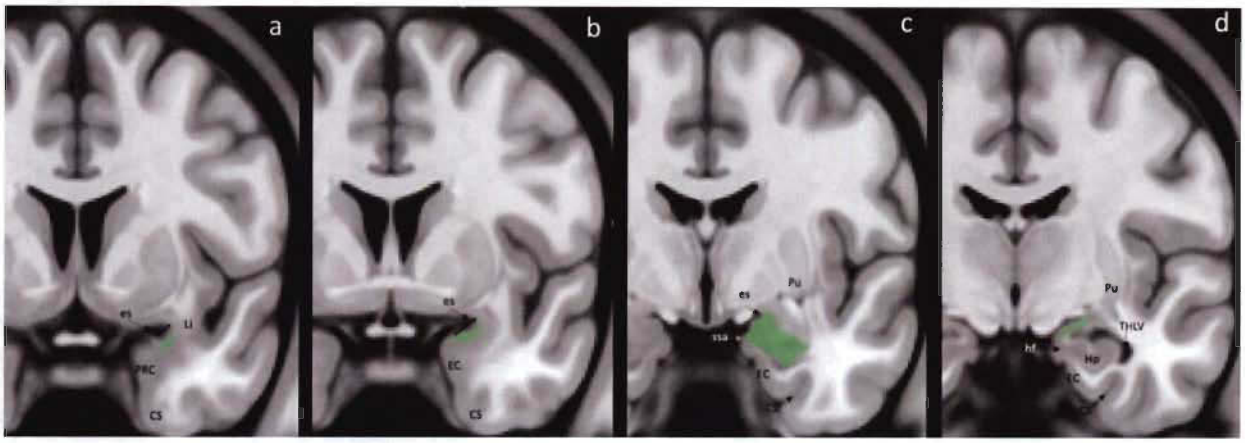


(a) Coronal section of the most rostral part of paleocortex at the level of limen insulae. At this level, piriform-cortical amygdala extends 30% of the distance between the entorhinal sulcus to the most convex point of the medial temporal cortex. (b) The piriform-cortical amygdala occupies 50% of the distance of the entorhinal sulcus – MTL convexity. (c) Coronal section at the level where the piriform-cortical amygdala extends from the entorhinal sulcus down to the sulcus semiannularis. (d) The most caudal section of paleocortex appearance at the level of hippocampal fissure opening.

es= entorhinal sulcus; Li= limen insulae; PRC= perirhinal cortex; CS= collateral sulcus; EC= entorhinal cortex; ssa= sulcus semiannularis; Pu= putamen; hf= hippocampal fissure; Hp= hippocampus; THLV= temporal horn of lateral. ventriculus.

Laterally, the gray matter of the AG transitions towards the ventral putamen. The posterior end was defined in the coronal plane at the level of the opening of the hippocampal fissure and at the point where grey matter appears superior to the alveus and laterally to the HH [5].

***ROI 3. Peri-archicortex manual segmentation:***

We included the perirhinal and parahippocampal cortices [14]. The anterior segment of CS served for determining the rostral limit of PeriAC [15]. If the CS stretched further anterior than the Li, then anterior tip of the CS was considered as the anterior border of the PeriAC [7]. If the CS was shorter or as long as the Li, then the border was determined to be 1 mm anterior to it. The most posterior part of parahippocampal cortex was defined as the first posterior slice where the pulvinar was no longer visible [7], and it was funnel-shaped, progressively merging with the retrosplenial region. The medial edge stretched from the shoulder of the medial bank of the CS to the medial apex of the parahippocampal gyrus. Laterally, the boundary between the perirhinal and

inferotemporal cortices was at the lateral edge of the CS, but if two CS were present, then we considered the fundus of the more lateral CS [11, 12], see Figure 5.

**Figure 5:** MRI anatomical landmarks of the Peri-archicortex limits.

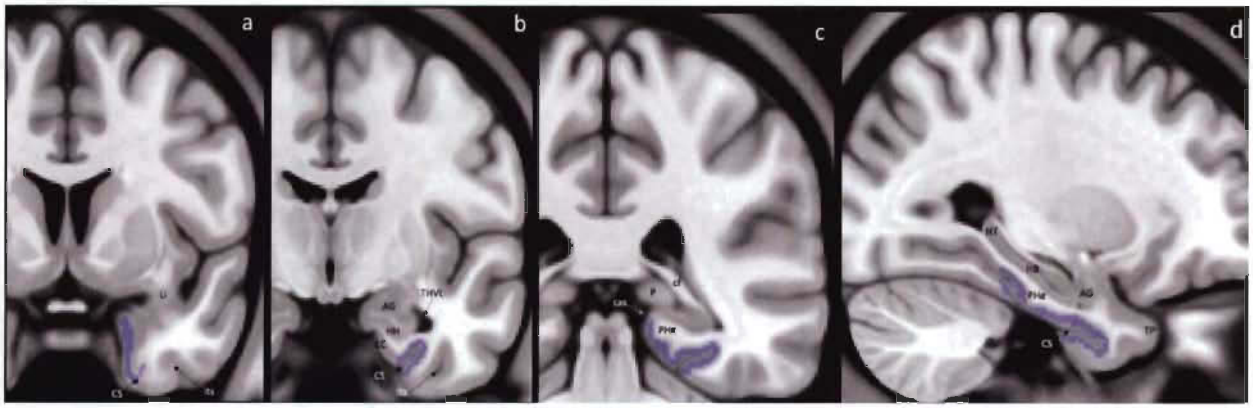


(a) Coronal view of the temporal lobe section where the perirhinal cortex is segmented at the level of the collateral sulcus appearance. (b) Coronal section of the temporal lobe at the level of the perirhinal cortex boundaries with the entorhinal and inferior temporal cortices. (c) Coronal view of the posterior slide where the parahippocampal cortex presents. This is the most posterior level where the pulvinar is present. (d) Sagittal section with visualisation of the peri-archi cortex folded around the collateral sulcus.

Li= limen insulae; CS= collateral sulcus; its= inferior temporal sulcus; AG= amygdala; HH= hippocampal head; HB= hippocampal body; HT= hippocampal tail; EC= entorhinal cortex; THVL= temporal horn of ventriculus lateralis; cf= crus of the fornix; P= pulvinar; PHg= parahippocampal gyrus; cas= calcarine sulcus; TP= temporal pole.

***ROI 4. Proisocortex manual segmentation:***

We included the gray matter of the supra- and sub-callosal areas of the anterior, middle and posterior cingulate gyrus (CinG) [9]. In the middle cingulate gyrus, we only considered the proisocortical section (IRd, area infraradiatadorsalis) [2] which is immediately adjacent to the location of the indusium griseum and perpendicular to the isocortical part of the cingulate gyrus that occupies the medial surface of the hemisphere (MR, area mediorata) by [10].

The anterior limit was defined when the CinG was no longer present anterior to the corpus callosum. The gray matter of the CinG around the splenium of the corpus callosum formed the posterior border of proisocortex. Medially, in the more anterior region, the cortex was limited by gray matter of the superior shoulder of the callosal sulcus (CalS) (gray matter of the CinG), and in

the more posterior region by the ventral shoulder of CalS (gray matter of the retrosplenial cortex) [2].

Laterally, the gray matter was segmented up to the deepest point of the bottom of the CalS (for the perigenou part) or at the level of the white matter of the CinG and deepest point of the calcarine fissure for the middle and posterior parts respectively: see Figure 6.

**Figure 6:** MRI anatomical landmarks of the proisocortex limits.

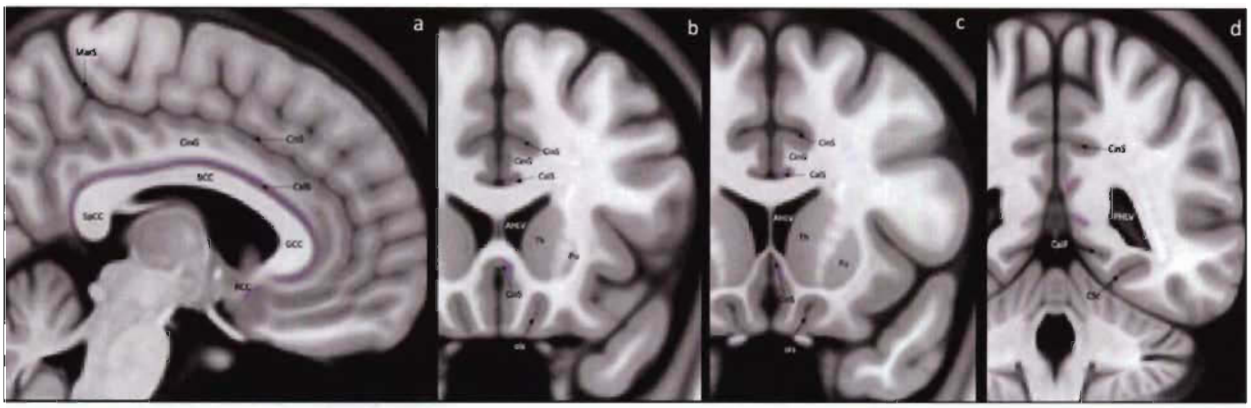


(a) Sagittal view of medial surface of a hemisphere, visualizing supra- and sub-callosal areas of anterior, middle and posterior cingulate gyrus where the proisocortex is present. (b) Coronal section of subcollosal CinC transition to subgenual CinC at the level where the putamen is first visualized within the basal ganglia. (c) Coronal view of the subgenual region at the level of the last slice after which the CinG is no longer present. (d) Coronal section of posterior CinC at the level of calcarine fissure.

GCC= genu corpus collosum; BCC= body corpus collosum, SpCC= splenium corpus collosum; RCC= rostrum corpus collosum; CalS= callosal sulcus; CinS= cingulate sulcus; CinG= cingulate gyrus; MarS= marginal sulcus; AHLV= anterior horn of lateral ventriculus; PHLV= posterior horn of lateral ventriculus; Th= thalamus; Pu= putamen; ols= olfactory sulcus; CalF= calcarine fissure; CSc= collateral sulcus caudal segment.

### *ROI. 5.1. Temporopolar neocortex manual segmentation*

The anterior limit was determined as the most prominent part of the temporal pole where the grey matter of the temporal cortex is first visible in the middle cranial fossa [7]. The visualization of the CS or gray matter of the Li defined the posterior border. The superolateral end was determined by the fundus of the temporo-polar sulcus (tps) and thus, the gyrus of Schwailbe [14] and the inferolateral limit was given by the medial bank of inferior temporal sulcus [11, 12], see Figure 7.

**Figure 7:** MRI anatomical landmarks of the temporopolar neocortex limits.

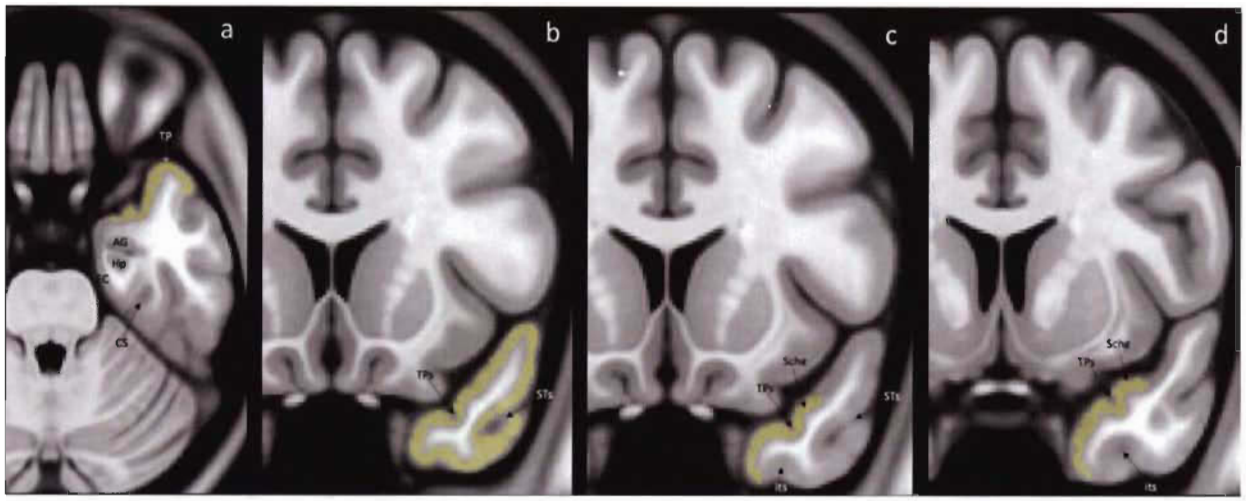


(a) Axial section of temporal lobe with visualisation of most prominent part of temporal pole. (b) The coronal view of anterior section of temporal lobe, when the inferior temporal sulcus was not yet visible and the section (c) where inferolateral and superolateral borders can be found. (d) The most posterior coronal section of temporopolar neocortex presence before limen insulae gray matter appearance. TP, temporal pole; AG, amygdala; Hp, hippocampus; EC, entorhinal cortex; CS, collateral sulcus; Schg, gyrus of Schwalbe; TPs, temporopolar sulcus; its, inferior temporal sulcus; STs, superior temporal sulcus.

***ROI 5.2. Post-central gyral cortex (somatosensory)***

Corresponding to the somatosensory region, which was modified from the CerabrA atlas [1], by removing partial volume voxels adjacent to CSF and WM of the original masks labeled as 13 (right hemisphere) and 64 (left hemisphere) of the CerebrA atlas. The editing of the CerebrA mask was done using Display, which allowed saving our final atlas mask of the post central gyral cortex.

***ROI 5.3. pre-central cortex (motor)***

The original mask of the CerebrA atlas [1] was uploaded using Display and all the voxels of partial volume with either the adjacent juxtacortical white matter or the sulci cerebrospinal fluid were removed for regions 35 (right hemisphere) and 86 (left hemisphere) from CerebrA. The corrected mask was saved as the final atlas label for the pre-central gyrus.

***ROI 5.4. pericalcarine cortex (visual)***

A similar procedure as that described in point 5.3. was performed with the original masks labeled 6 (right hemisphere) and 57 (left hemisphere).

***ROI 5.5. superior temporal cortex***

A similar procedure as that described in point 5.3. was performed with the original masks 45 (right hemisphere) and 96 (left hemisphere). The area overlapping the segmentation of the temporopolar cortex was also excluded from the original CerebrA mask.

***ROI 5.6. middle temporal cortex***

A similar procedure as that described in point 5.3. was performed with the original masks 28 (right hemisphere) and 79 (left hemisphere). The area overlapping the segmentation of the temporopolar cortex was also excluded from the original CerebrA mask.

***ROI 5.7. precuneus cortex (association)***

A similar procedure as that described in point 5.3. was performed with the original masks 31 (right hemisphere) and 82 (left hemisphere).

***ROI 5.8. insular cortex***

A similar procedure as that described in point 5.3. was performed with the original masks 23 (right hemisphere) and 74 (left hemisphere).

***ROI 5.9. inferior parietal cortex***

A similar procedure as that described in point 5.3. was performed with the original masks 10 (right hemisphere) and 61 (left hemisphere).

***ROI 5.10. caudal anterior cingulate cortex***

A similar procedure as that described in point 5.3. was performed with the original masks 30 (right hemisphere) and 81 (left hemisphere).

***ROI 5.11. posterior cingulate cortex***

A similar procedure as that described in point 5.3. was performed with the original masks 47 (right hemisphere) and 98 (left hemisphere).

***ROI 5.12. lingual cortex***

A similar procedure as that described in point 5.3. was performed with the original masks 12 (right hemisphere) and 63 (left hemisphere).

***ROI 5.13. caudal middle frontal cortex***

A similar procedure as that described in point 5.3. was performed with the original masks 42 (right hemisphere) and 93 (left hemisphere).

***ROI 5.14. cuneus cortex***

A similar procedure as that described in point 5.3. was performed with the original masks 43 (right hemisphere) and 94 (left hemisphere).

***ROI 5.15. fusiform cortex***

A similar procedure as that described in point 5.3. was performed with the original masks 24 (right hemisphere) and 75 (left hemisphere).

***ROI 5.16. inferior temporal cortex***

A similar procedure as that described in point 5.3. was performed with the original masks 3 (right hemisphere) and 54 (left hemisphere).

***ROI 5.17. isthmus cingulate cortex***

A similar procedure as that described in point 5.3. was performed with the original masks 33 (right hemisphere) and 84 (left hemisphere).

***ROI 5.18. lateral occipital cortex***

A similar procedure as that described in point 5.3. was performed with the original masks 34 (right hemisphere) and 85 (left hemisphere).

***ROI 5.19. lateral orbitofrontal cortex***

A similar procedure as that described in point 5.3. was performed with the original masks 7 (right hemisphere) and 58 (left hemisphere).

***ROI 5.20. medial orbitofrontal cortex***

A similar procedure as that described in point 5.3. was performed with the original masks 15 (right hemisphere) and 66 (left hemisphere).

***ROI 5.21. paracentral cortex***

A similar procedure as that described in point 5.3. was performed with the original masks 16 (right hemisphere) and 67 (left hemisphere).

***ROI 5.22. cortex of the pars opercularis***

A similar procedure as that described in point 5.3. was performed with the original masks 32 (right hemisphere) and 83 (left hemisphere).

***ROI 5.23. cortex of the pars orbitalis***

A similar procedure as that described in point 5.3. was performed with the original masks 44 (right hemisphere) and 95 (left hemisphere).

***ROI 5.24. cortex of the pars triangularis***

A similar procedure as that described in point 5.3. was performed with the original masks 22 (right hemisphere) and 73 (left hemisphere).

***ROI 5.25. rostral anterior cingulate cortex***

A similar procedure as that described in point 5.3. was performed with the original masks 8 (right hemisphere) and 59 (left hemisphere).

***ROI 5.26. rostral middle frontal cortex***

A similar procedure as that described in point 5.3. was performed with the original masks 1 (right hemisphere) and 52 (left hemisphere).

***ROI 5.27. superior frontal cortex***

A similar procedure as that described in point 5.3. was performed with the original masks 38 (right hemisphere) and 89 (left hemisphere).

***ROI 5.28. superior parietal cortex***

A similar procedure as that described in point 5.3. was performed with the original masks 9 (right hemisphere) and 60 (left hemisphere).

***ROI 5.29. supramarginal cortex***

A similar procedure as that described in point 5.3. was performed with the original masks 51 (right hemisphere) and 102 (left hemisphere).

***ROI 5.30. transverse temporal cortex (auditory)***

A similar procedure as that described in point 5.3. was performed with the original masks 14 (right hemisphere) and 65 (left hemisphere).

Fig. 8 illustrates the different masks identifying the ROIs in a coronal section of the MNI-ICBM152 2009c T1-weighted average template.

**Figure 8:** PAN-Atlas masks. From left to right, various inferior to superior axial slices (top two rows), right to left sagittal slices (middle two rows), and posterior to anterior axial slices (bottom two rows) of the masks of the ROIs.

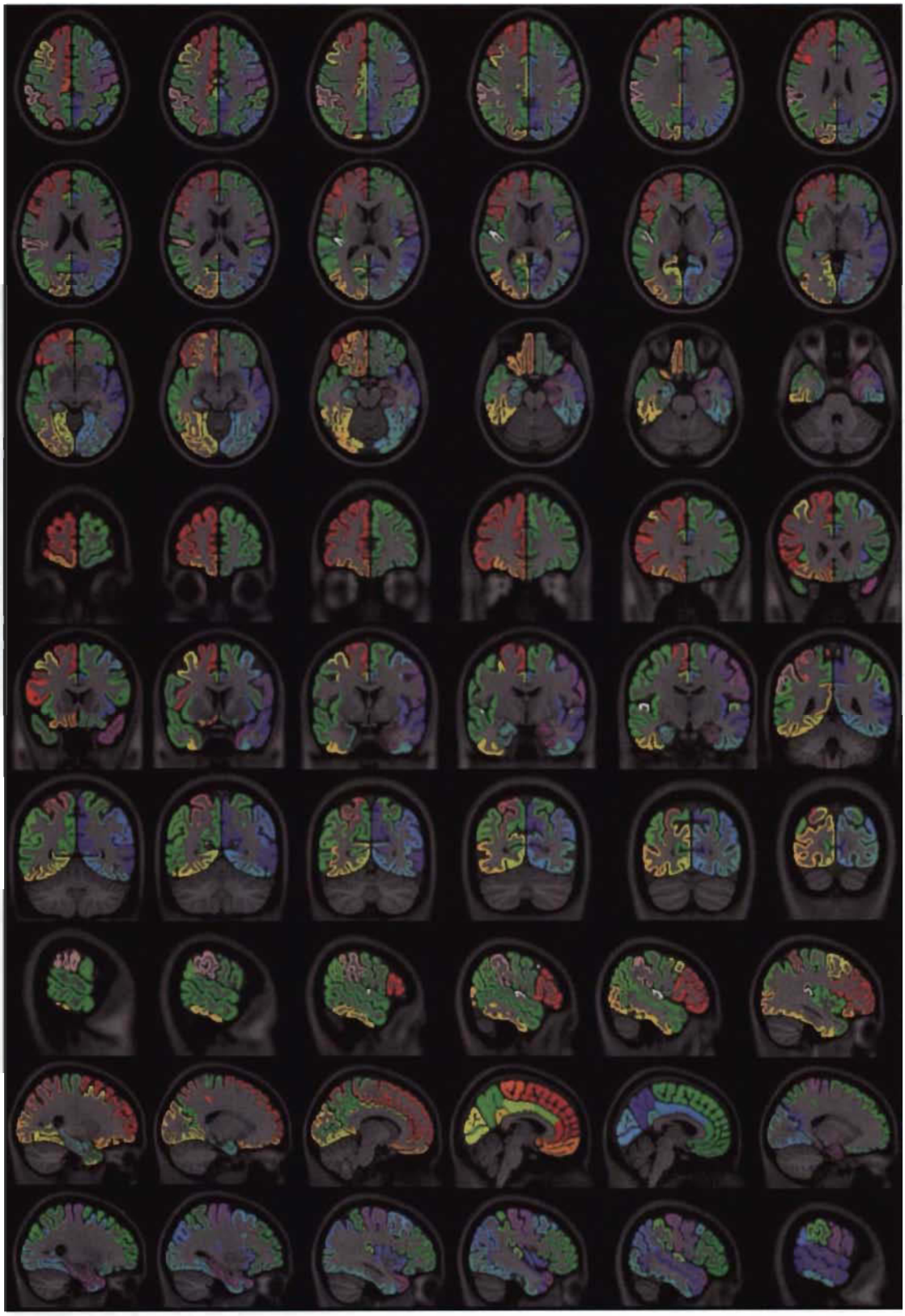

The final masks of each ROI of the PaleoArchiNeo Human Brain Atlas are available at https://gin.g-node.org/Maryna.Zhernovaia/MRI/. Table 1 indicates the numbers of the MINC format masks of each ROI, in the right and left sides, and the number of voxels (volume in cubic milimeters) of each ROI.

The T1w template is available at http://nist.mni.mcgill.ca/?p=904. The imaging data is available in compressed MINC [16] and NIfTI formats.

**Table 01:** ROIs names and numbers of the final labels in MINC format

| LABEL NAME | Atlas ID Right Hemisphere labels | Atlas ID Left Hemisphere labels | Number of voxels: volume in $mm^3$ |
|---|---|---|---|
| archicortex: ROI 1 | 1 | 21 | 3317 |
| paleocortex: ROI 2 | 2 | 22 | 1134 |
| periarchicortex: ROI 3 | 3 | 23 | 2238 |
| proisocortex: ROI 4 | 4 | 24 | 596 |
| temporopolar cortex: ROI 5.1 | 5 | 25 | 3752 |
| post-central cortex: ROI 5.2 | 6 | 26 | 12136 |
| pre-central cortex: ROI 5.3 | 7 | 27 | 11989 |
| pericalcarine cortex: ROI 5.4 | 8 | 28 | 3015 |
| superior temporal cortex: ROI 5.5 | 9 | 29 | 13572 |
| middle temporal cortex: ROI 5.6 | 10 | 30 | 17509 |
| precuneus cortex: ROI 5.7 | 11 | 31 | 12736 |
| insular cortex: ROI 5.8 | 12 | 32 | 7611 |
| inferior parietal cortex: ROI 5.9 | 13 | 33 | 16518 |
| caudal anterior cingulate: ROI 5.10 | 14 | 34 | 1587 |
| posterior cingulate: ROI 5.11 | 15 | 35 | 3016 |
| lingual gyrus cortex: ROI 5.12 | 16 | 36 | 8381 |
| caudal middle frontal: ROI 5.13 | 17 | 37 | 6597 |
| cuneus: ROI 5.14 | 18 | 38 | 3780 |
| fusiform: ROI 5.15 | 19 | 39 | 7576 |
| inferior temporal: ROI 5.16 | 20 | 40 | 8944 |
| isthmus cingulate: ROI 5.17 | 21 | 41 | 2133 |
| lateral occipital: ROI 5.18 | 22 | 42 | 12746 |
| lateral orbitofrontal: ROI 5.19 | 23 | 43 | 7153 |
| medial orbitofrontal: ROI 5.20 | 24 | 44 | 4417 |
| paracentral: ROI 5.21 | 25 | 45 | 4266 |

| | | | |
|---|---|---|---|
| pars opercularis: ROI 5.22 | 26 | 46 | 4356 |
| pars orbitalis: ROI 5.23 | 27 | 47 | 2184 |
| pars triangularis: ROI 5.24 | 28 | 48 | 4440 |
| rostral anterior cingulate: ROI 5.25 | 29 | 49 | 1650 |
| rostral middle frontal: ROI 5.26 | 30 | 50 | 10998 |
| superior frontal: ROI 5.27 | 31 | 51 | 30276 |
| superior parietal: ROI 5.28 | 32 | 52 | 9468 |
| Supramarginal: ROI 5.29 | 33 | 53 | 8535 |
| transverse temporal: ROI 5.30 | 34 | 54 | 1289 |

## Validation

### *Intra-rater variability assessment*

The manual segmentations of the archicortex, paleocortex, periarchicortex, proisocortex, and temporopolar cortex were performed by M.Z.

The correction of the CerebrA masks that were used as the starting point for the various neocortical areas considered in our atlas were performed by J.M.

All segmentations (either fully manual or the correction of pre-existing masks) were done twice, to allow the assessment of the intra-rater variability using Dice Kappa similarity index, which determines the proportion of voxels that are common (in the same special location) to the two masks. A Dice Kappa of 1 indicates a perfect spatial overlap, whereas a Dice Kappa of 0 implies no overlap between the two masks.

The Dice Kappa values of the different ROIs were as follows: 0.85 for the archicortex, 0.81 for the paleocortex, 0.69 for the periarchicortex, 0.64 for the proisocortex, 0.72 for the neocortical temporopolar cortex, 0.94 for the neocortical post-central gyrus, 0.79 for the neocortical pre-central gyrus, 0.83 for the neocortical pericalcarine region, 0.81 for the neocortical superior temporal gyrus, 0.99 for the neocortical middle temporal gyrus, 0.95 for the neocortical pre-cuneus region, 0.87 for the insular cortex, and 0.80 for the neocortical inferior parietal gyrus, indicating excellent intra-rater agreement.

The volumes of each cortical area, obtained in the first and second segmentation, showed a normal distribution, thus they were also assessed using a pair t-test and Pearson correlation coefficient.

There was no statistically significant difference between the volumes obtained in the first and second segmentation (t=-0.6; p=0.6). The Pearson correlation coefficient was 0.99 (p<0.0001).

***Inter-rater variability assessment***

All the cortical areas were also independently segmented by a second rater to assess inter-rater variability also using the Dice Kappa similarity index.

The manual segmentations of the archicortex, paleocortex, periarchicortex, proisocortex, and temporopolar cortex were also segmented by J.M. an expert neuroanatomist with more than 15 years of experience in segmentation of the brain structures on MRI scans.

The corrections of the CerebrA neocortical masks were also performed by M.Z. a specialist in neuroanatomy who has two years of experience in cortical segmentation on MRI scans.

The Dice Kappa values of the different ROIs were as follows: 0.91 for the archicortex, 0.89 for the paleocortex, 0.82 for the periarchicortex, 0.81 for the proisocortex, 0.85 for the neocortical temporopolar cortex, 0.80 for the neocortical post-central gyrus, 0.79 for the neocortical pre-central gyrus, 0.86 for the neocortical pericalcarine region, 0.82 for the neocortical superior temporal gyrus, 0.79 for the neocortical middle temporal gyrus, 0.82 for the neocortical pre-cuneus region, 0.84 for the insular cortex, and 0.80 for the neocortical inferior parietal gyrus, indicating excellent inter-rater agreement.

The volumes of each cortical area obtained by the two raters were also assessed using an independent t-test and Pearson correlation coefficient. There was no statistically significant difference between the volumes obtained by the two raters (t=-0.2; p=0.9). The Pearson correlation coefficient was 0.99 (p<0.0001).

## Ethics Statement

The present work did not involve the use of human subjects, nor animal experiments.

## CRediT author statement

**Maryna Zhernovaia:** Study concept and design, manual segmentation of the labels, analysis and interpretation of the data, drafting and revision of the manuscript.

**Mahsa Dadar**: Study concept and design, analysis and interpretation of the data, revising the manuscript.

**Sawsan Mahmoud**: analysis and interpretation of the data, revising the manuscript.

**Yashar Zeighami**: analysis and interpretation of the data, revising the manuscript.

**Josefina Maranzano**: Study concept and design, manual correction of the labels and supervision of the manual segmentations, analysis and interpretation of the data, drafting and revision of the manuscript

### Declaration of competing interests

The authors declare no competing interests

### References


[1] Manera, A., M. Dadar, V. Fonov and L. Collins (2020). CerebrA, registration and manual label correction of Mindboggle-101 atlas for MNI-ICBM152 template. Sci Data 7, 237.

[2] Mai, J. r. K. and G. Paxinos (2012). The human nervous system. Amsterdam; Elsevier Academic Press.

[3] Klingler, E. (2017). "Development and Organization of the Evolutionarily Conserved Three-Layered Olfactory Cortex." eNeuro **4**(1).

[4] Fleischhauer, K. (1976). "Handbuch der mikroskopischen Anatomie des Menschen, Bd. 4, Teil 9: Nervensystem, Allocortex — bearbeitet von H. Stephan:W.v. Möllendorf, W. Bargmann (Editors). (Springer-Verlag, Berlin-Heidelberg-New York, 1975, 1080 p., 465 Abb., DM 544.00)." Electroencephalography and Clinical Neurophysiology **41**(4): 448-448.

[5] Pruessner, J. C., L. M. Li, W. Serles, M. Pruessner, D. L. Collins, N. Kabani, S. Lupien and A. C. Evans (2000). "Volumetry of hippocampus and amygdala with high-resolution MRI and three-dimensional analysis software: minimizing the discrepancies between laboratories." Cereb Cortex **10**(4): 433-442.

[6] Gonçalves Pereira, P. M., R. Insausti, E. Artacho-Pérula, T. Salmenperä, R. Kälviäinen and A. Pitkänen (2005). "MR volumetric analysis of the piriform cortex and cortical amygdala in drug-refractory temporal lobe epilepsy." AJNR Am J Neuroradiol **26**(2): 319-332.

[7] Frankó, E., A. M. Insausti, E. Artacho-Pérula, R. Insausti and C. Chavoix (2014). "Identification of the human medial temporal lobe regions on magnetic resonance images." Hum Brain Mapp **35**(1): 248-256.

[8] Mikhael, S., C. Hoogendoorn, M. Valdes-Hernandez and C. Pernet (2018). "A critical analysis of neuroanatomical software protocols reveals clinically relevant differences in parcellation schemes." Neuroimage **170**: 348-364.

[9] McCormick, L. M., S. Ziebell, P. Nopoulos, M. Cassell, N. C. Andreasen and M. Brumm (2006). "Anterior cingulate cortex: an MRI-based parcellation method." Neuroimage **32**(3): 1167-1175.

[10] Palomero-Gallagher, N., H. Mohlberg, K. Zilles and B. Vogt (2008). "Cytology and receptor architecture of human anterior cingulate cortex." J Comp Neurol **508**(6): 906-926.

[11] Pruessner, J. C., S. Köhler, J. Crane, M. Pruessner, C. Lord, A. Byrne, N. Kabani, D. L. Collins and A. C. Evans (2002). "Volumetry of temporopolar, perirhinal, entorhinal and parahippocampal cortex from high-resolution MR images: considering the variability of the collateral sulcus." Cereb Cortex **12**(12): 1342-1353.

[12] Insausti, R., K. Juottonen, H. Soininen, A. M. Insausti, K. Partanen, P. Vainio, M. P. Laakso and A. Pitkänen (1998). "MR volumetric analysis of the human entorhinal, perirhinal, and temporopolar cortices." AJNR Am J Neuroradiol **19**(4): 659-671.

[13] Ding, S. L., J. J. Royall, S. M. Sunkin, L. Ng, B. A. Facer, P. Lesnar, A. Guillozet-Bongaarts, B. McMurray, A. Szafer, T. A. Dolbeare, A. Stevens, L. Tirrell, T. Benner, S. Caldejon, R. A. Dalley, N. Dee, C. Lau, J. Nyhus, M. Reding, Z. L. Riley, D. Sandman, E. Shen, A. van der Kouwe, A. Varjabedian, M. Wright, L. Zöllei, C. Dang, J. A. Knowles, C. Koch, J. W. Phillips, N. Sestan, P. Wohnoutka, H. R. Zielke, J. G. Hohmann, A. R. Jones, A. Bernard, M. J. Hawrylycz, P. R. Hof, B. Fischl and E. S. Lein (2016). "Comprehensive cellular-resolution atlas of the adult human brain." J Comp Neurol **524**(16): 3127-3481.

[14] Ulmer, S. and O. Jansen (2013). FMRI : basics and clinical applications. Berlin ;, Springer.

[15] Huntgeburth, S. C. and M. Petrides (2012). "Morphological patterns of the collateral sulcus in the human brain." Eur J Neurosci **35**(8): 1295-1311.

[16] Vincent, R. D., P. Neelin, N. Khalili-Mahani, A. L. Janke, V. S. Fonov, S. M. Robbins, L. Baghdadi, J. Lerch, J. G. Sled, R. Adalat, D. MacDonald, A. P. Zijdenbos, D. L. Collins and A. C. Evans (2016). "MINC 2.0: A Flexible Format for Multi-Modal Images." Frontiers in Neuroinformatics **10**(35).

# CHAPTER 3: A Human Cortical Atlas Following a Phylogenetic approach on MRI: initial results.

The content of this chapter has been presented as: Zhernovaia M, Dadar M, Zeighami Y, Maranzano, J. *Building a cortical brain MRI atlas following a phylogenetic approach: first quantitative results.* Poster Presentation at the Quebec Bio-Imaging Network Scientific Day Conference (QBIN). Montreal, QC, CA: February 7, 2020.

The work in this chapter has also been presented by Zhernovaia M. as an oral presentation intitled *A Human Cortical Atlas Following a Phylogenetic approach on MRI: initial results,* at the Scientific Week, organized by the Centre intégré en neuroimagerie et neurostimulation de Québec (CINQ). Québec, QC, CA: 25-29 May 2020.

## Introduction

Our group has created a new voxel-based human brain MRI atlas using a phylogenetic approach that we have named the PAN Human Brain Atlas. The atlas divides the cortex into five main regions of interest (ROIs): archicortex, paleocortex, peri-archicortex, proisocortex, and neocortex, which is subdivided in thirty sub-ROIs.

The atlas was built on the MNI-ICBM 152 2009c symmetric average brain MRI model, which allows the registration of single subjects' scans (which are in their native space) to the ICBM model (template space) and the use of the inverse subject-to-template transformation to obtain the atlas' masks in the original native space of the subject. In other words, this registration process allows the creation of automatic atlas' masks for individual subjects' scans.

Hence, using this registration principle, we sought to test the performance of 5 ROIs of our PAN Atlas using T1-w and MTR images of healthy participants (HP).

## General Objective

To assess, in ten HP, the registration, volumetric and MTR characteristics of 5 ROIs of the PAN-Atlas: 1- archicortex (AC), 2- paleocortex (PC), 3- peri-archicortex (PAC) 4- proisocortex (PIC), 5- temporopolar-isocortex (TPIC) (one of the sub-ROIs of the neocortex).

**Specific Objectives**

1. To perform a manual correction of the 5 ROIs and quantitatively assess the differences between the automatic masks and the manually corrected masks.
2. To assess and compare the volume of the 5 ROIs between the left and right hemispheres
3. To assess and compare the mean MTR values across the 5 ROIs and left and right.

## Materials and Methods

***Study Population:*** Ten HP (5 men and 5 women, between 20 and 30 years of age) were randomly selected from the Cambridge Center for Aging and Neuroscience (Cam-CAN) data repository (https://www.cam-can.org/index.php?content=) (Taylor et al., 2017).

***MRI scans:***

All participants were imaged on the same 3Tesla MRI scanner using an identical standardized acquisition protocol.

In our work we used T1w images (MPRAGE) to generate the ROIs' masks and calculate the cortical volume, and MTR images, to generate mean MTR values as a surrogate of the myelin content of the area (Details in Table 02).

**Table 2**: MRI acquisition parameters

| | T1w (MPRAGE) | MTR |
|---|---|---|
| TE (ms) | 2.99 | 5 |
| TR (ms) | 2250 | 30[a] |
| TI (ms) | 900 | NA |
| Voxel size (mm) | 1x1x1 | 1.5x1.5x1.5 |
| Number of slices | 192 | 192 |

TE=Echo time; TR=Repetition time; TI=Inversion time; NA=non-applicable

[a]TR = 50 used if SAR exceeded limits

***MRI processing and analysis***

The native T1w of each HP was non-linearly registered to the ICBM model. A hierarchical multiscale non-linear fitting algorithm technique was used to obtain the deformation vector field that maps the HP T1w to the template, and the inverse of the non-linear HP-to-template transformation was used to obtain the native T1w cortical masks of the ROIs (Collins & Evans,

1997). The masks obtained (that we referred to as automatic masks) were manually corrected following the anatomical landmarks presented in Chapter 2. The correction of the automatic masks was done using the interactive software package 'Display' and saved as the final manually corrected masks. Finally, the MTR images were linearly registered to the native T1w images to allow the calculation of the mean MTR values of the voxels included in each ROI (Dadar, Fonov, & Collins, 2018).

Figure 9 shows a screenshot that illustrates how the software Display presents the images of the brain in the coronal, axial, and sagittal space simultaneously, along with the Display Menu and the Terminal necessary to perform the manual corrections of the masks. Figure 10 shows a schematic representation of all the steps involved in the generation of the final manually corrected masks.

**Figure 9**: Example of one MRI case visualised using 'Display'.

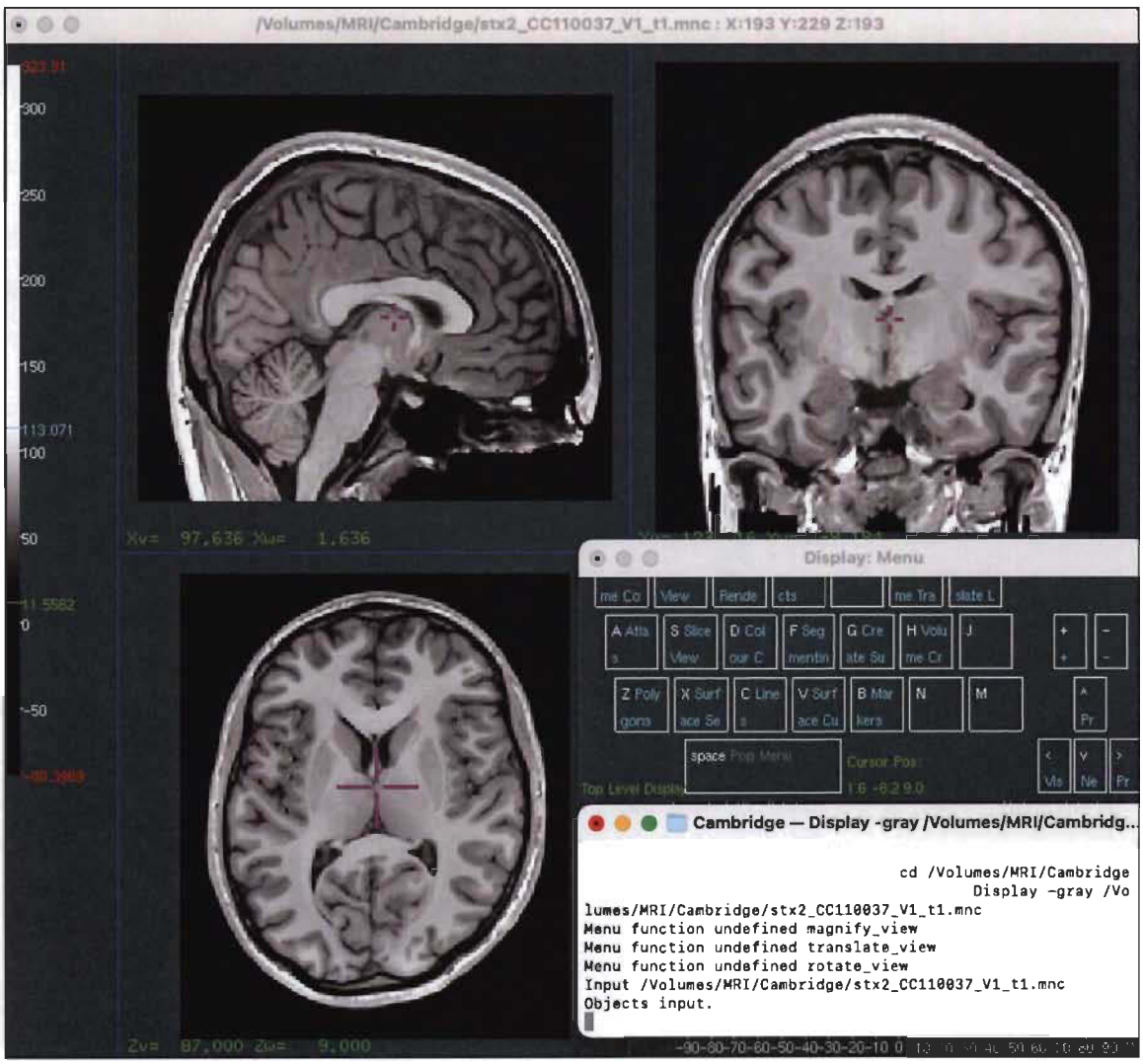

**Figure 10**: Representation of the image processing steps

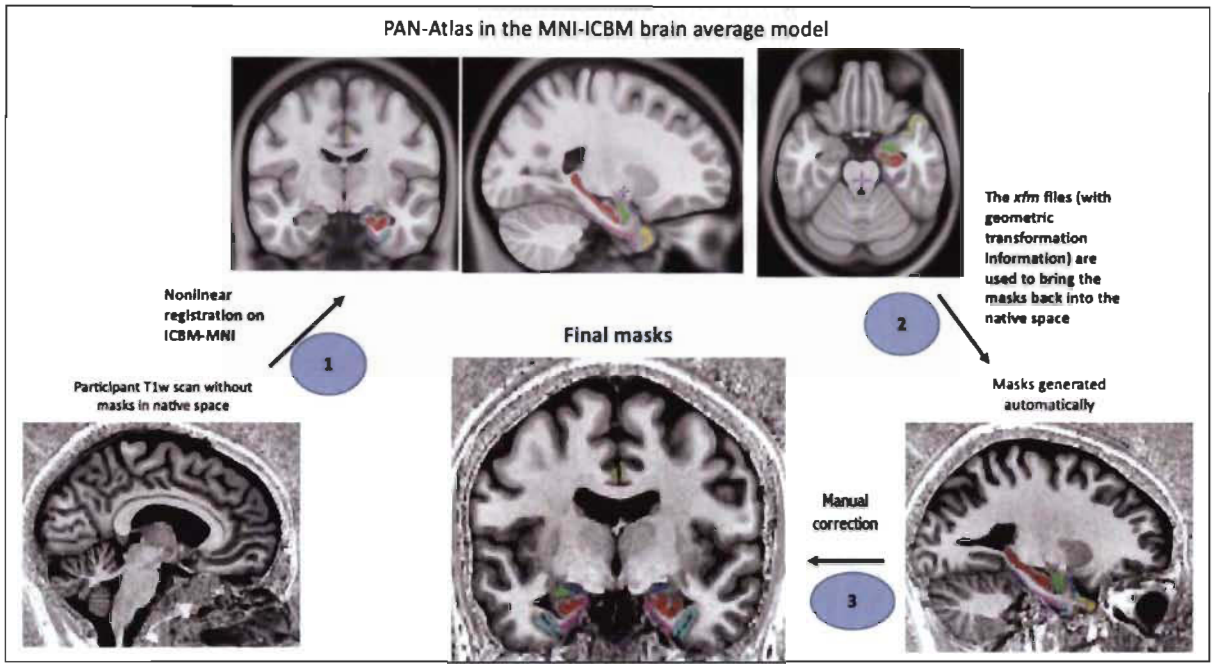


## Statistical analysis

The amount of correction needed for each ROI's mask was evaluated using Dice-Kappa similarity index between the automatic masks and the final manually corrected masks. As described in Chapter 2, a Dice-kappa of 0 indicates lack of spatial co-localization and a Dice-kappa of 1 indicates perfect co-localization between two masks (in this case automatic vs. manually corrected masks). Dice-kappa values between 0.72 and 0.90 are considered very good to excellent agreement regarding the reliability of a quantification technique (Bartko, 1991).

Cortical Dice-kappa values, ROIs volumes (in cubic centimeters) and MTR values are presented using the mean and standard deviation or median and range, according to their distributions.

A T-test (repeated or dependent T-test) was used to assess differences in cortical volumes and MTR values between the right and left hemispheres.

ANOVA (with Bonferroni correction) we used to determine if there were significant differences between MTR values across the different phylogenetic ROIs. A difference was considered

significant when p values were < 0.05. IBM SPSS Statistics software v.26 was used to perform all statistical analyses.

**Results**

All automated masks, with the exception of the PAC, have a very good to excellent performance, with median Dice-kappa values that are higher than 0.72 (details in Table 3 and Figure 11) (Bartko, 1991).

**Table 3**: Median Dice-kappa values of the automatic vs. manually corrected masks, expressed as median and a range.

| Cortex | Right | Left |
|---|---|---|
| **Archi** | 0.88 (0.82-0.93) | 0.88 (0.84-0.94) |
| **Paleo** | 0.92 (0.84-1.00) | 0.94 (0.80-1.00) |
| **Periarchi** | 0.65 (0.50-0.74) | 0.65 (0.43-0.71) |
| **Proiso** | 0.76 (0.68-0.82) | 0.78 (0.74-0.91) |
| **Iso (Temporopolar)** | 0.77 (0.64-0.86) | 0.77 (0.65-0.83) |

**Figure 11**: Dice-kappa values of the automatic vs. manual corrected masks of 5 ROIs.

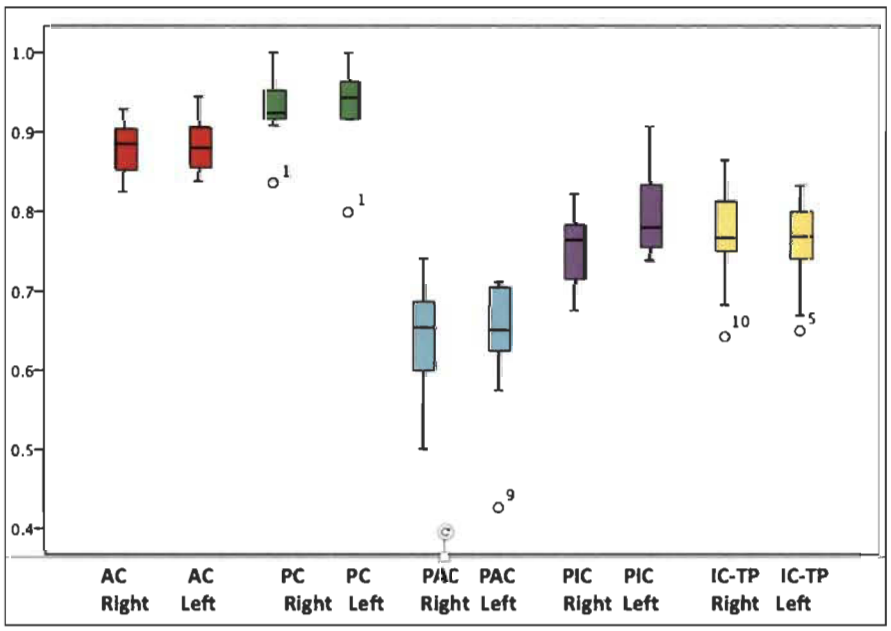

The right AC, PC, PAC, PIC volumes were not significantly different than the left volumes. The respective right and left volumes were AC 3.54cc ± 0.25 vs 3.45cc ± 0.25 (t=1.6, p=0.14); PC 1.13cc ± 0.06 vs 1.1cc ± 0.08 (t=1.1, p=0.3); PAC 3.32cc± 0.47 vs 3.29cc ± 0.47 (t=0.2, p=0.87); PIC 1.16cc ± 0.2vs 0.99cc ± 0.15 (t=1.9, p=0.09).

The right TPIC was significantly larger than the left one: 3.9cc ± 0.66 vs 3.33cc ± 0.71 (t=3.4, p=0.008) (Table 4 and Figure12).

**Table 4**: Cortices' volumes expressed as means and standard deviations

| Cortex | Right | Left |
|---|---|---|
| **Archi** | 3.54cc ± 0.25 | 3.45cc ± 0.25 |
| **Paleo** | 1.13cc ± 0.06 | 1.1cc ± 0.08 |
| **Periarchi** | 3.32cc ± 0.47 | 3.29cc ± 0.47 |
| **Proiso** | 1.16cc ± 0.2 | 0.99cc ± 0.15 |
| **Iso (Temporopolar)** | 3.9cc ± 0.66 * | 3.33cc ± 0.71 * |

cc=cubic centimeters

**Figure 12**: Cortical volumes (in cubic centimeters) of the five ROIs in the right and left hemisphere.

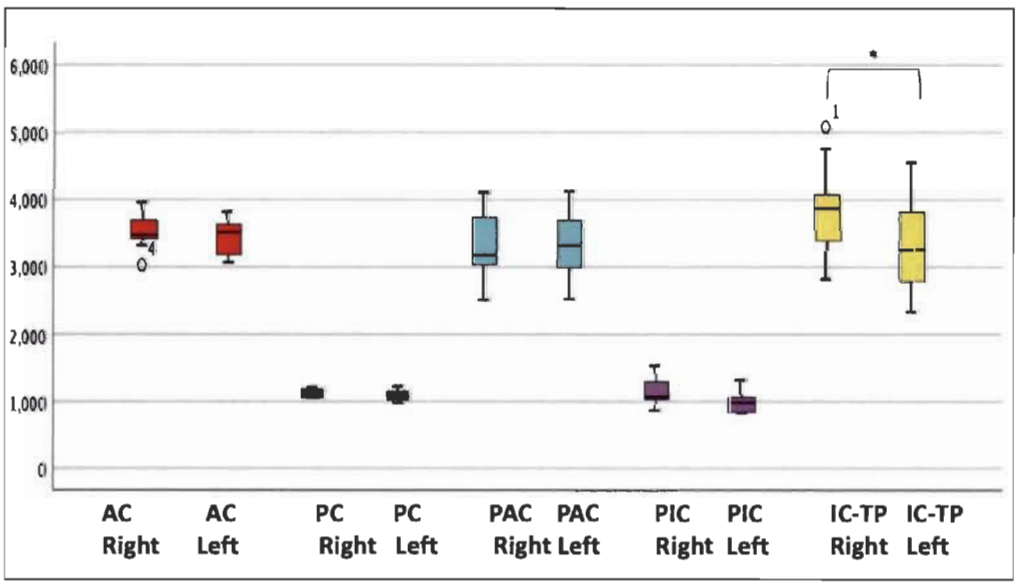

The mean MTR values of the right AC, PC, PIC, and TPIC were not significantly different than the left MTR values. The respective right and left values were AC 36.63 vs 36.48 (t=1.0, p=0.32); PC 36.78 vs 36.39 (t=1.1, p=0.29); PAC 37.62 vs 36.86 (t=3.12, p=0.01); PIC 37.3 vs 36.6 (t=1.2, p=0.25); TPIC 33.49 vs 33.39 (t=0.3, p=0.75).

The mean MTR value of the left PAC was significantly lower than the right PAC: 36.86 vs 37.62 (t=3.1, p=0.01) (Table 5 and Figure 13)

**Table 5**: MTR values of the cortical ROIs expressed as means and standard deviations.

| Cortex | Right | Left |
|---|---|---|
| **Archi** | 36.63 ± 0.73 | 36.48 ± 0.81 |
| **Paleo** | 36.78 ± 1.08 | 36.39 ± 1.3 |
| **Periarchi** | 37.62 ± 0.65* | 36.86 ± 0.89* |
| **Proiso** | 37.33 ± 1.12 | 36.58 ± 1.19 |
| **Iso (Temporopolar)** | 33.49 ± 1.82 | 33.39 ± 1.53 |

**Figure 13**: MTR values of the five ROIs in the right and left hemisphere.

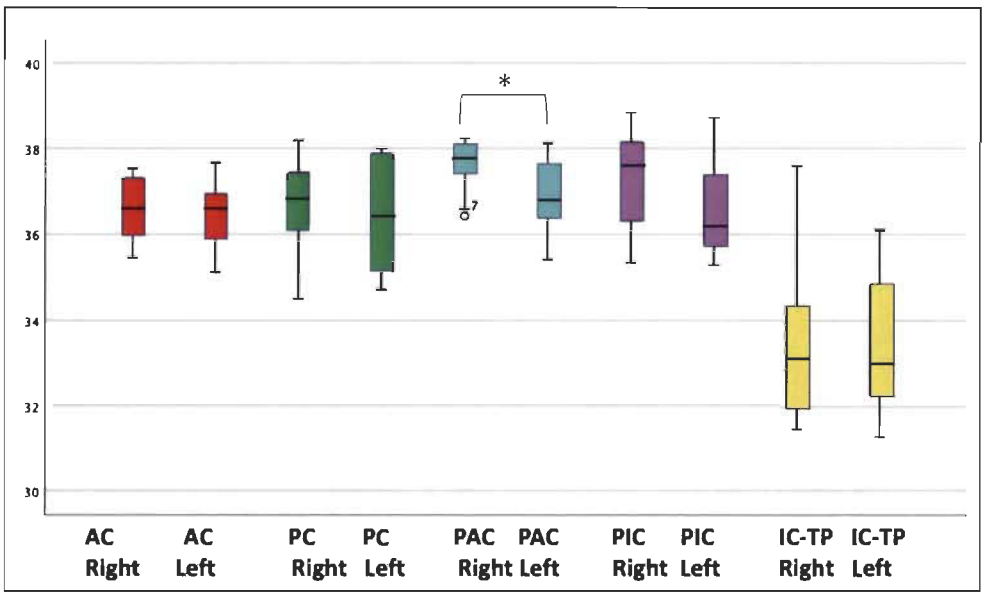

Finally, the mean MTR value of the TPIC (33.43 ± 1.63) was significantly lower than the other 4 ROIs: AC 36.55 ± 0.73, PC 36.58 ± 1.07, PAC 37.24 ± 0.68, PIC 37.04 ± 0.63 ($F=23.28$; $p<0.0001$) (Figure14).

**Figure 14**: The MTR values of IC-TP versus all other ROIs in both hemispheres.

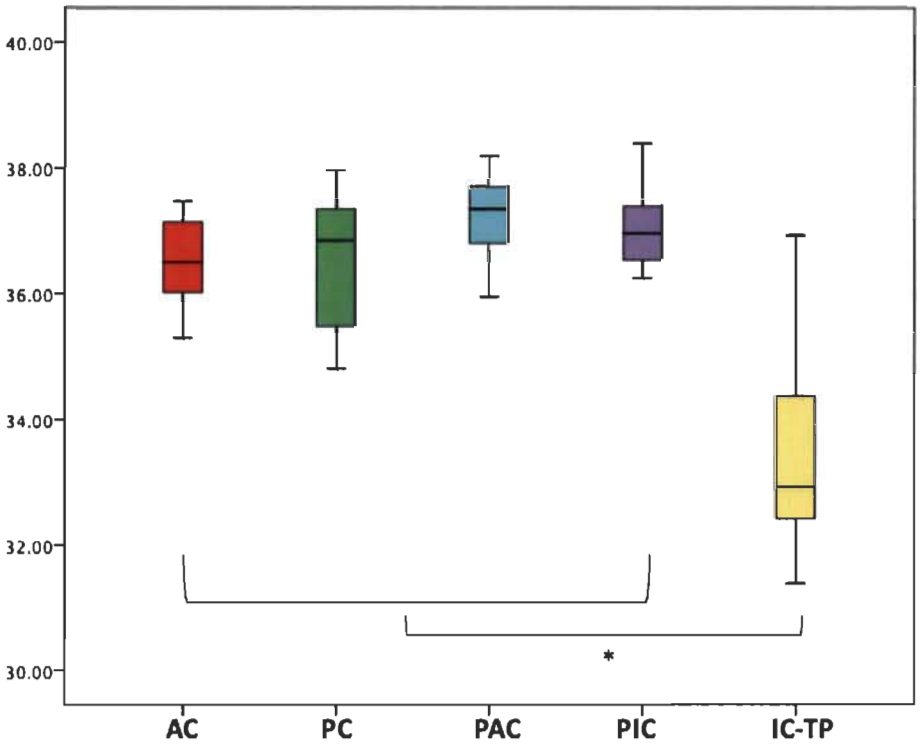


## Discussion

We know that there are differences between cortices of the left and right hemispheres from a functional point of view (Wernicke area, and other language related areas), which are manifested in structural asymmetries of the corresponding areas (Toga & Thompson, 2003). The information provided by structural MRI studies reflecting those anatomical differences using volumetric analysis are very contradictory and non-homogenous (Carne et al., 2006). Our preliminary results of volumetric analysis of 5 ROIs did not show a significant volumetric difference between the hemispheres except for the cortex of the temporal pole, which was larger in the right hemisphere of our small sample. These results must be corroborated with analyses of larger datasets of healthy participants, before a meaningful interpretation is possible. However, we can conclude that our atlas correctly segments the cortex and is a useful tool to perform this type of volumetric analysis in future studies. Moreover, we think that our atlas could be of use in the cortical volumetric

analysis of different neurodegenerative diseases, which may show, as an early sign, decrease in volume of specific cortical areas. Perhaps, different neurodegenerative diseases have their specific cortical targets, and they would show volumetric changes in different portions of cortex, even evolving/changing chronologically in different manners.

In addition to volumetric changes, the cerebral cortex may also experience histological changes without impacting its volume. For example, changes in myelin content might not necessary impact the overall cortical volume or thickness, but might still be captured by MTR images (Heim et al., 2017); (Ridha et al., 2007). Our atlas was successfully used on MTR images of $1mm^3$ isotropic voxel resolution, finding significant differences in the MTR values of the temporal pole cortex. However, these are only preliminary results, and further studies using larger datasets are warranted to corroborate regional differences in MTR values, using a voxel-based method such as our atlas.

Finally, regarding the need of manual correction of the automatic labels, the Dice-kappa values obtained translate a very good to excellent agreement. However, to increase the accuracy, the correction of the automatic masks is necessary, so manual correction is recommended if quantitative analysis is required (e.g. cortical volumes, MTR values, diffusion, etc.). This is of particular importance for the periarchicortex ROI, which shows the lowest kappa value. This is due to the anatomical location of this cortex, around the collateral sulcus, which is known to be highly variable across individuals (Huntgeburth & Petrides, 2012). Future projects, using corrected segmentations of the ROIs in larger datasets, could be used as training data (deep learning) to improve the automatic detection of all ROIs.

**Conclusions**

Our results show that the regional division of the cortex on MRI using a phylogenetic approach is possible using our PAN Human Brain Atlas.

Dividing the cortex with a phylogenetic approach is useful to detect differences between the right and left hemispheres. Future studies performed in healthy participants and patients affected by neurodegenerative disorders could show differential changes in phylogenetic cortical areas.

# DISCUSSION AND CONCLUSION

This thesis presents a new voxel-based brain MRI atlas that divides the cortex according to its phylogenetic evolution. The motivation of this project was dual: 1) the observation that certain neurodegenerative diseases preferentially affect portions of the cortex that have a common phylogenetic origin (i.e. AD) (Adams et al., 2017) and that could then benefit from a tool that approaches the study of the cortical changes following a phylogenetic approach, and 2) the lack of a brain MRI atlas that grouped common phylogenetic areas and that could be easily used (by image registration) on MRI scans of individual subjects (either healthy or affected by neurodegenerative changes). We then set to fill a void in the repertoire of brain MRI atlases currently available to researchers working in neurosciences and neurology. To our knowledge, this is the first MRI atlas in standard ICBM-MNI space that divides the cortex into phylogenetic ROIs.

## Comparison of the ROIs of the PAN-Atlas with the ROIs of other available atlases

If we compare our PAN atlas with any of the purely histology atlases, such as Brodmann's atlas (Brodmann & Gary, 2006), or Von-Economo-Koskinas' atlas (von Economo & Koskinas, 1925), or the myeloarchitectonic atlases (R. Nieuwenhuys, 2013), the main difference resides in that they parcel the cortex only on the basis of cytological or myeloarchitectonic structural characteristics and they do not consider macroscopic anatomical landmarks as the limits of the cortical areas. Additionally, these histological atlases do not fully cover the cortical ribbon, but they concentrate their analysis to the surfaces of the gyri (crown of the gyri), disregarding the cortex of the deepest parts of the sulci.

Having said this, there are conceptual similarities between our PAN atlas and the histological atlas, since both cytoarchitectonic atlases consider a general developmental division. However, the developmental division of these histologic atlases is less extensive than ours: they mainly consider two orders of cortex (heterogenetic and homogenetic), while our atlas considers five main categories.

When comparing our atlas to other neuroimaging/MRI atlases, we can observe some similarities and several differences regarding the ROIs included by the different groups. The Talairach Daemon atlas can be seen as an adaptation/translation of the Brodmanns' areas on to a brain MRI in Talairach space (Lancaster et al., 1997). However, this translation did not follow a protocol validated through MRI and histological analysis of the same brain specimen, but just the expert

identification on MRI of the Brodmann's areas depicted in illustrations and anatomical descriptions by Brodmann. Conversely, our atlas, when identifying the cortical area/ROI of a particular type of phylogenetic cortex (e.g. archicortex), based the selection of the boundaries on studies that validated the MRI landmarks with histology (Insausti et al., 1998); (Pruessner et al., 2000); (Gonçalves Pereira et al., 2005); (Frankó et al., 2014); (McCormick et al., 2006); (Palomero-Gallagher, Mohlberg, Zilles, & Vogt, 2008).

The Harvard-Oxford atlas (Caviness et al., 1996) is a purely anatomical atlas on MRI (topography-based mapping system) that exclusively parcellates the neocortex. Our PAN Atlas shares similarities in the treatment of the neocortex, since all the sub-ROIs of the neocortex (except for the temporopolar cortex) were created following an anatomical approach that uses the sulci and fissures as landmarks of the different gyri. The area that our atlas treats differently is the temporal pole, which was segmented following an MRI protocol validated with histology (Insausti et al., 1998).

Several other anatomical atlases (described in the first chapter of this thesis) share similar characteristics amongst themselves and with our PAN atlas: namely the division of the cortex using the sulci and fissures, and correlating some specific ROIs (e.g. cingulate gyrus) with histology when necessary. These atlases are: the Desikan-Killiany (Desikan et al., 2006), the Destrieux (Destrieux et al., 2010), the Mindboggle-101 (Klein & Tourville, 2012), and the Cerebrum Atlas (A. L. Manera et al., 2020). Specifically, the division of the neocortex performed by the Cerebrum Atlas, also constructed on the T1w MNI-ICBM 2009 average brain template, was used as the starting point for the neocortical sub-ROIs of our atlas. However, the changes that we introduced to the Cerebrum Atlas' ROIs provide several advantages. First, the exclusion of all partial volume voxels along the cortical-WM surface and the cortical-CSF surface, allow the use of our atlas for quantitative and semiquantitative MRI projects: for example, we used our atlas to measure MTR values in cortical GM voxels in the different phylogenetic ROIs. Other groups could use this same approach to measure relaxation times or diffusion measurements, to assess biological modifications (e.g. axonal integrity) in normal and/or pathological individual scans. Another advantage is the consideration of the temporal polar cortex as a separate ROI, which is a cytoarchitectonic area that has been underexplored, and could be of interest when assessing the medial temporal cortices, known to be selectively affected by some neurodegenerative diseases.

The neuroimaging atlases that differ the most with our atlas, are the ones that consider specific pathologies, since the ROIs may be almost exclusively subcortical, as it is the case of the atlas of Parkinson disease (Xiao et al., 2017). Also, the atlases that consider function, using resting-state fMRI, task fMRI, and MEG/EEG (Glasser et al., 2016); (Yeo et al., 2011), include ROIs that do not compare with the ones included in our atlas, since they do not necessary follow cytoarchitectonic, nor classical anatomical landmarks.

Among the atlases that combined MRI and histology, several protocols presented in Chapter I were a reference for the segmentation of specific ROIs of our atlas. The protocols developed by Insausti's group guided the segmentation on MRI of the entorhinal, perirhinal, and associated temporopolar cortices using anatomic landmarks defined on the basis of cytoarchitectonic analyses (Insausti et al., 1998). That histological data identified the anatomical landmarks used by Pruessner's group to segment the hippocampus, amygdala (Pruessner et al., 2000), temporopolar, perirhinal, entorhinal, and parahippocampal cortices (Pruessner et al., 2002) in living subjects. However, our atlas differs from these specific protocols in that we combined some of the cortical areas (e.g. hippocampus and entorhinal cortex) into a single ROI (e.g. archicortex).

Other MRI-histology atlases are more complex in their conception, such as the JuBrain atlas which is based on probabilistic cytoarchitectonic maps automatically generated using a gray scale index on digitalized images, and correlated with anatomical and functional imaging data (S. B. Eickhoff et al., 2005). The ROIs included in the JuBrain only include some portions of the cortex: motor, somatosensory, visual, auditory and language, which can all be found in homologous neocortical sub-ROIs of our PAN atlas. For example, the motor cortex of the JuBrain would correspond to the ROI 5.3 of the PAN atlas (pre-central cortex), and although we acknowledge that the detailed limits provided by the JuBrain are likely more accurate than ours regarding the cytoarchitectonic characteristics/boundaries of the motor cortex, most of the voxels included in the ROIs of both atlases will be the same.

Finally, there are three more modern histological-MRI atlases that share some key features: they combine the cytoarchitecture analysis of the whole hemispheric slices reconstructed onto the MRI, either of a template MRI or of the specimen MRI (Katrin Amunts et al., 2003); (J. K. Mai et al., 2015); (Ding et al., 2016). These atlases are used to correlate the classical cytoarchitecture of Brodmann and Von Ekonomo-Koskinas with MRI in a more accurate fashion than that provided

by the Talairach Daemon atlas. They also provide a classical anatomical division of the cortex using the sulci and fissures. In this sense, our anatomical neocortical sub-ROIs are similar to the anatomical ROIs of these atlases. However, these three atlases do not present the various cortical areas that are included in our phylogenetic ROIs (e.g. hippocampus and entorhinal cortex combined in a unique archicortex ROI) as single ROIs. Additionally, these atlases are created as high-resolution images, and their translation and applicability to lower-resolution, clinical research MRI scans may be more challenging. Our PAN-atlas is created based on an MRI template that is easily registered to clinical research scans of $1mm^3$ isotropic voxel resolution, i.e. the typical resolution used in most current T1w acquisitions (Taylor et al., 2017).

**Using the PAN-atlas: comparing how different atlases are used**

Regarding how atlases are used or applied to single subject scans, several computational tools and programs have been developed by different groups. Some of the tools have been specifically tailored to particular atlases: for example, the Alice™ and Dipstation™ image processing software used by the authors of the Talairach Daemon atlas. However, as surface atlases gained popularity given their claimed precision and ease of use (Desikan et al., 2006), three main groups emerged as the most popular software toolboxes that could be used by the neuroscientific community: 1) SPM toolbox (developed by the University College London), 2) FSL (developed by the University of Oxford), and 3) FreeSurfer (developed by Harvard University). Most of the atlases presented in Chapter 1 of this thesis have been developed or adapted to work with these toolboxes. For example, the Talairach Daemon atlas is currently available in SPM (Evans et al., 2012), the JuBrain atlas is also available in SPM (S. B. Eickhoff et al., 2005), the Desikan–Killiany (Desikan et al., 2006), the Destrieux (Destrieux et al., 2010), and the Mindboggle-101 atlas (Klein & Tourville, 2012) use FreeSurfer, and the Human Connectome Project (Van Essen et al., 2013) has used both FSL and Freesurfer tools. The main motivation to have these atlases available in these popular toolboxes has been the analysis of fMRI (and in a lesser degree the analysis of cortical thickness) in large datasets (Evans et al., 2012).

Our PAN-atlas is different in this regard. Ours is a voxel-based atlas created in ICBM-MNI standard space, so it can be used by any toolbox/software that performs linear and non-linear registration accurately. We tested (Chapter 3) our atlas using minc-tools registration scripts (Collins & Evans, 1997); (Dadar et al., 2018), showing very good to excellent automatic

performance for almost all types of cortices. Furthermore, the automated labels can be edited manually, following the anatomical guidelines described in detail in our PAN-atlas manuscript (Chapter 2). This allows further improvement for cases that do not properly register to the standard space.

Our atlas is open-source and available in a public repository, both in nifti (nii) -the most widely used image format- and in minc (mnc) format, so groups interested in surface analysis may choose to transform our volume/voxel-masks to surfaces, if they deem it necessary. This way of applying the PAN-atlas gives users more flexibility than the use in a single designated, specific tool-box, designed to analyse functional MRI data. Our goal was to provide voxel-based masks that can be used in multiple image modalities, once they are registered to ICBM-MNI standard space, by any given registration software, allowing the analysis of semi-quantitative and quantitative MRI sequences. In this regard, we successfully tested the performance of our atlas in MTR images, assessing the registration of this modality and calculating MTR values in the different ROIs. The same type of analysis could be done using other MRI sequences, for example to assess relaxation times, or diffusion properties. We see our atlas as a versatile tool, capable of being used in multiple modalities, through robust registration pipelines, and, eventually, transformable to surface-based masks if needed.

**Limitations:**

This master's project is not without limitations. The main limitation does not concern the creation of the atlas, but its application. As mentioned above, we used a small sample size of MRI scans. However, this first application of the atlas, did not seek the generation of novel biological knowledge, but just proof of concept that the atlas was operational. In particular, we were interested in assessing the performance of the ROIs that were created by fully manual segmentation, which is why we did not test all the neocortical sub-ROIs, but just the main phylogenetic ROIs. Future studies, increasing the number of scans, might corroborate some of the volumetric and MTR differences that we captured in our first test. Also, future studies in larger datasets will include all the neo-cortical sub-ROIs.

Another limitation of this work concerns the application of the atlas in certain areas, namely the periarchicortex. We transformed the atlas' masks to single individual scans using nonlinear registration, but in areas where nonlinear registration accuracy is lower due to the high anatomical

variability (Huntgeburth & Petrides, 2012) (in the case of the periarchicortex the variability is determined by the collateral sulcus variations), the resulting individual level mask is not as accurate as in other ROIs. Future experiments, using segmentation techniques (e.g. deep learning) instead of nonlinear registration might help improve the individual level accuracy of the periarchicortex masks.

Finally, we only tested the performance of our atlas using T1w and MTR images of young healthy adults. Future studies using other MRI modalities (either non-quantitative or quantitative) and older participants, or participants affected by neurodegenerative diseases, will test its applicability in a wider range of projects.

**Conclusion:**

This work presents a new voxel-based MRI parcellation approach of the human cortex following a phylogenetic approach: the PAN Human Brain Atlas, and it proves its functionality in MRI scans of individual subjects to probe volumetric and MTR characteristics.

## REFERENCES


Adams, S. L., Benayoun, L., Tilton, K., Chavez, O. R., Himali, J. J., Blusztajn, J. K., . . . Delalle, I. (2017). Methionine Sulfoxide Reductase-B3 (MsrB3) Protein Associates with Synaptic Vesicles and its Expression Changes in the Hippocampi of Alzheimer's Disease Patients. *J Alzheimers Dis, 60*(1), 43-56. doi:10.3233/jad-170459

Amunts, K., Lepage, C., Borgeat, L., Mohlberg, H., Dickscheid, T., Rousseau, M., . . . Evans, A. C. (2013). BigBrain: an ultrahigh-resolution 3D human brain model. *Science, 340*(6139), 1472-1475. doi:10.1126/science.1235381

Amunts, K., Schleicher, A., Ditterich, A., & Zilles, K. (2003). Broca's region: cytoarchitectonic asymmetry and developmental changes. *Journal of Comparative Neurology, 465*(1), 72-89.

Amunts, K., & Zilles, K. (2015). Architectonic Mapping of the Human Brain beyond Brodmann. *Neuron, 88*(6), 1086-1107. doi:10.1016/j.neuron.2015.12.001

Augustinack, J. C., van der Kouwe, A. J., & Fischl, B. (2013). Medial temporal cortices in ex vivo magnetic resonance imaging. *J Comp Neurol, 521*(18), 4177-4188. doi:10.1002/cne.23432

Azevedo, F. A., Carvalho, L. R., Grinberg, L. T., Farfel, J. M., Ferretti, R. E., Leite, R. E., . . . Herculano-Houzel, S. (2009). Equal numbers of neuronal and nonneuronal cells make the human brain an isometrically scaled-up primate brain. *Journal of Comparative Neurology, 513*(5), 532-541.

Bae, J. R., & Kim, S. H. (2017). Synapses in neurodegenerative diseases. *BMB Rep, 50*(5), 237-246. doi:10.5483/bmbrep.2017.50.5.038

Bartel, F., Visser, M., de Ruiter, M., Belderbos, J., Barkhof, F., Vrenken, H., . . . van Herk, M. (2019). Non-linear registration improves statistical power to detect hippocampal atrophy in aging and dementia. *Neuroimage Clin, 23*, 101902. doi:10.1016/j.nicl.2019.101902

Bartko, J. J. (1991). Measurement and reliability: statistical thinking considerations. *Schizophr Bull, 17*(3), 483-489. doi:10.1093/schbul/17.3.483

Batool, S., Raza, H., Zaidi, J., Riaz, S., Hasan, S., & Syed, N. I. (2019). Synapse formation: from cellular and molecular mechanisms to neurodevelopmental and neurodegenerative disorders. *J Neurophysiol, 121*(4), 1381-1397. doi:10.1152/jn.00833.2018

Boivin, J. R., & Nedivi, E. (2018). Functional implications of inhibitory synapse placement on signal processing in pyramidal neuron dendrites. *Curr Opin Neurobiol, 51*, 16-22. doi:10.1016/j.conb.2018.01.013

Brady, S., Siegel, G., Albers, R. W., & Price, D. (2011). *Basic neurochemistry: principles of molecular, cellular, and medical neurobiology*: Academic press.

Brant-Zawadzki, M., Gillan, G. D., & Nitz, W. R. (1992). MP RAGE: a three-dimensional, T1-weighted, gradient-echo sequence--initial experience in the brain. *Radiology, 182*(3), 769-775. doi:10.1148/radiology.182.3.1535892

Brickman, A. M., Tosto, G., Gutierrez, J., Andrews, H., Gu, Y., Narkhede, A., . . . Mayeux, R. (2018). An MRI measure of degenerative and cerebrovascular pathology in Alzheimer disease. *Neurology, 91*(15), e1402-e1412. doi:10.1212/wnl.0000000000006310

Brodmann, K., & Gary, L. J. (2006). *Brodmann's localization in the cerebral cortex : the principles of comparative localisation in the cerebral cortex based on cytoarchitectonics* [1 online resource (xv, 298 pages) : illustrations]. doi:10.1007/b138298

Carne, R. P., Vogrin, S., Litewka, L., & Cook, M. J. (2006). Cerebral cortex: an MRI-based study of volume and variance with age and sex. *J Clin Neurosci, 13*(1), 60-72. doi:10.1016/j.jocn.2005.02.013

Carpenter, T. A., & Williams, E. J. (1999). MRI - from basic knowledge to advanced strategies: hardware. *Eur Radiol, 9*(6), 1015-1019. doi:10.1007/s003300050787

Caspers, S., Eickhoff, S. B., Zilles, K., & Amunts, K. (2013). Microstructural grey matter parcellation and its relevance for connectome analyses. *Neuroimage, 80*, 18-26. doi:10.1016/j.neuroimage.2013.04.003

Caviness, V. S., Jr., Meyer, J., Makris, N., & Kennedy, D. N. (1996). MRI-Based Topographic Parcellation of Human Neocortex: An Anatomically Specified Method with Estimate of Reliability. *J Cogn Neurosci, 8*(6), 566-587. doi:10.1162/jocn.1996.8.6.566

Chakravarty, M. M., Bertrand, G., Hodge, C. P., Sadikot, A. F., & Collins, D. L. (2006). The creation of a brain atlas for image guided neurosurgery using serial histological data. *Neuroimage, 30*(2), 359-376. doi:10.1016/j.neuroimage.2005.09.041

Collins, D. L., & Evans, A. C. (1997). Animal: validation and applications of nonlinear registration-based segmentation. *International journal of pattern recognition and artificial intelligence, 11*(08), 1271-1294.

Cragg, B. G. (1976). Ultrastructural features of human cerebral cortex. *Journal of anatomy, 121*(Pt 2), 331-362.

Dadar, M., Fonov, V. S., & Collins, D. L. (2018). A comparison of publicly available linear MRI stereotaxic registration techniques. *Neuroimage, 174*, 191-200. doi:10.1016/j.neuroimage.2018.03.025

de Flores, R., La Joie, R., & Chételat, G. (2015). Structural imaging of hippocampal subfields in healthy aging and Alzheimer's disease. *Neuroscience, 309*, 29-50. doi:10.1016/j.neuroscience.2015.08.033

Desikan, R. S., Ségonne, F., Fischl, B., Quinn, B. T., Dickerson, B. C., Blacker, D., . . . Killiany, R. J. (2006). An automated labeling system for subdividing the human cerebral cortex on MRI scans into gyral based regions of interest. *Neuroimage, 31*(3), 968-980. doi:10.1016/j.neuroimage.2006.01.021

Destrieux, C., Fischl, B., Dale, A., & Halgren, E. (2010). Automatic parcellation of human cortical gyri and sulci using standard anatomical nomenclature. *Neuroimage, 53*(1), 1-15. doi:10.1016/j.neuroimage.2010.06.010

Dickerson, B. C., & Wolk, D. A. (2012). MRI cortical thickness biomarker predicts AD-like CSF and cognitive decline in normal adults. *Neurology, 78*(2), 84-90. doi:10.1212/WNL.0b013e31823efc6c

Ding, S. L., Royall, J. J., Sunkin, S. M., Ng, L., Facer, B. A., Lesnar, P., . . . Lein, E. S. (2016). Comprehensive cellular-resolution atlas of the adult human brain. *J Comp Neurol, 524*(16), 3127-3481. doi:10.1002/cne.24080

Dinse, J., Härtwich, N., Waehnert, M. D., Tardif, C. L., Schäfer, A., Geyer, S., . . . Bazin, P. L. (2015). A cytoarchitecture-driven myelin model reveals area-specific signatures in human primary and secondary areas using ultra-high resolution in-vivo brain MRI. *Neuroimage, 114*, 71-87. doi:10.1016/j.neuroimage.2015.04.023

Dugger, B. N., Hentz, J. G., Adler, C. H., Sabbagh, M. N., Shill, H. A., Jacobson, S., . . . Beach, T. G. (2014). Clinicopathological outcomes of prospectively followed normal elderly brain bank volunteers. *J Neuropathol Exp Neurol, 73*(3), 244-252. doi:10.1097/nen.0000000000000046

Duvernoy, H. M. (1999). *The human brain: surface, three-dimensional sectional anatomy with MRI, and blood supply*: Springer Science & Business Media.

Eickhoff, S., Walters, N. B., Schleicher, A., Kril, J., Egan, G. F., Zilles, K., . . . Amunts, K. (2005). High-resolution MRI reflects myeloarchitecture and cytoarchitecture of human cerebral cortex. *Hum Brain Mapp, 24*(3), 206-215. doi:10.1002/hbm.20082

Eickhoff, S. B., Constable, R. T., & Yeo, B. T. T. (2018). Topographic organization of the cerebral cortex and brain cartography. *Neuroimage, 170*, 332-347. doi:10.1016/j.neuroimage.2017.02.018

Eickhoff, S. B., Stephan, K. E., Mohlberg, H., Grefkes, C., Fink, G. R., Amunts, K., & Zilles, K. (2005). A new SPM toolbox for combining probabilistic cytoarchitectonic maps and functional imaging data. *Neuroimage, 25*(4), 1325-1335. doi:10.1016/j.neuroimage.2004.12.034

Eickhoff, S. B., Thirion, B., Varoquaux, G., & Bzdok, D. (2015). Connectivity-based parcellation: Critique and implications. *Hum Brain Mapp, 36*(12), 4771-4792. doi:10.1002/hbm.22933

Erkkinen, M. G., Kim, M.-O., & Geschwind, M. D. (2018). Clinical Neurology and Epidemiology of the Major Neurodegenerative Diseases. *Cold Spring Harbor Perspectives in Biology, 10*(4). doi:10.1101/cshperspect.a033118

Eroschenko, V. P., & Di Fiore, M. S. H. (2017). *DiFiore's atlas of histology with functional correlations* (13th ed. ed.). Philadelphia: Wolters Kluwer.

Evans, A. C., Janke, A. L., Collins, D. L., & Baillet, S. (2012). Brain templates and atlases. *Neuroimage, 62*(2), 911-922. doi:10.1016/j.neuroimage.2012.01.024

Farhy-Tselnicker, I., & Allen, N. J. (2018). Astrocytes, neurons, synapses: a tripartite view on cortical circuit development. *Neural Dev, 13*(1), 7. doi:10.1186/s13064-018-0104-y

Fatterpekar, G. M., Naidich, T. P., Delman, B. N., Aguinaldo, J. G., Gultekin, S. H., Sherwood, C. C., . . . Fayad, Z. A. (2002). Cytoarchitecture of the human cerebral cortex: MR microscopy of excised specimens at 9.4 Tesla. *AJNR Am J Neuroradiol, 23*(8), 1313-1321.

Fernandez-Gonzalez, P., Benavides-Piccione, R., Leguey, I., Bielza, C., Larrañaga, P., & DeFelipe, J. (2017). Dendritic-branching angles of pyramidal neurons of the human cerebral cortex. *Brain Struct Funct, 222*(4), 1847-1859. doi:10.1007/s00429-016-1311-0

Fornito, A., Wood, S. J., Whittle, S., Fuller, J., Adamson, C., Saling, M. M., . . . Yücel, M. (2008). Variability of the paracingulate sulcus and morphometry of the medial frontal cortex: associations with cortical thickness, surface area, volume, and sulcal depth. *Hum Brain Mapp, 29*(2), 222-236. doi:10.1002/hbm.20381

Frankó, E., Insausti, A. M., Artacho-Pérula, E., Insausti, R., & Chavoix, C. (2014). Identification of the human medial temporal lobe regions on magnetic resonance images. *Hum Brain Mapp, 35*(1), 248-256. doi:10.1002/hbm.22170

Gerfen, C. R., Economo, M. N., & Chandrashekar, J. (2018). Long distance projections of cortical pyramidal neurons. *J Neurosci Res, 96*(9), 1467-1475. doi:10.1002/jnr.23978

Glasser, M. F., Coalson, T. S., Robinson, E. C., Hacker, C. D., Harwell, J., Yacoub, E., . . . Van Essen, D. C. (2016). A multi-modal parcellation of human cerebral cortex. *Nature, 536*(7615), 171-178. doi:10.1038/nature18933

Gonçalves Pereira, P. M., Insausti, R., Artacho-Pérula, E., Salmenperä, T., Kälviäinen, R., & Pitkänen, A. (2005). MR volumetric analysis of the piriform cortex and cortical amygdala in drug-refractory temporal lobe epilepsy. *AJNR Am J Neuroradiol, 26*(2), 319-332.

Griauzde, J., & Srinivasan, A. (2018). Advanced Neuroimaging Techniques: Basic Principles and Clinical Applications. *J Neuroophthalmol, 38*(1), 101-114. doi:10.1097/wno.0000000000000539

Guillery, R. (2000). Brodmann's 'Localisation in the Cerebral Cortex'. *Journal of anatomy, 196*(Pt 3), 493.

Harris, J., Tomassy, G. S., & Arlotta, P. (2015). Building blocks of the cerebral cortex: from development to the dish. *Wiley Interdiscip Rev Dev Biol, 4*(5), 529-544. doi:10.1002/wdev.192

Harris, K. D., & Shepherd, G. M. (2015). The neocortical circuit: themes and variations. *Nat Neurosci, 18*(2), 170-181. doi:10.1038/nn.3917

Heim, B., Krismer, F., De Marzi, R., & Seppi, K. (2017). Magnetic resonance imaging for the diagnosis of Parkinson's disease. *J Neural Transm (Vienna), 124*(8), 915-964. doi:10.1007/s00702-017-1717-8

Hess, A., Hinz, R., Keliris, G. A., & Boehm-Sturm, P. (2018). On the Usage of Brain Atlases in Neuroimaging Research. *Mol Imaging Biol, 20*(5), 742-749. doi:10.1007/s11307-018-1259-y

Huntgeburth, S. C., & Petrides, M. (2012). Morphological patterns of the collateral sulcus in the human brain. *European Journal of Neuroscience, 35*(8), 1295-1311.

Insausti, R., Juottonen, K., Soininen, H., Insausti, A. M., Partanen, K., Vainio, P., . . . Pitkänen, A. (1998). MR volumetric analysis of the human entorhinal, perirhinal, and temporopolar cortices. *American journal of neuroradiology, 19*(4), 659-671.

Jahn, H. (2013). Memory loss in Alzheimer's disease. *Dialogues Clin Neurosci, 15*(4), 445-454. doi:10.31887/DCNS.2013.15.4/hjahn

Johnson, M. B., & Walsh, C. A. (2017). Cerebral cortical neuron diversity and development at single-cell resolution. *Curr Opin Neurobiol, 42*, 9-16. doi:10.1016/j.conb.2016.11.001

Kalia, L. V., & Lang, A. E. (2015). Parkinson's disease. *Lancet, 386*(9996), 896-912. doi:10.1016/s0140-6736(14)61393-3

Kharlamova, A. S., Godovalova, O. S., Junemann, O. I., & Saveliev, S. V. (2018). Developmental dynamics of prepiriform cortex in prenatal human ontogenesis. *J Chem Neuroanat, 92*, 61-70. doi:10.1016/j.jchemneu.2018.06.002

Klein, A., & Tourville, J. (2012). 101 labeled brain images and a consistent human cortical labeling protocol. *Front Neurosci, 6*, 171. doi:10.3389/fnins.2012.00171

Klingler, E. (2017). Development and Organization of the Evolutionarily Conserved Three-Layered Olfactory Cortex. *eNeuro, 4*(1). doi:10.1523/eneuro.0193-16.2016

Kuhn, S., Gritti, L., Crooks, D., & Dombrowski, Y. (2019). Oligodendrocytes in Development, Myelin Generation and Beyond. *Cells, 8*(11). doi:10.3390/cells8111424

Kutová, M., Mrzílková, J., Riedlová, J., & Zach, P. (2018). Asymmetric Changes in Limbic Cortex and Planum Temporale in Patients with Alzheimer Disease. *Curr Alzheimer Res, 15*(14), 1361-1368. doi:10.2174/1567205015666181004142659

Lancaster, J. L., Rainey, L. H., Summerlin, J. L., Freitas, C. S., Fox, P. T., Evans, A. C., . . . Mazziotta, J. C. (1997). Automated labeling of the human brain: a preliminary report on the development and evaluation of a forward-transform method. *Hum Brain Mapp, 5*(4), 238-242. doi:10.1002/(sici)1097-0193(1997)5:4<238::Aid-hbm6>3.0.Co;2-4

Leverenz, J. B., Umar, I., Wang, Q., Montine, T. J., McMillan, P. J., Tsuang, D. W., . . . Zhang, J. (2007). Proteomic identification of novel proteins in cortical lewy bodies. *Brain Pathol, 17*(2), 139-145. doi:10.1111/j.1750-3639.2007.00048.x

Li, G., Nie, J., Wang, L., Shi, F., Lyall, A. E., Lin, W., . . . Shen, D. (2014). Mapping longitudinal hemispheric structural asymmetries of the human cerebral cortex from birth to 2 years of age. *Cereb Cortex, 24*(5), 1289-1300. doi:10.1093/cercor/bhs413

Lifshits, S., Tomer, O., Shamir, I., Barazany, D., Tsarfaty, G., Rosset, S., & Assaf, Y. (2018). Resolution considerations in imaging of the cortical layers. *Neuroimage, 164*, 112-120. doi:10.1016/j.neuroimage.2017.02.086

Liu, J., Heinsen, H., Grinberg, L. T., Alho, E., Amaro, E., Jr., Pasqualucci, C. A., . . . Danek, A. (2019). Pathoarchitectonics of the cerebral cortex in chorea-acanthocytosis and Huntington's disease. *Neuropathol Appl Neurobiol, 45*(3), 230-243. doi:10.1111/nan.12495

Llorens, F., Thüne, K., Tahir, W., Kanata, E., Diaz-Lucena, D., Xanthopoulos, K., . . . Zerr, I. (2017). YKL-40 in the brain and cerebrospinal fluid of neurodegenerative dementias. *Mol Neurodegener, 12*(1), 83. doi:10.1186/s13024-017-0226-4

Lodato, S., & Arlotta, P. (2015). Generating neuronal diversity in the mammalian cerebral cortex. *Annu Rev Cell Dev Biol, 31*, 699-720. doi:10.1146/annurev-cellbio-100814-125353

Lyttelton, O. C., Karama, S., Ad-Dab'bagh, Y., Zatorre, R. J., Carbonell, F., Worsley, K., & Evans, A. C. (2009). Positional and surface area asymmetry of the human cerebral cortex. *Neuroimage, 46*(4), 895-903. doi:10.1016/j.neuroimage.2009.03.063

Mai, J. K., Majtanik, M., & Paxinos, G. (2015). *Atlas of the human brain*: Academic Press.

Mai, J. r. K., & Paxinos, G. (2012). *The human nervous system* [1 online resource (xi, 1415 pages) : illustrations (some color)](3rd ed. ed.). Retrieved from http://www.clinicalkey.com/dura/browse/bookChapter/3-s2.0-C20090027214

Maintz, J. B., & Viergever, M. A. (1998). A survey of medical image registration. *Med Image Anal, 2*(1), 1-36. doi:10.1016/s1361-8415(01)80026-8

Maldjian, J. A., Laurienti, P. J., Kraft, R. A., & Burdette, J. H. (2003). An automated method for neuroanatomic and cytoarchitectonic atlas-based interrogation of fMRI data sets. *Neuroimage, 19*(3), 1233-1239. doi:10.1016/s1053-8119(03)00169-1

Malva, J. o. O. (2007). *Interaction between neurons and glia in aging and disease* [1 online resource (ix, 521 pages) : illustrations (some color)]. doi:10.1007/978-0-387-70830-0.

Manera, A., Dadar, M., Fonov, V., & Collins, L. (2019). CerebrA: Accurate registration and manual label correction of Mindboggle-101 atlas for MNI-ICBM152 template. In: bioRxiv.

Manera, A. L., Dadar, M., Collins, D. L., & Ducharme, S. (2019). Deformation based morphometry study of longitudinal MRI changes in behavioral variant frontotemporal dementia. *Neuroimage Clin, 24*, 102079. doi:10.1016/j.nicl.2019.102079

Manera, A. L., Dadar, M., Fonov, V., & Collins, D. L. (2020). CerebrA, registration and manual label correction of Mindboggle-101 atlas for MNI-ICBM152 template. *Sci Data, 7*(1), 237. doi:10.1038/s41597-020-0557-9

Marinelli, S., Basilico, B., Marrone, M. C., & Ragozzino, D. (2019). Microglia-neuron crosstalk: Signaling mechanism and control of synaptic transmission. *Semin Cell Dev Biol, 94*, 138-151. doi:10.1016/j.semcdb.2019.05.017

Mazziotta, J., Toga, A., Evans, A., Fox, P., Lancaster, J., Zilles, K., . . . Mazoyer, B. (2001). A four-dimensional probabilistic atlas of the human brain. *J Am Med Inform Assoc, 8*(5), 401-430. doi:10.1136/jamia.2001.0080401

McCormick, L. M., Ziebell, S., Nopoulos, P., Cassell, M., Andreasen, N. C., & Brumm, M. (2006). Anterior cingulate cortex: an MRI-based parcellation method. *Neuroimage, 32*(3), 1167-1175. doi:10.1016/j.neuroimage.2006.04.227

McKhann, G. M., Knopman, D. S., Chertkow, H., Hyman, B. T., Jack, C. R., Jr., Kawas, C. H., . . . Phelps, C. H. (2011). The diagnosis of dementia due to Alzheimer's disease: recommendations from the National Institute on Aging-Alzheimer's Association workgroups on diagnostic guidelines for Alzheimer's disease. *Alzheimers Dement, 7*(3), 263-269. doi:10.1016/j.jalz.2011.03.005

Molyneaux, B. J., Arlotta, P., Menezes, J. R., & Macklis, J. D. (2007). Neuronal subtype specification in the cerebral cortex. *Nature reviews neuroscience, 8*(6), 427-437.

Morell, P., & Norton, W. T. (1980). Myelin. *Scientific American, 242*(5), 88-119.

Mountcastle, V. B. (1997). The columnar organization of the neocortex. *Brain : a journal of neurology, 120*(( Pt 4)), 701-722.

Na, H., Chunyan, L., Wenjing, Z., Xiyue, Y., Yuan, X., John, A. S., . . . Qiyong, G. (2020). Hippocampal subfield alterations in schizophrenia: A selective review of structural MRI studies. *Biomarkers in Neuropsychiatry, 3*, 100026. doi:10.1016/j.bionps.2020.100026

Nieuwenhuys, R. (1994). The neocortex : An overview of its evolutionary development, structural organization and synaptology. *Anatomy and Embryology, 190*(4), 307-337. doi:10.1007/BF00187291

Nieuwenhuys, R. (2013). The myeloarchitectonic studies on the human cerebral cortex of the Vogt-Vogt school, and their significance for the interpretation of functional neuroimaging data. *Brain structure & function, 218*(2), 303-352. doi:10.1007/s00429-012-0460-z

Nieuwenhuys, R., Voogd, J., & Huijzen, C. v. (2008). *The human central nervous system* (Fourth edition. ed.). Berlin: Springer.

Oishi, K., & Nakajima, K. (2018). Subtype Specification of Cerebral Cortical Neurons in Their Immature Stages. *Neurochem Res, 43*(1), 238-244. doi:10.1007/s11064-017-2441-3

Ono, M., Kubik, S., & Abernathey, C. D. (1990). *Atlas of the cerebral sulci*: Thieme Medical Publishers.

Palomero-Gallagher, N., Mohlberg, H., Zilles, K., & Vogt, B. (2008). Cytology and receptor architecture of human anterior cingulate cortex. *J Comp Neurol, 508*(6), 906-926. doi:10.1002/cne.21684

Palomero-Gallagher, N., & Zilles, K. (2019). Cortical layers: Cyto-, myelo-, receptor- and synaptic architecture in human cortical areas. *Neuroimage, 197*, 716-741. doi:10.1016/j.neuroimage.2017.08.035

Partridge, L., Deelen, J., & Slagboom, P. E. (2018). Facing up to the global challenges of ageing. *Nature, 561*(7721), 45-56. doi:10.1038/s41586-018-0457-8

Paus, T. (2018). Imaging microstructure in the living human brain: A viewpoint. *Neuroimage, 182*, 3-7. doi:10.1016/j.neuroimage.2017.10.013

Petrides, M. (2012). *The human cerebral cortex: an MRI atlas of the sulci and gyri in MNI stereotaxic space*: Elsevier/Academic Press.

Pruessner, J. C., Köhler, S., Crane, J., Pruessner, M., Lord, C., Byrne, A., . . . Evans, A. C. (2002). Volumetry of temporopolar, perirhinal, entorhinal and parahippocampal cortex from high-resolution MR images: considering the variability of the collateral sulcus. *Cerebral Cortex, 12*(12), 1342-1353.

Pruessner, J. C., Li, L. M., Serles, W., Pruessner, M., Collins, D. L., Kabani, N., . . . Evans, A. C. (2000). Volumetry of hippocampus and amygdala with high-resolution MRI and three-dimensional analysis software: minimizing the discrepancies between laboratories. *Cerebral Cortex, 10*(4), 433-442.

Purger, D., Gibson, E. M., & Monje, M. (2016). Myelin plasticity in the central nervous system. *Neuropharmacology, 110*(Pt B), 563-573. doi:10.1016/j.neuropharm.2015.08.001

Purves, D., Augustine, G. J., Fitzpatrick, D., Hall, W. C. P. D., LaMantia, A.-S., Mooney, R. D., . . . White, L. E. (2018). *Neuroscience* (Sixth edition. ed.). Sunderland, Massachusetts: Oxford University Press.

Ramaswamy, S., & Markram, H. (2015). Anatomy and physiology of the thick-tufted layer 5 pyramidal neuron. *Front Cell Neurosci, 9*, 233. doi:10.3389/fncel.2015.00233

Ridha, B. H., Symms, M. R., Tozer, D. J., Stockton, K. C., Frost, C., Siddique, M. M., . . . Tofts, P. S. (2007). Magnetization transfer ratio in Alzheimer disease: comparison with volumetric measurements. *AJNR Am J Neuroradiol, 28*(5), 965-970.

Ross, M. H., & Pawlina, W. (2011). *Histology : a text and atlas : with correlated cell and molecular biology* (6th ed. ed.). Philadelphia: Wolters Kluwer/Lippincott Williams & Wilkins Health.

Rüb, U., Seidel, K., Heinsen, H., Vonsattel, J. P., den Dunnen, W. F., & Korf, H. W. (2016). Huntington's disease (HD): the neuropathology of a multisystem neurodegenerative disorder of the human brain. *Brain Pathol, 26*(6), 726-740. doi:10.1111/bpa.12426

Scholtens, L. H., de Reus, M. A., de Lange, S. C., Schmidt, R., & van den Heuvel, M. P. (2018). An MRI Von Economo - Koskinas atlas. *Neuroimage, 170*, 249-256. doi:10.1016/j.neuroimage.2016.12.069

Scholtens, L. H., de Reus, M. A., & van den Heuvel, M. P. (2015). Linking contemporary high resolution magnetic resonance imaging to the von Economo legacy: A study on the comparison of MRI cortical thickness and histological measurements of cortical structure. *Hum Brain Mapp, 36*(8), 3038-3046. doi:10.1002/hbm.22826

Sengupta, S., Fritz, F. J., Harms, R. L., Hildebrand, S., Tse, D. H. Y., Poser, B. A., . . . Roebroeck, A. (2018). High resolution anatomical and quantitative MRI of the entire human occipital lobe ex vivo at 9.4T. *Neuroimage, 168*, 162-171. doi:10.1016/j.neuroimage.2017.03.039

Simic, G., Bexheti, S., Kelovic, Z., Kos, M., Grbic, K., Hof, P. R., & Kostovic, I. (2005). Hemispheric asymmetry, modular variability and age-related changes in the human entorhinal cortex. *Neuroscience, 130*(4), 911-925.

Simpson, D. S. A., & Oliver, P. L. (2020). ROS Generation in Microglia: Understanding Oxidative Stress and Inflammation in Neurodegenerative Disease. *Antioxidants (Basel), 9*(8). doi:10.3390/antiox9080743

Spalletta, G., Piras, F., & Gili, T. (2018). *Brain morphometry*: Springer.

Specht, K., & Wigglesworth, P. (2018). The functional and structural asymmetries of the superior temporal sulcus. *Scand J Psychol, 59*(1), 74-82. doi:10.1111/sjop.12410

Stephenson, J., Nutma, E., van der Valk, P., & Amor, S. (2018). Inflammation in CNS neurodegenerative diseases. *Immunology, 154*(2), 204-219. doi:10.1111/imm.12922

Strominger, N. L., Demarest, R. J., & Laemle, L. B. (2012). *Noback's human nervous system: structure and function*: Springer Science & Business Media.

Symms, M., Jäger, H. R., Schmierer, K., & Yousry, T. A. (2004). A review of structural magnetic resonance neuroimaging. *J Neurol Neurosurg Psychiatry, 75*(9), 1235-1244. doi:10.1136/jnnp.2003.032714

Szabo, C. A., Xiong, J., Lancaster, J. L., Rainey, L., & Fox, P. (2001). Amygdalar and hippocampal volumetry in control participants: differences regarding handedness. *AJNR Am J Neuroradiol, 22*(7), 1342-1345.

Taylor, J. R., Williams, N., Cusack, R., Auer, T., Shafto, M. A., Dixon, M., . . . Henson, R. N. (2017). The Cambridge Centre for Ageing and Neuroscience (Cam-CAN) data repository: Structural and functional MRI, MEG, and cognitive data from a cross-sectional adult lifespan sample. *Neuroimage, 144*(Pt B), 262-269. doi:10.1016/j.neuroimage.2015.09.018

Toga, A. W., & Thompson, P. M. (2003). Mapping brain asymmetry. *Nat Rev Neurosci, 4*(1), 37-48. doi:10.1038/nrn1009

Trampel, R., Bazin, P. L., Pine, K., & Weiskopf, N. (2019). In-vivo magnetic resonance imaging (MRI) of laminae in the human cortex. *Neuroimage, 197*, 707-715. doi:10.1016/j.neuroimage.2017.09.037

Triarhou, L. C. (2007). The Economo-Koskinas Atlas Revisited: Cytoarchitectonics and Functional Context. *Stereotactic and Functional Neurosurgery, 85*(5), 195-203. doi:10.1159/000103258

Ulmer, S., & Jansen, O. (2013). *FMRI : basics and clinical applications* [1 online resource (vi, 325 pages) : illustrations (some color)](2nd ed. ed.). doi:10.1007/978-3-642-34342-1

Van Essen, D. C., Donahue, C. J., & Glasser, M. F. (2018). Development and Evolution of Cerebral and Cerebellar Cortex. *Brain Behav Evol, 91*(3), 158-169. doi:10.1159/000489943

Van Essen, D. C., Glasser, M. F., Dierker, D. L., Harwell, J., & Coalson, T. (2012). Parcellations and hemispheric asymmetries of human cerebral cortex analyzed on surface-based atlases. *Cereb Cortex, 22*(10), 2241-2262. doi:10.1093/cercor/bhr291

Van Essen, D. C., Smith, S. M., Barch, D. M., Behrens, T. E., Yacoub, E., & Ugurbil, K. (2013). The WU-Minn Human Connectome Project: an overview. *Neuroimage, 80*, 62-79. doi:10.1016/j.neuroimage.2013.05.041

Vogt, B. A., Vogt, L., & Laureys, S. (2006). Cytology and functionally correlated circuits of human posterior cingulate areas. *Neuroimage, 29*(2), 452-466. doi:10.1016/j.neuroimage.2005.07.048

von Economo, C. F., & Koskinas, G. N. (1925). *Die cytoarchitektonik der hirnrinde des erwachsenen menschen*: J. Springer.

von Economo, C. F., Koskinas, G. N., & Triarhou, L. C. (2008). *Atlas of cytoarchitectonics of the adult human cerebral cortex* (Vol. 10): Karger Basel.

Walsh, D. M., Landman, K. A., & Hughes, B. D. (2017). What is the optimal distribution of myelin along a single axon? *Neurosci Lett, 658*, 97-101. doi:10.1016/j.neulet.2017.08.037

Watson, C., Kirkcaldie, M., & Paxinos, G. (2010). *The brain an introduction to functional neuroanatomy* [1 ressource en ligne (ix, 203 p.) : illustrations (principalement en coul.)](1st ed. ed.). Retrieved from http://www.sciencedirect.com/science/book/9780123738899

Wisse, L. E. M., Adler, D. H., Ittyerah, R., Pluta, J. B., Robinson, J. L., Schuck, T., . . . Yushkevich, P. A. (2017). Comparison of In Vivo and Ex Vivo MRI of the Human Hippocampal Formation in the Same Subjects. *Cereb Cortex, 27*(11), 5185-5196. doi:10.1093/cercor/bhw299

Xiao, Y., Fonov, V., Chakravarty, M. M., Beriault, S., Al Subaie, F., Sadikot, A., . . . Collins, D. L. (2017). A dataset of multi-contrast population-averaged brain MRI atlases of a Parkinson's disease cohort. *Data Brief, 12*, 370-379. doi:10.1016/j.dib.2017.04.013

Yeo, B. T., Krienen, F. M., Sepulcre, J., Sabuncu, M. R., Lashkari, D., Hollinshead, M., . . . Buckner, R. L. (2011). The organization of the human cerebral cortex estimated by intrinsic functional connectivity. *J Neurophysiol, 106*(3), 1125-1165. doi:10.1152/jn.00338.2011

Zilles, K., & Amunts, K. (2010). Centenary of Brodmann's map--conception and fate. *Nat Rev Neurosci, 11*(2), 139-145. doi:10.1038/nrn2776